Vol. 292, No. 3, July 11, 1994
Completing Volume 292

ISSN 0003-2670

ANALYTICA CHIMICA ACTA

An international journal devoted to all branches of analytical chemistry

ELSEVIER

ANALYTICA CHIMICA ACTA

Scope. *Analytica Chimica Acta* publishes original papers, rapid publication letters and reviews dealing with every aspect of modern analytical chemistry. Reviews are normally written by invitation of the editors, who welcome suggestions for subjects. Letters can be published within **four months** of submission. For information on the Letters section, see inside back cover.

Submission of Papers

Americas

Prof. Harry L. Pardue
Department of Chemistry
1393 BRWN Bldg, Purdue University
West Lafayette, IN 47907-1393
USA

Tel:(+1-317) 494 5320
Fax:(+1-317) 496 1200

Computer Techniques

Prof. J.T. Clerc
Universität Bern
Pharmazeutisches Institut
Baltzerstrasse 5, CH-3012 Bern
Switzerland

Tel:(+41-31) 6314191
Fax:(+41-31) 6314198

Prof. Sarah C. Rutan
Department of Chemistry
Virginia Commonwealth University
P.O. Box 2006
Richmond, VA 23284-2006
USA
Tel:(+1-804) 367 7517
Fax:(+1-804) 367 8599

Other Papers

Prof. Alan Townshend
Department of Chemistry
The University
Hull HU6 7RX
Great Britain

Tel:(+44-482) 465027
Fax:(+44-482) 466410

Prof. Willem E. van der Linden
Laboratory for Chemical Analysis
Department of Chemical Technology
Twente University of Technology
P.O. Box 217, 7500 AE Enschede
The Netherlands
Tel:(+31-53) 892629
Fax:(+31-53) 356024

Prof. Paul Worsfold
Dept. of Environmental Sciences
University of Plymouth
Plymouth PL4 8AA
Great Britain

Tel:(+44-752) 233006
Fax:(+44-752) 233009

Submission of an article is understood to imply that the article is original and unpublished and is not being considered for publication elsewhere. *Anal. Chim. Acta* accepts papers in English only. There are no page charges. Manuscripts should conform in layout and style to the papers published in this issue. See inside back cover for "Information for Authors".

Publication. *Analytica Chimica Acta* appears in 16 volumes in 1994 (Vols. 281-296). *Vibrational Spectroscopy* appears in 2 volumes in 1994 (Vols. 6 and 7). Subscriptions are accepted on a prepaid basis only, unless different terms have been previously agreed upon. It is possible to order a combined subscription (*Anal. Chim. Acta* **and** *Vib. Spectrosc.*).
Our p.p.h. (postage, packing and handling) charge includes surface delivery of all issues, except to subscribers in the U.S.A., Canada, Australia, New Zealand, China, India, Israel, South Africa, Malaysia, Thailand, Singapore, South Korea, Taiwan, Pakistan, Hong Kong, Brazil, Argentina and Mexico, who receive all issues by air delivery (S.A.L.-Surface Air Lifted) at no extra cost. For Japan, air delivery requires 25% additional charge of the normal postage and handling charge; for all other countries airmail and S.A.L. charges are available upon request.

Subscription orders. Subscription prices are available upon request from the publisher. Subscription orders can be entered only by calendar year and should be sent to: Elsevier Science B.V., Journals Department, P.O. Box 211, 1000 AE Amsterdam, The Netherlands. Tel: (+31-20) 5803 642, Telex: 18582, Telefax: (+31-20) 5803598, to which requests for sample copies can also be sent. Claims for issues not received should be made within six months of publication of the issues. If not they cannot be honoured free of charge. Readers in the U.S.A. and Canada can contact the following address: Elsevier Science Inc., Journal Information Center, 655 Avenue of the Americas, New York, NY 10010, U.S.A. Tel: (+1-212) 6333750, Telefax: (+1-212) 6333990, for further information, or a free sample copy of this or any other Elsevier Science journal.
Advertisements. Advertisement rates are available from the publisher on request.

US mailing notice - Analytica Chimica Acta (ISSN 0003-2670) is published 3 times a month (total 48 issues) by Elsevier Science B.V. (Molenwerf 1, Postbus 211, 1000 AE Amsterdam). Annual subscription price in the USA US$ 3035.75 (valid in North, Central and South America), including air speed delivery. Second class postage paid at Jamaica, NY 11431. *USA Postmasters*: Send address changes to Anal. Chim. Acta, Publications Expediting, Inc., 200 Meacham Av., Elmont, NY 11003. Airfreight and mailing in the USA by Publication Expediting.

ANALYTICA CHIMICA ACTA

An international journal devoted to all branches of analytical chemistry

(Full texts are incorporated in CJELSEVIER, a file in the Chemical Journals Online database available on STN International; Abstracted, indexed in: Aluminum Abstracts; Anal. Abstr.; Biol. Abstr.; BIOSIS; Chem. Abstr.; Curr. Contents Phys. Chem. Earth Sci.; Engineered Materials Abstracts; Excerpta Medica; Index Med.; Life Sci.; Mass Spectrom. Bull.; Material Business Alerts; Metals Abstracts; Sci. Citation Index)

VOL. 292 NO. 3 CONTENTS JULY 11, 1994

ELSEVIER

Analytica Chimica Acta 292 (1994) 219–234

ANALYTICA CHIMICA ACTA

Classification of multicomponent analytical data of olive oils using different neural networks

Jure Zupan *, Marjana Novič

National Institute of Chemistry, SLO-61115 Ljubljana, Slovenia

Xinzhi Li, Johann Gasteiger [1]

Organisch Chemisches Institut, Technische Universität München, 81477 Garching, Germany

(Received 19th July 1993; revised manuscript received 4th October 1993)

Abstract

A comparison of classification abilities of two different neural network methods, namely, back-propagation of errors and Kohonen learning is made and discussed. The classification is performed on a set of 572 Italian olive oils on the basis of an analysis of eight fatty acids. The comparison of methods is carried out by different neural network architectures for each learning strategy separately. It was found that for the applied classification problem Kohonen learning is superior to the back-propagation of errors. Additionally, the levels of weights in the Kohonen neural network can be exploited to give more detailed information about the separation ability of each individual variable, i.e. of each individual fatty acid in our case.

Key words: Multicomponent analysis; Neural networks; Olive oils

1. Introduction

One of the simplest and most frequently used task in handling complex multivariate data is classification. To some extent, classification is similar to the mapping of objects from a m-dimensional to the 2-dimensional space. In standard clustering or classification one is mainly concerned with two questions: first, how many clusters are formed, and second, to which cluster or class a given object belongs. In mapping the additional concern is the visual representation – the form of and the inter-relations between the clusters, i.e. the features like: how many distinguished areas can be identified on the map, what are the shapes of these areas, how can the map's features be correlated with the objects from which the map was obtained, etc.

Classification or mapping can be successfully applied to a problem presently of high interest: the monitoring of the origin of goods. To be more specific: how can be shown that an object comes from the region specified by its label or no Hence, the problem is reduced to a stand

* Corresponding author.

[1] Present address: Computer-Chemie-Centrum, Universität Erlangen-Nürnberg, Nürnberg, Nägelsbachstrasse 25, D-91052, Erlangen, Germany.

SSDI 0003-2670(94)00085-Z

classification: from a list of possible regions the analyst has to determine to which region the sample belongs. Here, usually the analyst is faced with the additional problem that a short answer like 'yes' or 'no' is not good enough.

A clear and easy-to-understand presentation of analytical results is important not only from the consumer's point of view, but it also has many advantages for the producer. The method used for the presentation of data must not only show a clear picture, but must be robust enough to allow an easy test for unknown objects to decide whether they fit into the proposed classification or not. A robust approach to the classification problem can be made by mapping the original multivariate objects into a 2-dimensional plane and observe if the clusters of object projections formed on the map can be assigned to the sought clusters.

Until now the most widely used method for the purpose of mapping multivariate data into a 2-dimensional plane is the principal component analysis (PCA) [1,2]. Recently the neural network approach for solving classification problems was tried. For example, Smits et al. [3] used multilayer feedforward networks trained with the back-propagation of errors learning strategy for classification of algae. In the present paper we will show that for classification purposes different neural network architectures and strategies can be used. However, it is argued here that among different neural network approaches this can best be achieved by a Kohonen learning strategy [4–8].

2. Data

In order to show how the problem of classifying multivariate objects can be treated by neural networks a data set that has already been extensively studied by various statistical and pattern recognition methods [1,9–12] is used. This data set consists of analytical data from 572 Italian olive oils [11,12]. For each of the 572 olive oils produced at nine different regions in Italy a chemical analysis was made to determine the percentage of eight different fatty acids. In the same order as they are given here, the percentages of the following fatty acids: palmitic, palmitoleic, stearic, oleic, linoleic, arachidic (eicosanoic), linolenic and eicosenoic fatty acid, are listed as variables in the representation of each olive oil in the study. Because the contents of different fatty acids differ by two orders of magnitude, all values belonging to a given variable (concentration of a particular fatty acid) were scaled from 0 to 100 with respect to the range between the smallest and the largest concentration.

Table 1
Regions of origin in Italy and number of samples of olive oils used in this study

Numbering	Region	Number of samples
1	North Apulia	25
2	Calabria	56
3	South Apulia	206
4	Sicily	36
5	Inner Sardinia	65
6	Coastal Sardinia	33
7	East Liguria	50
8	West Liguria	50
9	Umbria	51
Total		572

Table 1 shows the numbering of regions in Italy and how many different oils were analysed from each part. Fig. 1 shows the corresponding regions in Italy by their identification numbers.

Fig. 1. Regions of origins in Italy of the olive oils: (1) North Apulia; (2) Calabria; (3) South Apulia; (4) Sicily; (5) Inner Sardinia; (6) Coastal Sardinia; (7) East Liguria; (8) West Liguria; (9) Umbria.

3. Learning strategies

To show the advantages and drawbacks, the same set of data is treated by a number of networks each having a different architecture. The research was focused on two neural network learning strategies each with several different architectures. The neural network methods believed to solve the classification problem best were learning by back-propagation of errors [13,14,6–8] and Kohonen learning [4–8].

A major reason for the selection of these two neural network models was to explore two fundamentally different learning strategies: supervised and unsupervised learning. The back-propagation of errors learning method involves supervised learning where the desired classification is used in the correction of the weights of the network. For such cases, both the number of classes and the assignments of the objects in the training set to a particular class should be known in advance. Learning in the Kohonen network, on the other hand, is unsupervised, i.e. no prior information, either how many clusters can be distinguished in the population or to which cluster an object belongs, is employed in the adjustment of the weights of the network. The basic difference between the supervised and unsupervised methods is that in the former case the in advance possessed knowledge is forced to the decision system, while in the second case the sought information is extracted from the data automatically.

The learning procedure in any neural network strategy is achieved via correction of weights in the neural network after one object represented as a multivariate signal passes through the network. Neural network learning strategies basically differ in two things: first, in the way how the weights for correction are selected, and second, how the amount of correction is calculated. As both methods, back-propagation of error and Kohonen learning, are well described in the literature [4–8,13,14] we shall give here only the final formulas for correction of weights which were used in this study.

In the back-propagation of error strategy the correction of weights is calculated for all weights of a given layer as a two-term expression. The

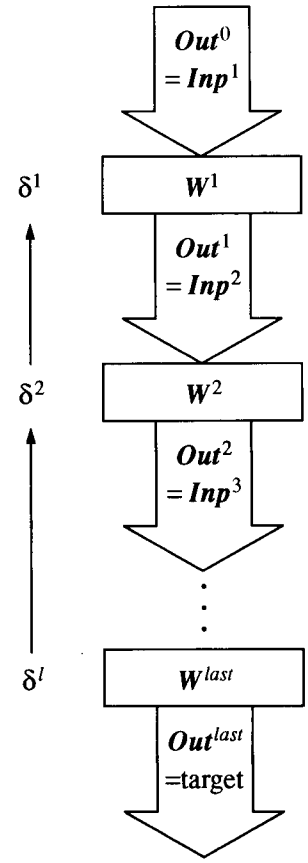

Fig. 2. Labelling of layers of neurons in a multilayer back-propagation neural network. Matrices of weights W of each layer are drawn as boxes and carry the layer assignation as a superscript. Inputs and outputs are drawn as arows: output of the upper layer is the input to the next (lower) one. Errors produced in each layer are marked as δ.

labelling of layers follows the scheme of multilayer neural network shown in Fig. 2.

The first term in the expression for weight correction led by a constant η is called the learning term, while the second one, multiplied by a constant μ, is the momentum term:

$$\Delta w_{ji}l = \eta\delta_j l \ \mathrm{out}_i^{l-1} + \mu\Delta w_{ji}^l \ \text{(previous)} \qquad (1)$$

In this equation, δ_j^l is the correction for the j-th neuron in the l-th layer, out_i^{l-1} is the input (output from the $l-1$ layer) to each i-th weight on all neurons in the l-th layer. Weights are first corrected in the last layer by substituting δ_j^{last} for δ_j^l into Eq. 1, where y_j is the expected output

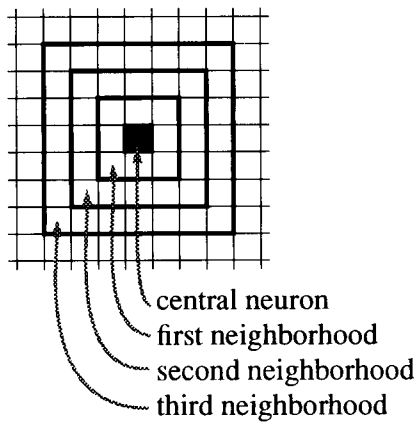

Fig. 3. The correction of weights in the Kohonen network is applied in the neighbouring neurons concentrically around the selected (central) neuron which shows the best response. Each ring of neighbours further from the center is corrected less than the closer neighbours.

value (object's target value):

$$\delta_j^{\text{last}} = \left(y_j - \text{out}_j^{\text{last}}\right) \text{out}_j^{\text{last}} \left(1 - \text{out}_j^{\text{last}}\right) \quad (2)$$

and for the hidden layers the correction δ_j^l (Eq. 1) is calculated from the corrections of one layer below δ_j^{l+1} using Eq. 3,

$$\delta_j^l = \left(\sum_{k=1}^{r} \delta_k^{l+1} w_{kj}^{l+1} \right) \text{out}_j^l \left(1 - \text{out}_j^l\right) \quad (3)$$

In the Kohonen learning the correction of weights is applied concentrically around the selected central neuron c (Fig. 3). A different central neuron c represented by the weight vector $\mathbf{W}_c$ is selected by Eq. (4) for each input object X

$$\mathbf{W}_c = \mathbf{W}_j \leftarrow \min \left\{ \sum_{i=1}^{m} \left(x_{si} - w_{ji}\right)^2 \right\} \text{ for all } \mathbf{W}_j,$$

$$j = 1, 2, \ldots, n \quad (4)$$

After the central neuron c (also called the "excited" neuron) has been selected, the correction Δw_{ji} for each i-th weight in the j-th neuron, $w_{ji}^{(\text{old})}$ in its neighbourhood is calculated by:

$$\Delta w_{ji} = \eta(t) a(c - j) \left(x_i - w_{ji}^{(\text{old})}\right) \quad (5)$$

where the range of correction $a(c - j)$ depends on the topological distance between the central neuron c and the j-th neuron. During training the range of the correction $a(.)$ monotonically shrinks from the entire network at the beginning of the learning to a single neuron (the central one) at the end of the process. At the same time the amount of correction decreases according to the function $\eta(t)$:

$$\eta(t) = (a_{\max} - a_{\min}) \frac{t_{\max} - t}{t_{\max} - 1} + a_{\min} \quad (6)$$

Here, t is the number of objects that have already been passed through the network, while $a_{\max}$ and $a_{\min}$ ($a_{\max} \geq a_{\min}$) are the maximal and minimal correction factors that should be determined at the beginning (must be between 1.0 and a very small number).

4. Preliminary exploration of possible neural networks

As a preliminary study, a simple classification using all 572 objects was tried by eight different neural networks: four back-propagation and four Kohonen neural networks. In this first attempt the emphasis was put more on answering what architecture should be chosen for the particular study rather than on obtaining the best classification. The architectures of four back-propagation and four Kohonen neural networks are shown in Figs. 4 and 5, respectively.

The use of the back-propagation networks was aimed at finding the most promising architecture (i.e. the number of layers and the number of neurons in each layer) of the network. For the Kohonen networks it was tried to estimate the proper size of the resulting map. The classification results for all preliminary networks are summarized in Table 2.

The best recall in the back-propagation network was defined as the smallest number of objects that cannot be learnt after 400 epochs. The time needed on a SUN Sparc workstation to learn the classification of all 572 objects in back-propagation networks was limited to 400 epochs because in the case of larger data sets and larger networks much longer time would be needed to obtain the same recall. One epoch of learning

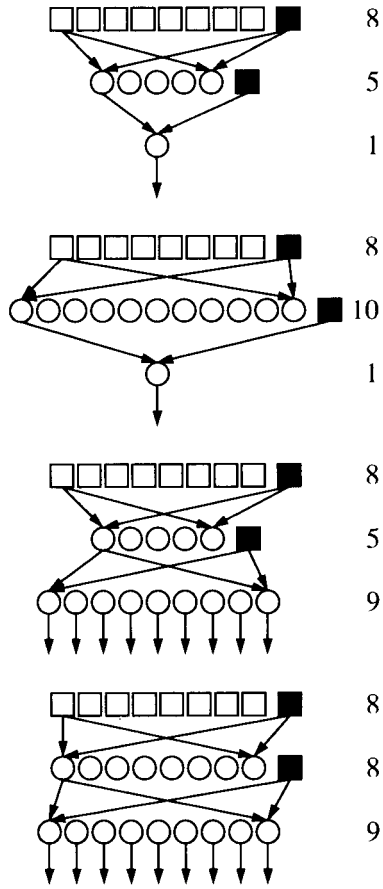

Fig. 4. The architecture of the back-propagation neural networks used in the preliminary study. The squares indicate the input neurons (8 in all 4 networks, black square is bias), while the circles represent the neurons in the hidden (5, 10, 5 and 8) and in the output (1, 1, 9 and 9) layer, respectively.

means that the network is exposed to all 572 objects.

For this particular problem, first it has to be decided whether to make a network with one or a network with nine output neurons, and second, how many neurons should be in the hidden layer? In a one output neural network the range of values from 0 to 1 is divided into nine ranges with each range corresponding to a different area. In Fig. 4, two (out of four) neural networks with nine output neurons can be seen.

By comparing networks 3 and 4 with networks 1 and 2 in Table 2, the question on the number of output neurons can be settled easily: the net-

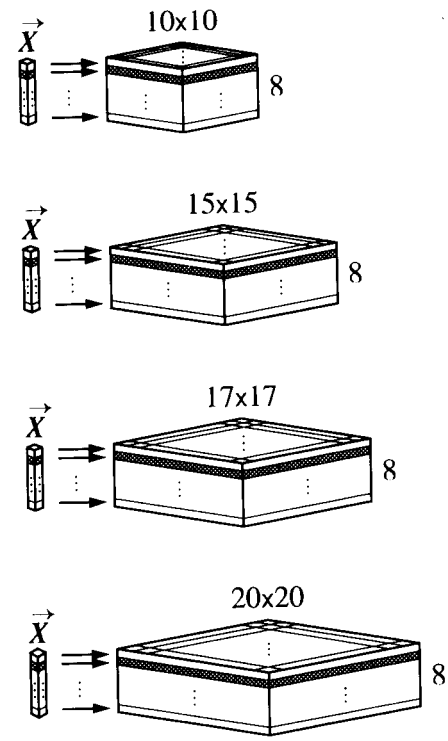

Fig. 5. The Kohonen networks used in the preliminary study. The architecture or layout of the Kohonen networks can be viewed as flat and square bricks: each vertical column in the brick represents one neuron, the number of weights in each neuron is equal to the number of inputs, i.e. to the number of variables representing each object. All neurons in the network obtain the 8-dimensional input simultaneously.

Table 2
The characteristic data for neural networks used in the preliminary step

Network	Type	Dimension	Weights	Time (min)	Errors on 572 objects
1	BPN	8×5×1	51	15.0	138
2	BPN	8×10×1	101	20.0	71
3	BPN	8×5×9	108	45.0	23
4	BPN	8×8×9	153	75.0	15
5	Kohonen	10×10×8	800	1.0	24
6	Kohonen	15×15×8	1800	2.0	14
7	Kohonen	17×17×8	2512	2.5	14
8	Kohonen	20×20×8	3200	3.0	12

For BPN (back-propagation network) each error represents a wrong recall of the object that was used in the training set, while for the Kohonen network the error means a conflict, i.e. two objects belonging to different classes excite the same neuron.

works with nine outputs perform far better than those with one. Although using many different initial random weight settings, the networks 1 and 2 always begin to oscillate in recall answers. This means that not only a large proportion (up to 25%) of training objects was not classified correctly in each epoch, but also these objects differ from epoch to epoch, i.e. the networks begin to "oscillate" in recognition of certain groups of objects early in the training process. In Table 2 the best performances are given.

In general, there is a deeper reason for rejecting the one-output neural network for classification of objects into more than two classes. Namely, a single-output answer is always confined with the interval (0,1), which means that for the classification of objects into one of n classes, this interval must be divided into n sequential intervals. Because the sequence of intervals inherently implies the similarity of the intervals, i.e. the classes predicted by the two consecutive intervals are more similar to each other than two classes predicted by the intervals from two different ends of the (0,1) range, such an assumption cannot be justified for most of the actual applications.

Although the networks with nine output neurons give better recalls than those with one output, the problem of oscillation shows up exactly in the same way as in the networks with one output. By increasing the number of neurons in the hidden layer we were able to diminish this problem, but not to solve it entirely. By increasing the number of weights only, the complete classification was not possible.

If regarded as "boxes", all Kohonen neural networks (Fig. 5) differ only by the size of the bases. They all have the same height which means that they have the same number of input nodes (eight). The size of the base, i.e. the number of neurons, defines the area of each map. The two criteria for the selection of the best Kohonen network architecture are the number of conflicts and the number of empty spaces produced in the map. The conflict occurs when two objects from different classes trigger the same neuron, while an empty space is a neuron that is not triggered by any of the 572 oils. Too many conflicts indicate poor recognition ability, while too many empty spaces indicate that either the network is too large for a given set, or that the network of a proper size does not spread the objects well enough into the projection plane.

The results shown in Table 2 show that the training time of the Kohonen networks is more than one order of magnitude smaller than that needed for training the back-propagation networks. While the back-propagation network requires 400 epochs, the Kohonen networks need about 40 epochs to yield approximately the same results. In spite of the fact that the product between the number of weights (column 4 in Table 2) and the number of epochs for the Kohonen and for the back-propagation networks is roughly of the same size, the learning process in the Kohonen networks is still one order of magnitude faster (cf. column 5 in Table 2) than those of the back-propagation networks.

5. Learning to make predictions

The preliminary work described above was done with the intention to inspect the behaviour of different networks when trained with the same set of data rather than to inspect the results itself. Therefore, all data (572 multicomponent analyses) were involved in the training. In this part, however, we will concentrate on finding out how good neural networks can be for predictions. Learning will be performed by one group of data to "teach" the network to be able to make predictions about class membership for objects contained in a second (test) group.

To begin with, the entire group of analytical data on 572 olive oils was divided into two sets: the training and the test set. While splitting the entire group into two sets we are trying to satisfy two conditions. First, both sets should be approximately of the same size with possibly the test group being slightly larger than the training set. Secondly, the learning set should be as homogeneous as possible. This means that the training set must contain approximately the same number of objects from each class. A good choice would be a set of 270 objects for learning and a set of 302 for testing. The number of 270 objects in the

Table 3
Splitting the data into the training and test group

No.	Region	Label	Training	Test
1	North Apulia	NA	15	10
2	Calabria	CA	35	21
3	South Apulia	SA	40	166
4	Sicily	SI	20	16
5	Inner Sardinia	IS	30	35
6	Coastal Sardinia	CS	20	13
7	East Liguria	EL	30	20
8	West Liguria	WL	30	20
9	Umbria	UM	30	21
Total			250	322

training set would ask for 30 objects of each of 9 classes. Due to the heavily unbalanced number of objects within various classes the desired number of 30 objects cannot be achieved for each group. Therefore, with some trade-off between smaller and larger groups the distribution of objects as shown in Table 3 was selected. The objects within each group were selected at random with no prior inspection of their behaviour or knowledge on how they will group together.

The training set was first investigated by the four back-propagation networks described above (Fig. 4). According to the previous explanation the first two networks having only one output neuron will yield worse predictions than those with nine output neurons. In spite of this, they were included in the experiment for the purpose of comparison. They demonstrate, in fact, how deficient a bad design of a neural network can be (Table 4).

All learning procedures were carried out by applying the set of equations given above (Eqs. 1–3) and using the learning rate η equal to 0.2 and momentum μ equal to 0.4, for all networks. The values of 0.2 and 0.4 for the learning rate η and for the momentum μ, respectively, were chosen because they yield the fastest learning convergence to the minimal number of errors.

Table 4
Recall and prediction errors made by different back-propagation neural networks

Network	Dimension	Errors	
		Recall from 250 (training set)	Predictions from 322 (test set)
1	8×5×1	104 (42)	121 (38)
2	8×10×1	89 (36)	117 (36)
3	8×5×9	5 (2.2)	25 or 27 (8)
4	8×8×9	1 (0.4)	31 (10)

Percentages of errors are given in parentheses.

The networks with only one output neuron gave almost 40% wrong predictions and thus have clearly an inadequate design for a nine-class identification. When considering the networks with nine outputs it is surprising that the larger network with eight neurons in the hidden layer is less successful in learning compared to the smaller one having only five nodes. Although the difference in the number of errors in predictions is not very large, this example demonstrates quite well that larger networks do not necessarily provide better performance.

Thus, the best performer is the network with an $8 \times 5 \times 9$ architecture giving only 25 (7.8%) wrong classifications for the 322 objects in the test set. The number 27 shown in Table 4 parallel to the number 25 means that two more objects will be classified wrongly when a stricter criterion is selected for deciding class membership, as explained now in detail.

For a neural network with nine output neurons nine-element target vectors **Y** have to be provided. In the ideal case, only one output neuron should have the output signals equal to 1, while all other output neurons should have an output of zero. The non-zero signal should be associated with the class of the object that has activated this neuron. The 9-dimensional targets are considered in the form:

Class	NA	CA	SA	SI	IS	CS	EL	WL	UM
Y(1) =	(1	0	0	0	0	0	0	0	0)
Y(2) =	(0	1	0	0	0	0	0	0	0)
Y(3) =	(0	0	1	0	0	0	0	0	0)
Y(4) =	(0	0	0	1	0	0	0	0	0)
Y(5) =	(0	0	0	0	1	0	0	0	0)
Y(6) =	(0	0	0	0	0	1	0	0	0)
Y(7) =	(0	0	0	0	0	0	1	0	0)
Y(8) =	(0	0	0	0	0	0	0	1	0)
Y(9) =	(0	0	0	0	0	0	0	0	1)

The actual output from the networks is seldom like this. More often the output values of neurons that should be zero are only close to it and the values of the neurons signalling the correct class have values ranging from 1.0 to 0.5.

All of the 25 wrong predictions have produced the largest signal on the wrong neuron. Contrary to this 25 cases, the two additional errors had largest output on the neuron signalling the correct class. However, in one case this largest signal amounted only to 0.45, with all other signals being much smaller, while in the second case the largest output on the correct output was 0.9, but there was another signal of 0.55 (thus exceeding 0.5 threshold) on another output neuron.

Strictly speaking, the total error in both controversial answers was more than 0.5, hence both could be regarded as wrong. On the other hand, acquiring the criterion of the largest signal as a deciding factor, both can be regarded as correct answers.

The second learning experiment was set up by Kohonen networks. The learning was performed by the set of Eqs. 4–6. The correction function $a(.)$ has a simple triangular form [4,8] with parameters a_{max} and a_{min} being 0.5 and 0.01, respectively.

Because a Kohonen network is usually not exploited for making predictions, we have to discuss in more detail how predictions can be made with a Kohonen network.

The result of the Kohonen network is a 2-dimensional map of neurons each of which carries a "tag" or "label" of the object that has excited it at the final recall test. If more than one object excites one neuron it is hoped that all of them belong to the same class. Even more so, it is expected that the neurons excited by objects of the same class will form clusters or small regions on such a map. If the test object falls into such a cluster it can be classified as belonging to the group that forms this cluster. The region where the objects of a certain class excite the neurons can form tight borders with regions formed by other classes. Or, there can be an area with neurons not excited by any object from the training set between two or more regions. Such a part on the map is called an empty space. The empty

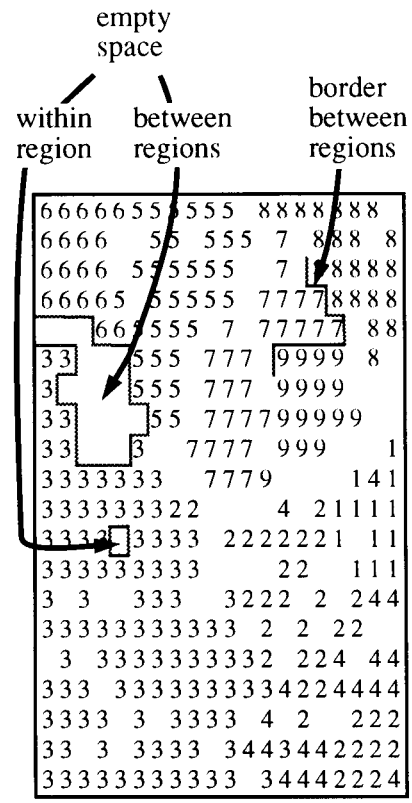

Fig. 6. 20×20 neuron Kohonen map. Numbers represent labels of objects (olive oils) that excite the neuron in the particular position. Empty spaces, i.e. non-labelled neurons that are not excited by any object, can appear between and within the classes representing different regions.

spaces do not appear only between classes, they can be located as well within the region of a class (Fig. 6). Hits of query objects into an empty region of the Kohonen network must obtain an individual treatment in the prediction procedure.

Along tight borders of two or more regions it can easily happen that the same neuron is excited by two objects belonging to different classes. Such cases are called conflicts and the neurons are called conflicting neurons. Conflicts can occur in the recall process, but much more often they happen during predictions of objects not involved in the training process. The smaller the number of conflicts is, the better is the prediction ability of the Kohonen network.

If the test object excites a neuron in a region on the map that belongs to a class different from

that of the test object this is clearly a conflict situation. On the other hand, if the excited neuron is located within an empty region, the answer whether the particular situation is a conflict or not can be decided to some extent by considering the class membership of the neighbouring neurons.

We could stay on the safe side and say that neurons in empty spaces cannot give predictions at all because these regions are not labelled. However, the situation is not that clear. In order to settle this question, it is useful to first inspect the prediction results made by different Kohonen networks. Table 5 shows the prediction abilities of eight Kohonen networks.

All objects were mapped by exactly the same Kohonen learning procedure with the same training set of 250 objects, the only difference being the size of the network. After learning was completed, i.e. when each neuron in the training set excited exactly the same neuron as in the previous epoch, the excited neurons were labelled as belonging to the class of the exciting object.

The learning produced only two conflicting neurons with the 10×10 and 17×17 networks and one conflicting neuron with the 15×15 network. The 20×20 network did not have any conflict at all. Thus, by selecting a proper design of the network of neurons, it can be said that the Kohonen learning can achieve good recall (recognition ability).

The prediction ability of each network was tested with the remaining set of 322 oils and it was found that an increase in the size of the Kohonen maps improves the prediction ability from 17 (10×10 map) to only 8 (20×20 map) mistakes (Table 5, rows 1–4). However, the number of hits into empty spaces increases at the same time by a factor of four: from 26 to 108. The factor of four is in excellent agreement with the increase in the size of the Kohonen maps from 100 (i.e. 10×10 map) to 400 neurons (i.e. 20×20 map).

With maps larger than 20×20 neurons, yet with the training and the test sets remaining the same, the number of hits into empty spaces still increases, but is always limited by the number of objects in the test set. Hence, the ratio between the number of hits into empty spaces and the size of the map is not constant anymore.

The fact that for a fixed number of objects in the training and test sets the relation between the hits into the empty spaces and the size of the network (map) remains constant over a given range of map sizes yields a hint how to select an appropriate size of the Kohonen network.

Supposing that the objects from the test sets have approximately the same distribution in the measurement space as the objects from the training set, then the proportionality between the increase in size of the network and the number of hits into empty spaces offers the following sugges-

Table 5
Number of empty spaces produced during the learning with 250 objects

No.	Dimension	Map size	Learning		Predictions		
			Empty spaces	Conflicts	Correct	Hits into empty space	Wrong predictions
1	$20 \times 20 \times 8$	400	193	0	216	108	8
2	$17 \times 17 \times 8$	289	108	2	215	96	11
3	$15 \times 15 \times 8$	225	98	1	229	83	10
4	$10 \times 10 \times 8$	100	19	2	280	26	17
5	$7 \times 7 \times 8$	49	5	9	290	3	29
6	$5 \times 5 \times 8$	25	1	27	285	0	37
7	$4 \times 4 \times 8$	16	2	33	247	0	75
8	$3 \times 3 \times 8$	9	0	57	267	0	55

Prediction ability for 322 oils as obtained from different Kohonen networks. The sum of correct and wrong predictions together with the hits into the empty space is 322.

tion: there is a significant correlation between the topology of clusters of objects represented in the multi-dimensional space and the topology of the 2-dimensional map of labelled neurons.

From the above observation, it can be concluded that an appropriate size of a Kohonen network should be within the range where it is linearly proportional to the number of hits into the empty space. In our case, this is somewhere between the 10×10 and 20×20 map.

Between the objects from different classes a certain amount of repulsive interaction always exists. Therefore, almost all maps, with the exception of the smallest ones, contain empty spaces. Empty spaces are not wasted neurons. On the contrary, they serve for "accommodating" the objects (signals) considerably different from those used in the training. Of course, a map containing too many empty spaces would have rather poor prediction ability due to the fact that many test objects would rather excite neurons on empty spaces than those that are labelled.

To investigate the number of empty spaces, four small Kohonen networks having $49 = 7 \times 7$, $25 = 5 \times 5$, $16 = 4 \times 4$, and $9 = 3 \times 3$ neurons were generated. It is obvious that the smaller the map, the less empty spaces it has, but on the other hand, small maps produce large number of conflicts in the training set and an even larger number of wrong predictions in the test set. In designing the Kohonen network a compromise between lowering the number of hits into empty spaces and the number of conflicts has to be found. As can be seen from Table 5 (rows 5–8), only the 3×3 map does not contain empty spaces; however, the number of conflicting recalls is obviously the highest: 57. The 4×4 map has two, the 5×5 map one, and the 7×7 network five empty spaces, while the number of conflicts is decreasing as 33, 27, and 9, respectively.

Because a hit into an empty space can in some circumstances yield valuable information, we shall now explore such cases in more detail. In order to make a prediction about the class membership of an object hitting into the empty space, the K-nearest neighbour technique is applied. The KNN [1] method determines the class by counting a certain neighbourhood of neurons, and the class membership of the majority of these neighbours determines the class of the "unknown" or tested object.

A detailed inspection of the eight closest neighbours was made for all 83 empty-space hits when the objects from the testing set passed the 15×15 network trained with the 20-epoch training procedure (Table 5, line 3). The class membership of the object that hits the empty space was determined according to the class to which the majority of the eight closest neighbours belong. The numbers of correct, undecided and

Table 6
Number of hits into empty spaces in predictions on the 322 object test set for different Kohonen networks

Class	No. of objects	Network			
		10×10	15×15	17×17	20×20
1	10	0	1 (– 1 –)	3	5
2	21	3	6 (4 1 1)	7	9
3	166	20	48 (40 7 1)	59	52
4	16	2	5 (2 – 3)	7	8
5	35	0	7 (6 – 1)	3	11
6	13	1	3 (3 – –)	0	4
7	20	0	5 (5 – –)	5	10
8	20	0	6 (5 1 –)	10	6
9	21	0	2 (1 1 –)	3	2
Total	322	26	83 (66 11 6)	96	108

Numbers in parentheses are decisions for hits into empty spaces made on counting the first neighbours: correct, undecided and wrong decisions.

wrong classification for each class are given in Table 6 in parentheses.

It was found that on the basis of the "majority vote" 66 of the hits (out of 83) were classified correctly. Eleven were undecided which means that an equal number of first eight neighbours belong to two different classes. Only six hits (out of 83) were classified wrongly. Altogether, this would mean that by considering the KNN decision for empty space hits in addition to the regular predictions made by hits on labelled neurons, the 15 × 15 network produces 295 (229 + 66) correct answers, 11 undecided, and 16 (10 + 6) wrong classifications. The numbers of correct (229) and wrong (10) answers, predicted by the 15 × 15 map, are taken from the third row of Table 5.

Fig. 7 shows the case in which decision could not be made on the basis of the majority vote. The empty space, where the test object has hit the map, has two neighbours from class 2, two neighbours from class 3, and four additional neighbouring empty spaces.

Besides the inspection of the empty space hits, wrong predictions occurring when the test objects hit the neurons carrying label different from that of the test object were also examined. During the test of all 322 objects, there are only 10 wrong classifications (predictions) made by the 15 × 15 network (cf. Table 5). Fig. 8 shows all neurons (in circles) that were excited by objects of the wrong class (indicated by the numbers given outside the map).

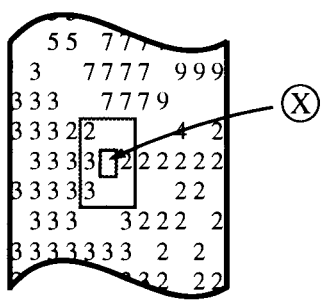

Fig. 7. Out of eight neighbours of the unlabelled neuron in the empty space two are members of class 2 and two members of class 4; the rest are empty spaces. The prediction to which class the object x belongs cannot be made.

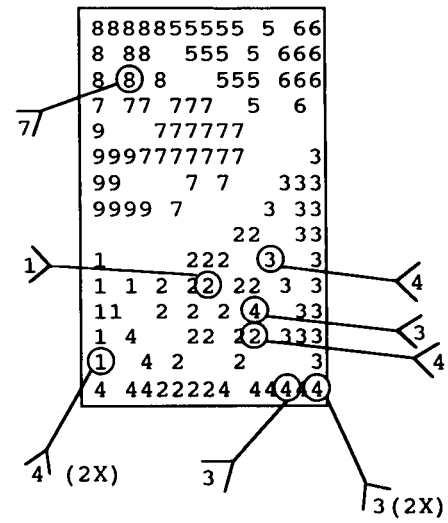

Fig. 8. Final (15 × 15) map obtained by 250 training objects for making predictions for 322 test objects. The origins of all 10 oils for which the prediction is wrong are explicitly marked outside the map. The labels of neurons which were excited by these misclassified oils are shown in open circles.

In the ten wrongly predicted objects shown in Fig. 8 it can be seen that in one case the East Ligurian oil (class No. 7) has been assigned as a West Liguria one (class No. 8), next that three out of four Sicilian oil mistakes (class No. 4) were predicted on the borders of Sicilian oils (twice with North Apulia, class No. 1, and once with Calabria, class No. 2), one Sicilian oil mistake was in the region of South Apulia oils, class No. 3, all four South Apulian oil mistakes, class No. 3 were made within the Sicilian oils, class No. 4, and finally that only one case, viz. the North Apulian oil, class No. 1, triggered a neuron far away from its own group, in the cluster of Calabrian oils.

It is interesting to note that even from the wrong predictions some valuable information can be obtained. All the errors are caused by objects belonging to the neighbouring classes in the sense of the actual geographical regions of the oils samples. For example: the north–south prediction of oil origins was 100% correct for all 322 test samples.

In order to see the influence of the number of training epochs on the prediction ability the 15 × 15 Kohonen network was trained with 10, 20, 50,

Table 7
Average errors per weight for the training (TR) and for the test (TE) set depending on the training period (in epochs) obtained in the 15×15 Kohonen network

Epochs	TR	TE	Training	
			Conflicts	Empty spaces
10	4.9	7.6	4	109
20	4.3	7.4	1	98
50	3.6	7.1	0	88
100	3.1	6.9	1	81
200	2.9	6.9	1	84
500	2.6	6.8	2	79
1000	2.5	6.8	2	80

100, 200, 500 and 1000 epochs (250 objects per epoch). In Table 7 the average errors per weight (i.e. per scaled fatty acid concentration), the numbers of conflicts, and the empty spaces produced during learning are given. Each error given in Table 7 is calculated as follows:

$$\mathrm{Err} = \left[1/(8N) \sum_{s=1}^{N} \sum_{i=1}^{8} (x_{si} - w_{ci})^2\right]^{1/2} \qquad (7)$$

Index s runs over the number of objects for the training (TR, $N = 250$) and for the test (TE, $N = 322$) set, respectively. Index c identifies the excited (central) neuron, while i identifies the weight on the neuron and the corresponding scaled variable of the input object.

By increasing the number of epochs in the training procedure lower recall error (TR) can be achieved, however, the error for test objects (TE, i.e. predictions) remains constant. Even more important, the number of conflicts produced during the training reaches its minimum in a relatively small number of training epochs (at 50 epochs). The same assumption is confirmed if a more thorough analysis of the predictions of networks generated by different number of training epochs is made (Table 8).

In Table 8, first the numbers of correct and wrong predictions followed by the number of hits into empty spaces are given. Then, for each case all hits into the empty space are analysed according to the KNN strategy (see Table 6 and Fig. 7). The classifications obtained for these hits are either correct, undecided, or wrong. The corresponding figures are given in columns 7, 8, and 9, respectively. Column 10 gives the total number of wrong classified objects (out of 322) and column 11 the percentage of wrongly predicted answers.

Although the averaged errors obtained with the training set decreases with the increasing number of epochs applied for learning, the smallest number of wrong predictions (16) is obtained already in the learning procedure of 20 epochs.

6. Use of weight maps within a Kohonen network

Besides obtaining the model for yielding the predictions about the origin of olive oils, the

Table 8
Prediction ability of the 15 × 15 Kohonen neural network depending on the number of training epochs (4 + 5 + 6 = 322)

Epochs	Trained 15 × 15 neural network		Direct predictions		Predictions from hits into empty spaces				Total	
	Conflicts	Empty spaces	Correct	Wrong	All hits into empty space	Correct	Undecided	Wrong	Total wrong	Pct. wrong (%)
(1)	(2)	(3)	(4)	(5)	(6) (6 = 7 + 8 + 9)	(7)	(8)	(9)	(10) (10 = 5 + 9)	(11)
10	4	109	231	16	75	66	5	4	20	6.2
20	1	98	229	10	83	66	11	6	16	5.0
50	0	88	224	9	89	73	9	7	16	5.0
100	1	81	213	9	100	77	13	10	19	5.9
200	1	84	229	4	89	73	4	12	16	5.0
500	2	79	224	10	82	71	7	10	20	6.2
1000	2	80	232	11	79	60	11	8	19	5.9

Kohonen networks can offer even more valuable information on the data representation with which they were trained. One among the common objections to the use of neural networks is the opinion that the parameters which are learned in the neural networks (i.e. the weights) do not bear any plausible relation to the problem involved. Therefore, the trained neural network is usually regarded as a complete black-box. In this paragraph we show how the levels of weights in the stabilised or trained Kohonen networks can be used to obtain maps of individual variables. These maps can be used for acquiring qualitative rules for classifying the objects into classes.

The inputs to the Kohonen networks are treated as eight-dimensional column vectors shown at the left-hand side of each network in Fig. 5. The same input vector (complete analysis of an olive oil) goes to all neurons in the network simultaneously. However, each component of the input vector, i.e. the percentage of a given fatty acid, is always put into the same level of weights. For example, the concentrations of the palmitoleic acid (second in order) are always put into the second level of weights (shown darker in Fig. 5). This means that after learning is completed each level of weights can be regarded as a map of concentration values of that particular fatty acid.

By inspecting the levels of weights, i.e. fatty acid concentration maps, it is possible to find in each map the contour (or threshold concentration) that most clearly divides or separates some of the classes of different olive oils. Note that we did not specify which classes this contour line should separate: what we are seeking, is just any clear division between the classes. To explain this procedure on the basis of Kohonen maps of weights, the maps of all eight fatty acids, i.e. eight weight levels in the 15×15 Kohonen network obtained by 20-epoch learning, are given in Fig. 9. For the sake of clarity, on each map only one iso-value contour line is drawn: the one which most clearly divides the classes of olive oils into two groups of classes. For example: in the first map of weights the 50% contour (50% of the scaled concentration of the palmitic fatty acid) divides the classes No. 2, No. 3 and No. 4 from the rest (classes No. 1 and Nos. 5–9) most clearly.

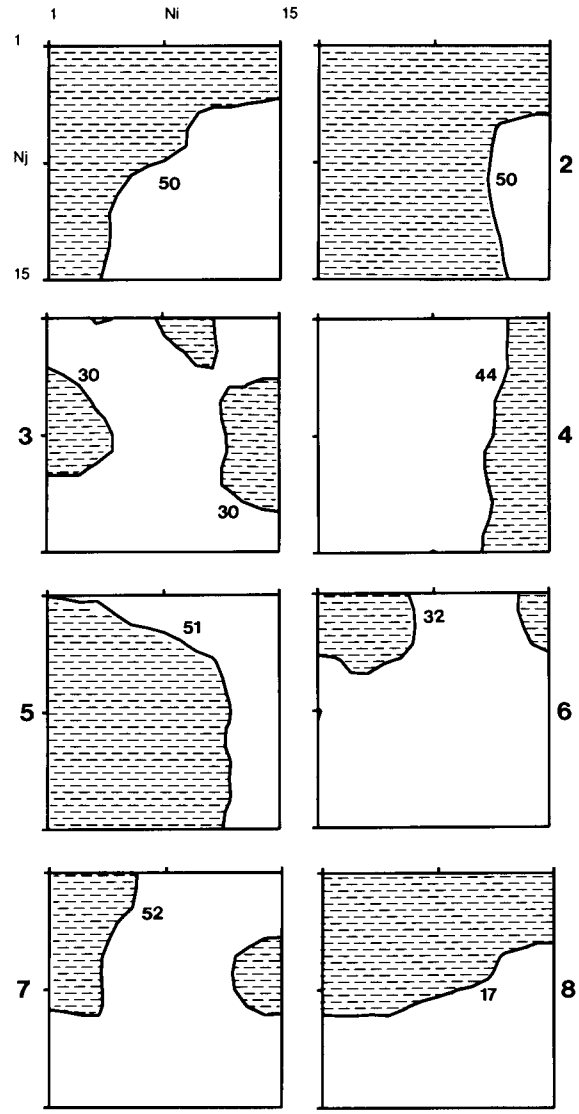

Fig. 9. Eight 15×15 weight maps obtained by the cross-sections of the Kohonen neural network at each weight level. The weights in each map reflect the distribution of particular scaled fatty acid concentration among all 250 objects from the training set. In each weight map only the iso-value contour that divides two arbitrary groups of classes in the most evident way is drawn. Areas with lower concentrations than the given iso-value line are shaded. The final map (map of labels) of this network is shown in Fig. 10.

Similarly, in the last map the 17% contour line divides clearly southern oils (classes No. 1, No. 2, No. 3 and No. 4) from the northern oils (classes No. 5, No. 6, No. 7, No. 8 and No. 9).

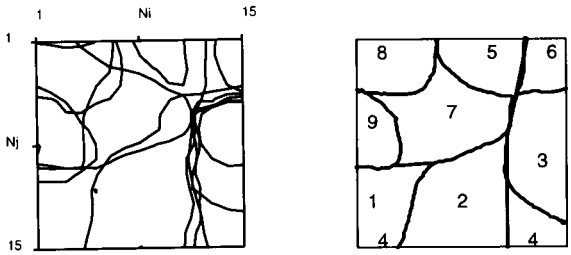

Fig. 10. Overlap of all eight weight maps (left) from Fig. 9 roughly shows the nine area belonging to nine oil classes (Fig. 8). In order to demonstrate the boundaries between the classes more clearly, the same overlap with smoothed contours is shown on the right.

Fig. 10 shows the result of overlapping all eight maps. By slightly smoothing these most significant contours, but still in qualitative accordance with the actual values, a very good separation between all nine classes is obtained (Fig. 10, right). As a matter of fact, in Fig. 10 only one separation is not outlined by the one-contour overlap. This is the separation between the class No. 1 (North Apulian oils) and one part of the class No. 4 (Sicilian oils). The group of Sicilian oils is intersected by the group of Calabrian oils (group No. 2). It is interesting to note that most of the classification errors are produced by the oils from these two regions. This is true not only in the present neural network application, but as well in the other chemometric methods.

By inspection of weight maps that overlap certain labelled cluster (comparing Fig. 8 with Fig. 9 or 10) the rules for classification of this cluster can be derived. For example: cluster No. 8, West Liguria oils, lies in the upper left corner of the 15×15 map (Fig. 8). The inspection of the weight maps, i.e. the concentrations of the fatty acids (Fig. 9), reveals that characteristic concentrations for this particular group forms the following rule: if the concentration of:

palmitic acid	$< 50\%$
palmitoleic acid	$< 50\%$
stearic acid	$> 30\%$,
oleic acid	$> 44\%$
linoleic acid has an arbitrary value	
arachidic acid	$< 32\%$
linolenic acid	$< 52\%$
eicosenoic acid	$< 17\%$

then the origin of the oil is West Liguria.

It has to be emphasized that such rules were obtained for all groups formed on the top, i.e. the map of labels. Hence, it can be safely said that the Kohonen network has the ability to produce complex decision rules.

As was said before, other statistical studies on the classification of these oils, including principal

Table 9
Prediction ability (number of wrong prediction results) of standard classification methods with comparison to back-propagation and Kohonen neural networks for 9 classes of Italian olive oils

Method (Ref.)	Class									
	1	2	3	4	5	6	7	8	9	All (%)
TIMM [18]	–	1	–	2	–	–	0	2	–	5 (7.8)
EX-TRAN [18]	–	3	–	6	–	–	2	2	–	13 (20.3)
1NN [a] [18]	–	1	–	2	–	–	1	4	–	8 (12.5)
5NN [a] [18]	–	1	–	1	–	–	1	4	–	7 (10.9)
LDA [18]	–	0	–	1	–	–	3	2	–	6 (9.4)
1NN [16]	4	3	4	2	0	1	1	1	0	16 (5.9)
3NN [16]	3	3	3	3	0	1	1	0	0	14 (5.2)
3-DM [16]	5	2	4	3	0	1	2	2	0	20 (7.3)
Back-propagation [b]	2	2	8	3	2	3	5	0	0	25 (7.8)
Kohonen [c]	1	1	5	7	1	0	1	0	0	16 (5.0)

[18] on 64 test objects for 4 classes only (class No 2, 4, 7 and 8).
[16] on 272 test objects.
[a] Autoscaled data.
[b] $8 \times 5 \times 9$ error back-propagation network architecture, 322 test objects.
[c] 15×15 Kohonen network architecture, 322 test objects.
Dash indicates absence of the analysis for a particular class.

component analysis (PCA [15]), nearest neighbour technique (KNN [16]), SIMCA [17], or three distance clustering (3-DC [16]), gave a comparable percentage (5.2–20.3%) misclassifications or errors. The numbers of errors in Table 2 (last column) are well in the range within these results obtained from statistical or pattern recognition methods. In Table 9 the results of standard classification methods [16–18] are shown in comparison with the results of the present study.

Most of the objects (oils) that cause the errors are either wrongly assigned or subjects of too large an experimental error. In any case, in a pool of more than 4500 (572×8) measurements it is hard to make less than 2% errors. Hence, even an ideal computational method could not yield significantly better predictions on this experimental data set. Therefore, it is not the quality of the results itself, but the presentation of them and the possibility for obtaining some additional information that should be possible with a new method of neural networks.

7. Conclusions

The question that should be answered by the present paper is: what advantage can offer a neural network approach over standard statistical classification techniques?

From the presentation point of view, clustering of objects on a two-dimensional map is much more informative compared to a clustering made by standard clustering techniques or a blackbox device which separates the objects by simple labelling. The two-dimensional map, in our case the map of nine regions in Italy, shows a clear separation between the southern and northern regions which cannot be easily perceived from the measured results or by a black-box prediction of classes. The prediction ability of Kohonen neural network is 95% for all the classes, if the network is trained with 250 objects and tested with 322 objects (see Tables 8 and Table 9). However, for certain classes the prediction ability is even 100% (0 errors for the classes 6, 8, 9, cf. Fig. 8 and Table 6).

Besides 95% prediction ability, the clustering obtained by Kohonen neural network can be regarded as remarkably good considering the simple learning scheme used to produce it. Not only is there a clear gap between the southern and the northern oils, there is even a clear topological separation between both types of Sardinian oils and of those two types from the rest. We can safely say that a clear correlation between the topology of labelled regions in the Kohonen map and the actual position of the oil producing areas in the geographic sense exists.

The example presented in this paper was intentionally selected to show advantages of the Kohonen network. We do not claim that the Kohonen network will always do the classification and display of clusters better than the standard statistical methods. However, we would like to imply that besides being very simple and understandable, this method is as good as any other statistical method (if not better), that the main advantage is in producing valuable additional information and offering a nice presentation tool. It should also be underlined that with this dataset (really not a difficult one) both neural networks and traditional classification methods produce very good results, hence the neural network can be selected only because of the simplicity. On the other hand, in cases where standard classification methods fail, neural networks may be successful because of their flexibility.

Acknowledgement

The financial assistance of the Ministry of Science and Technology of Slovenia and the Bundesministerium fuer Forschung und Technologie, Germany, is gratefully acknowledged.

References

[1] D.L. Massart, B.G.M. Vandeginste, S.N. Deming, Y. Michotte and L. Kaufmann, Chemometrics: a Textbook, Elsevier, Amsterdam, 1988.

[2] K. Varmuza and H. Lohninger, in J. Zupan (Ed.), Principal Component Analysis of Chemical Data, in PCs for Chemists, Elsevier, Amsterdam, 1990, pp. 43–64.

[3] J.R.M. Smits, L.W. Breedveld, M.W.J. Derksen, G. Kateman, H.W. Balfoort, J. Snoek and J.W. Hofstraat, Anal. Chim. Acta, 258 (1992) 11.
[4] T. Kohonen, Self-Organization and Associative Memory, Springer Verlag, Berlin, 3rd edn., 1989,
[5] T. Kohonen, Neural Networks, 1 (1988), 3.
[6] J. Zupan and J. Gasteiger, Anal. Chim. Acta, 248 (1991) 1.
[7] J. Gasteiger and J. Zupan, Angew. Chem., 105 (1993) 510; Angew. Chem. Intl. Ed. Engl. 32 (1993) 503.
[8] J. Zupan and J. Gasteiger, Neural Networks for Chemists: An Introduction, VCH, Weinheim, 1993.
[9] K. Varmuza, Pattern Recognition in Chemistry, Springer Verlag, Berlin, 1980.
[10] J. Zupan, Algorithms for Chemists, Wiley, Chichester, 1989.
[11] M. Forina and C. Armanino, Ann. Chim. (Rome), 72 (1982) 127.
[12] M. Forina and E. Tiscornia, Ann. Chim. (Rome), 72 (1982) 144.
[13] D.E. Rumelhart, G.E. Hinton and R.J. Williams, in D.E. Rumelhart and J.L. MacClelland (Eds.), Distributed Parallel Processing: Explorations in the Microstructures of Cognition, Vol. 1, MIT Press, Cambridge, MA, 1986, pp. 318–362.
[14] R.P. Lipmann, An Introduction to Computing with Neural Nets, IEEE ASSP Mag., April (1987) 155.
[15] M.P. Derde and D.L. Massart, Fresenius' Z. Anal. Chem., 313 (1982) 484.
[16] J. Zupan and D.L. Massart, Anal. Chem., 61 (1989) 2098.
[17] M.P. Derde and D.L. Massart, Anal. Chim. Acta, 191 (1986) 1.
[18] M.P. Derde, L. Buydens, C. Guns, D.L. Massart and P.K. Hopke, Anal. Chem., 59 (1987) 1868.

ELSEVIER

Analytica Chimica Acta 292 (1994) 235–241

ANALYTICA CHIMICA ACTA

Effect of climate on the chemical composition of virgin olive oil

R. Aparicio *[,a], L. Ferreiro [b], V. Alonso [a]

[a] *Instituto de la Grasa y sus Derivados (CSIC), Avda. Padre García Tejero 4, 41012 Seville, Spain*
[b] *Consejería de Salud, Junta de Andalucía, Luis Montoto s/n, 41018 Seville, Spain*

(Received 3rd November 1993; revised manuscript received 24th January 1994)

Abstract

The effect of climate on the chemical composition of virgin olive oil has received scant attention. In this work, the relationship between chemical composition and altitude, the latter being an indirect parameter related to climate and soil, was studied. Two altitudes, valley (< 400 m) and mountains (> 700 m) were studied; 126 samples of virgin olive oil were characterized by 53 compounds and it was found that sterols and some triterpenic alcohols and hydrocarbons changed systematically with altitude. Two linear discriminant equations, with correct classifications greater than 90%, were obtained and verified with samples of another crop. Similar results were obtained.

Key words: Gas chromatography; Altitude; Chemometrics; Climate; Olive oil

1. Introduction

Relationships between climate, soil aspects and lipids have been thoroughly studied. Thus, it is well known that climate has a great influence on ripeness and hence on the chemical composition of vegetables oils. Lotti et al. [1] demonstrated that punicic acid of *Mormodica balsamina* seed increased as the temperature decreased whilst they only detected irregular variations in the linoleic acid content. Subsequently, the same group [2] studied how the chemical composition of peanut oil was influenced by the latitude. They verified that the percentage of fatty acids followed Ivanov's rule: "the amount of linoleic acid rises when the temperature decreases, contrary to oleic acid". Further, they also found that the content of sterols showed great fluctuations. The concentration of β-sistosterol increased and those of campesterol and stigmasterol decreased as the climate became colder. Alberdi and Corcuera [3] studying the membrane effect, concluding that low temperatures stimulate the accumulation of linoleic acid, whilst from a biochemical point of view Sanchez et al. [4] analysed the effects of light and temperature on the formation of storage triacylglycerols and hence on fatty acid concentrations [5] in virgin olive oil.

Armanino et al. [6] reported the influence of altitude on the chemical composition of virgin olive oil, applying only a graphical representation to their results. They inferred that olives cultivated near the Mediterranean sea produce different olive oils from those harvested in the Alps. Later, statistical analyses applied to virgin olive

* Corresponding author.

SSDI 0003-2670(94)00065-T

oil samples from the province of Jaén (Spain) [5,7] resulted in the same conclusions. Recently, Ferreiro and Aparicio [8] analysed the combined influence of climate and olive varieties on the chemical composition of virgin olive oil by some multivariate procedures.

This paper, following on from previous work [8], analyses which compounds, from a set of 53, have a greater influence in characterizing virgin olive oil on the basis of the altitude of its cultivar. Thus not only a few series of compounds were studied but many, in fact the olive oil "fingerprint" [9,10]. Altitude was selected as it is related to environmental variations and so to more complex variables, such as soils and climate.

Two linear equations were derived to characterize the samples as belonging to one of two groups, one grown below 400 m and the other over 700 m. More than 90% of samples were correctly classified. The actual state-of-art only allows a discrete study of this subject.

The linear equations derived were applied to samples from the same cooperatives but from another crop and a similar percentage of correct classifications was obtained.

2. Experimental

2.1. Dataset and statistical procedures

Two datasets of 63 samples, all collected in Jaén, were characterized by 53 compounds (Table 1); the first set was used to build the regression equations and the second set to verify them. Each dataset corresponds to a different harvest (1988, 1989) from the same cooperatives. The province of Jaén was selected because it produces ca. 22% of the world production of this edible oil.

BMDP [11] was the statistical library used to develop this study. Student's t- and Hotelling T^2-tests were applied to accept or reject the null hypothesis on the similarity between the means of the altitude groups. The variables (compounds) of the linear equations were calculated by a stepwise linear discriminant analysis (SLDA). Selection was made taking into account the F-to-enter and F-to-remove values, F-distributions, in order to lessen the possibility of attaining conclusions by chance [5].

2.2. Analytical methodology

All the compounds (Table 1) were measured by gas chromatography using different procedures [12,13].

Fatty acids were measured as their methyl esters produced by inter-esterification, neutralization and subsequent methylation using a solution of HCl in methanol. Saturated NaCl solution was then added and the final solution was extracted with hexane. The organic phase was analysed with a Perkin-Elmer Sigma 2 gas chromatograph [2.5% EGS on Chromosorb W (80–100 mesh), 2 m × 2 mm i.d.]. An equal response factor was considered for the whole set of fatty acids.

Table 1
Compounds used to characterize the samples.

Palmitic acid	Stigmasterol
Palmitoleic acid	Obtusifoliol
Margaric acid	Gramisterol
Margaroleic acid	Cycloeucalenol
Stearic acid	24-Ethyllophenol
Oleic acid	Citrostadienol
Linoleic acid	
Linolenic acid	Oleanolic acid
Arachid acid	Phytol
Gadoleic acid	Erythrodiol
Behenic acid	
	Copaene
Docosanol	Valencene
Tetracosanol	Muurolene
Hexacosanol	Tridecene
Octacosanol	Heptadecene
Taraxerol	Heneicosane
Dammaradienol	Tricosane
β-Amirine	Tetracosane
Butyrospermol	Pentacosane
24-Methylene-24-dihydrolanosterol	Hexacosane
	Heptacosane
Cycloarthenol	Octacosane
24-Methylenecycloarthanol	Nonacosane
Cyclobranol	Triacontane
Campesterol	Hentriacontane
Δ^5-Avenasterol	Dotriacontane
β-Sitosterol	Tritriacontane
	Pentatriacontane

Alcohols, sterols and methylsterols were determined using 5 g of virgin olive oil to which was added 2 ml of a solution of 0.25 mg ml^{-1} heneicosanol and 0.25 mg ml^{-1} betulin in diisopropyl ether. The chemical series were then determined by saponification of the oils, fractionation by thin-layer chromatography (Whatman 20 × 20 cm plates, 250 mm layer) of the unsaponifiable matter using *n*-hexane–ethyl acetate (85 + 15, v/v) as developer. Three large bands were removed from the TLC plate. The first contained triterpenic alcohols, part of the phytol and aliphatic alcohols, the second contained the rest of the phytol and aliphatic alcohols, methylsterols and hydroxyaldehydetriterpene, and the third contained sterols and erythrodiol.

The three separated bands and the fractions recovered from them were extracted separately with diisopropyl ether (10 ml). The solutions were silanized (150 μl) with pyridine–hexamethyldisilane–trimethylchlorosilane (9 + 3 + 1); cholestane (2 ml of a 0.025 mg ml^{-1} solution in diisopropyl ether) was previously added to the first and second bands.

Two Hewlett-Packard HP-5890 gas chromatographs were fitted with a flame ionization detector and a split injection system. Separation was carried out on capillary columns (25 m × 0.3 mm i.d.) coated with methylphenylsilicone HP-5 of thickness 0.17 μm. For alcohols and methylsterols the operating conditions were oven temperature, 250°C for 1 min, subsequently increased at 0.6°C min^{-1} to 280°C; injector temperature, 275°C; detector temperature, 300°C; and carrier gas, nitrogen. For sterols the initial oven temperature was 275°C for 15 min, thereafter increased at 1°C min^{-1} to 285°C.

The phytol and aliphatic alcohol contents were determined by adding the data for the first and second portions, using the cholestane peak as weight and quantifying the results with heneicosanol.

Triterpenic alcohols, methylsterols and hydroxyaldehydetriterpene were also determined with heneicosanol, whereas sterols and erythrodiol were determined with betulin.

Hydrocarbons were determined by saponification of virgin olive oil (20 g) with potassium hydroxide in ethanol (10% in 75 ml) for 90 min. Distilled water (100 ml) was then added and the solution was extracted twice with hexane (100 ml). The extracts were washed with three 100 ml volumes of ethanol–water (1 + 1) to achieve a pH of 7. The solution was passed through anhydrous sodium sulphate and then evaporated at 30°C to reduced volume (1 ml). The residue was divided into two fractions, which were separately analysed using a Hewlett-Packard HP 5890 gas chromatograph with a flame ionization detector. A wide-bore capillary column (30 m × 0.75 mm) coated with SPB-1 (chemically bonded dimethylsiloxane) 1 mm thickness was used.

Table 2
Student's *t* and significance level of the most important variables characterizing the two levels

Variable	*t*	*P*	Variable	*t*	*P*
Palmitoleic acid	4.65	0.0001	Taraxerol	−2.45	0.0209
Margaric acid	−0.42	0.6792	Dammaradienol	−1.78	0.0840
Margaroleic acid	1.10	0.2806	Butyrospermol	−2.44	0.0205
Linoleic acid	−1.82	0.0577	24-Methylene-24-dihydrolanosterol	−2.17	0.0373
Arachid acid	1.56	0.1276	Cycloarthenol	−4.04	0.0003
Gadoleic acid	1.45	0.1560	24-Methylenecycloarthanol	−4.24	0.0002
Behenic acid	0.88	0.3830	Phytol	−1.90	0.0692
			Erytrodiol	0.25	0.8050
Cycloeucalenol	−2.21	0.0345	Tridecene	5.43	> 0.0001
Citrostadienol	−1.76	0.0878	Copaene	−5.17	> 0.0001
Stigmasterol	3.65	0.0011	Heptadecene	2.56	0.0155
Campesterol	3.91	0.0006	Heneicosane	3.02	0.0057
β-Sitosterol	4.78	0.0001	Tricosane	1.78	0.0851
Δ^5-Avenasterol	1.28	0.2158	Muurolene	−4.54	0.0001

3. Results and conclusions

3.1. Chemical composition related to altitude

In a first step, the samples were classified into two groups. The first set consisted of samples collected below 400 m and the second set above 700 m. The intermediate group, collected between 400 m and 700 m, was not considered because the influence of altitude is only strong enough to find a discrete relationship with the chemical composition and not a continuous one. The collection region has no homogeneous characteristics with respect to materials, soil humidity, pH and cations among valleys and mountains [14].

Basic statistical studies, histograms and Student's t-test were used to determine whether there were compounds with a sufficient level of significance to distinguish between the two groups (Table 2). The most significant parameters were palmitoleic acid (fatty acid), β-sitosterol, campesterol and stigmasterol (sterols), cycloarthenol and 24-methylenecycloarthanol (triterpenic alcohols) and tridecene and copaene (hydrocarbons). However, a multivariate procedure, F-to-enter for each variable at step 0 of a discriminant analysis that is equal to an F statistic corresponding to a one-way analysis of variance (ANOVA), allowed the following compounds, classified according to Aparicio et al. [15], to be selected:

almost certainly significant:
- copaene (hydrocarbon)
- 24-methylenecycloarthanol (triterpenic alcohol)
- β-sitosterol (sterol)

Very possibly significant:
- linoleic acid (fatty acid)

Possibly significant:
- cycloarthenol (triterpenic alcohol)

Slightly possibly significant:
- phytol (alcohol)
- palmitoleic (fatty acid)

Thus, the results of the two tests allow us to ascertain which compounds were the best related to altitude. Linoleic acid and β-sistosterol were explained in the work cited above. However, the other chemical compounds were not mentioned in the literature concerning the effects of altitude, climate or soils on chemical composition. Consequently, a statistical study was performed to determine whether the relationship found here between these compounds and altitude occurred by chance.

Fig. 1 shows the probability distribution of each of the most significant compounds for the two altitude groups (< 400 m and > 700 m), using the algorithm described in [16]. The probability distributions try to show that there are two groups, although the compounds cannot clearly distinguish them. However, it can be seen that the contents of the compounds of olive oils from the mountain zone are lesser homogeneous than those from the valley.

3.2. Characterization of virgin olive oil by altitude

Once the compounds related to altitude had been found, the next step was to establish whether virgin olive oil could be characterized on the basis of altitude.

Hotteling's T^2-test indicated that there was a significant difference ($p = 0.0022$) between the two groups (altitude < 400 m and > 700 m) and hence that there are equations with sufficient

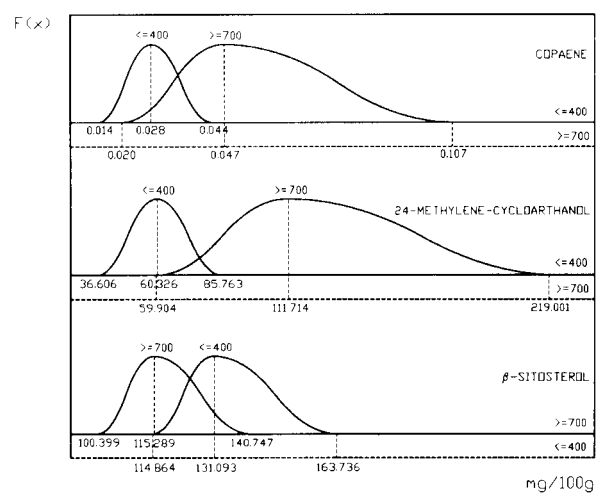

Fig. 1. Probability distribution (ordinate) versus contents of compounds (minimum, mean and maximum) in mg per 100 g of olive oil (abscissa). Number of samples = 63 (21 + 41); 1988 harvest.

ability to characterize the samples by altitude. Thus, Fig. 2 displays that a basic relational rule, the ratio between β-sitosterol and 24-methylenecycloarthanol, improves the results obtained independently with each of these compounds. Oils harvested at altitudes lower than 400 m have the highest contents of β-sitosterol and the lowest of 24-methylenecycloarthanol, and the opposite applies to oils harvested above 700 m.

Finally, stepwise linear discriminant analysis (SLDA) was used to determine the possibility of classifying virgin olive oil, using altitude (1, 2) as the dependent variable and the chemical compounds just described (Table 1) as independent variables. The number of samples of the first set (63) and groups (2) were used to calculate the F-to-enter and F-to-remove values from the F-distribution at 0.95 [17].

The first canonical equation that discriminates between the two groups uses copaene (hydrocarbon) and 24-methylenecycloarthanol (triterpenic alcohol) as the variables of the equation

$$y = 0.51 + 0.0055[\text{24-methylene-cycloarthanol}] - 12.24[\text{copaene}] \quad (1)$$

The equation has $R^2 = 0.85$ in terms of regression whilst the values of R^2 change [17], being 0.70 for copaene and 0.65 for 24-methylene-cycloarthanol. Knowing the standard deviation, the 95% confidence limits were estimated as ±0.55 (0.45–1.55 for the first group and 1.45–2.55 for the second), which means, in terms of altitude, ±165 m. Thus, 95.2% of the samples collected from the valleys were correctly classified versus only 78.1% of those from the second group.

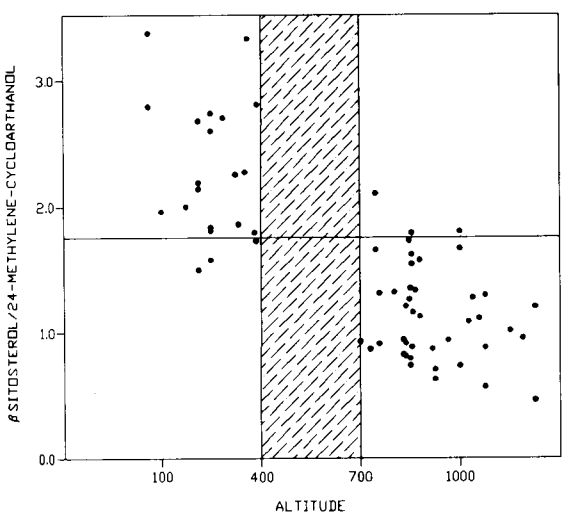

Fig. 2. Authentication of olive oil samples by the altitude of their cultivars using the β-sitosterol/24-methylenecycloarthanol ratio. Number of samples = 63 (21 + 41); 1988 harvest.

However, the hydrocarbon series requires a more complicated process and reagents than the other series. Consequently, we looked for another equation in which hydrocarbons were not used. The alternative is Eq. 2, the variables of which are palmitoleic and linoleic acid, the triterpenic alcohol cycloarthenol and the sterol β-sitosterol:

$$y = 2.49 - 1.21[\text{palmitoleic}] + 0.23[\text{linoleic}] - 0.01[\beta - \text{sitosterol}] + 0.02[\text{cycloarthenol}] \quad (2)$$

with $R^2 = 0.90$ and the 95% confidence limits of which were estimated as ±0.47 (0.53–1.47 for the first group and 1.53–2.47 for the second) which means, in terms of altitude, ±141 m. Thus, 95% of the samples collected from the first group were correctly classified against 88.9% of those from the second.

At first glance it is easy to conclude that the samples belonging to the first group, below 400 m, are more homogeneous than those in the second group. The explanation can be found either in the different climates affecting the mountains and valleys or the types of soils.

Thus, the most relevant variable is the topography. The soil depth is greater in the valley than on the mountains, so the valleys are richer in water, nutrients and organic materials, they have more cations (Ca^{2+}, Mg^{2+}, Na^{+}), higher pH and the water is retained longer in summer.

On the other hand, the mountain zones are less homogeneous; they are not equally affected by the action of surface water that produces micro-erosion, transporting and depositing materials in the valleys. They have very different levels of rainfall depending on the slope of the mountain, and this leads to the existence of alternate humid and dry zones without any uniformity [18]. In this study, some samples from the second group (altitude > 700 m) were classified in the

Table 3
Percentage of correct classifications by the two linear equations with the samples from two harvests (group 1 altitude < 400 m, group 2 altitude > 700 m)

Equation No.	Harvest	Percentage of correct classification		
		Group 1	Group 2	Total
1	1988	95.2	78.1	83.9
	1989	94.7	75.6	83.3
2	1988	95.0	88.9	90.8
	1989	90.0	83.7	85.7

first; 64% of these samples belong to zones that face the valleys and are affected by the Guadalquivir basin or the Mediterranean climate and this kind of climate (basically humid) has a greater influence than the altitude on the chemical composition of the oils. The oils produced, therefore, resemble those produced in the valley.

3.3. Verifying the functions

Every hypothesis, such as this one on the possibility of characterizing olive oils on the basis of the altitude of their cultivars, has to be validated before accepting its competence.

The proposed equations were obtained using a set of samples from olive trees of the picual variety (95%) harvested in 1988. A set of data from the same variety and cooperatives but harvested in 1989 were used to verify the equations.

The results were satisfactory. Table 3 shows a comparison between the percentages of correct classifications in the two crops. The results of both equations with respect to verification were fairly similar and once again the samples of the first group were the best classified. About 70% of the samples which were wrongly classified were thus classified in both years and consisted of samples from the same locations or from neighbouring locations. This means that the compounds selected are indeed related to the altitude and hence to the average conditions (climate and soil) pertaining in valleys and mountains.

There are three general groups of conclusions concerning the relationship between the qualitative chemical composition of olive oil and the altitude of its cultivar:

(a) The equality of group means was checked by the multivariate Hotelling's T^2-test, which rejected the null hypothesis of equality between the two sets of data with a probability of 99.6%. The level of significance of 55 chemical compounds was studied and 24-methylenecycloarthanol, cycloarthenol, copaene, palmitoleic acid linoleic acid and β-sitosterol seem to be the most related to altitude.

(b) The validation of the linear equations shows that it is possible to predict the altitude level of an unknown sample with a good range of probability, as shown in Table 3.

(c) The first equation shows that compounds with a cyclic structure (24-methylenecycloarthenol and copaene) seem affected by climate and soils, although their biochemical routes remain unknown.

Acknowledgements

This work was supported by CAYCIT (Spain), project ALI-91-0786, and the Dirección General de Investigación y Extensión Agraria de la Junta de Andalucía. The authors thank Drs. Cert and Lanzón and Mrs. Ferreiro, Miss Sanchez-Navarro, Mr. Martin and Mr. León for their collaboration in the chemical analyses of the samples.

References

[1] G. Lotti, G., R. Izzo and F. Nicolini, Riv. Ital. Sostanze Grasse, 50 (1973) 425.
[2] G. Lotti, S. Baragli and M. Gentili, Riv. Ital. Sostanze Grasse, 54 (1977) 506.
[3] M. Alberdi M. and L. Corcuera, Phytochemistry, 30 (1991) 3177.
[4] J. Sanchez, C. Osa and J.L. Harwood, in P.J. Quinn and J.L. Harwood (Eds.), Plant Lipids: Biochemistry Structure and Utilization, Portland Press, London, 1990, pp. 390–392.
[5] J. García and R. Aparicio, Anal. Chim. Acta, 271 (1993) 293.
[6] C. Armanino, R. Leardi, S. Lanteri and G. Modi, Chemometr. Intell. Lab. Syst., 5 (1989) 343.
[7] R. Aparicio, L. Ferreiro, R. Leardi and M. Forina, Cheometr. Intell. Lab. Syst., 10 (1991) 349
[8] L. Ferreiro and R. Aparicio, Grasas Aceites, 43 (1992) 149.

[9] R. Aparicio, J. Chemometr., 3 (1988) 175.
[10] R. Aparicio and V. Alonso, Grasas Aceites, 44 (1993) 18.
[11] W.J. Dixon, BMDP Statistical Software, University of California Press, Los Angeles, 1983.
[12] R. Aparicio, M. Sánchez-Navarro and M.S. Ferreiro, Grasas Aceites, 42 (1991) 356.
[13] R. Aparicio and V. Alonso, Prog. Lipid Res., 33 (1994) 29.
[14] F. Diaz-Pineda, Ecologia I. Ambiente Fisico y Organismos Vivos, Síntesis, Madrid, 1989.
[15] R. Aparicio, L. Ferreiro and J.L. Rodríguez, Characterization of Andalusian Virgin Olive Oil, Andalusian Ministry for Agriculture, Seville, 1992.
[16] M.T. Morales and R. Aparicio, Anal. Chim. Acta, 282 (1993) 423.
[17] B.G. Tabachnick and L.S. Fidell, Using Multivariate Statistics, Harper and Row, New York, 1983.
[18] G. Aubert and J. Boulaine, Pédologie Appliqueé, Mason, Paris, 1980.

ELSEVIER

Analytica Chimica Acta 292 (1994) 243–251

ANALYTICA CHIMICA ACTA

Application of neural networks for interpretation of ion mobility and x-ray fluorescence spectra

Zvi Boger *, Ze'ev Karpas

Nuclear Research Center Negev, P.O. Box 9001, 84190 Be'er-Sheva, Israel

(Received 3rd September 1992; revised manuscript received 1st July 1993)

Abstract

Neural networks (NN) have been successfully used to interpret spectral data, and to derive qualitative and quantitative information from ion mobility spectrometry (IMS) and x-ray fluorescence (XRF). It is shown that components of complex mixtures of up to six aliphatic amines may be automatically identified by NN methods from their ion mobility spectra with reasonable accuracy. The ability of NN to identify compounds even under low signal-to-noise conditions of IMS spectra is demonstrated. The use of XRF technique for quantitative determination of parts per million (ppm) amounts of mixtures of Re, Os, Ir and Pt in a polyethylene matrix, which could not be done successfully by conventional methods, was made possible by application of NN, with a root mean square error of a few ppm. The networks could be trained on a personal computer, in less than 10 min, from a surprisingly small data set of training samples to perform these tasks.

Key words: X-ray fluorescence; Amines; Ion mobility; Neural networks

1. Introduction

Neural networks (NN) have recently been used to interpret spectral data obtained by different experimental techniques [1–7]. Long et al. [1] and Borgaard and Thodberg [2] demonstrated that NN can be advantageously used to process near-infrared spectra. Olmos et al. [3] applied NN for γ-ray spectra processing and Bos and Weber [4] compared two types of NN for interpretation of x-ray fluorescence (XRF) spectroscopy. Morris et al. [5] compared NN with expert system techniques for infrared (IR) spectra analysis. Allanic et al. [6] utilized NN for two-dimensional fluorescence spectra identification. Wythoff et al. [7] verified IR peaks using NN. Tanabe et al. [8] applied NN to the identification of infrared spectra. Meyer and Weigelt [9] correlated IR spectra with chemical structures using NN. As spectra analysis requires a NN with a large number of inputs, which is difficult to train by the traditional NN algorithms, most authors [1–7] employed different methods of data reduction transformations to overcome these difficulties. Only in two cases were large NN with more than 100 inputs employed, by using a super-computer equivalent [8] or by training for many hours [9]. In a series of works [10] Boger has shown that NN can rapidly

* Corresponding author.

SSDI 0003-2670(94)00063-R

process several types of large input data sets, including the quantitative determination of ion mobility spectrometry (IMS) data [11].

In the present work, NN methods are applied to interpret spectral data from two different instrumental techniques, viz, IMS and XRF. The conventional mathematical methods were unable to successfully perform the required analysis of IMS spectra – automatic identification of individual components in complex mixtures or identification of single compounds under low signal-to-noise conditions. Determination of the concentrations of the individual elements in mixtures of rhenium, osmium, iridium and platinum in a polyethylene matrix could not be performed by these methods. However, the application of NN methods made these possible, with quite good levels of detection and accuracies.

1.1. Ion mobility spectrometry

Ion mobility spectrometry is a sensitive technique [12], that can be used for detecting, identifying and monitoring gases and vapors in air at sub parts per million (sub-ppm) concentrations. The technique is based on atmospheric pressure ionization of pollutant molecules in the reaction region at the entrance to a drift tube. A bunch of ions is then injected into the drift region of the tube. As they drift through a buffer gas in an electric field they are separated according to their mobility.

The technique is particularly suitable for compounds that readily form stable ions, under the atmospheric pressure ionization conditions of the IMS reaction region. Compounds that have high proton affinities, such as most reduced nitrogen [13] and phosphorus [14] compounds and ketones [15], are readily protonated and form stable positive ions. On the other hand, compounds that contain electronegative functional groups, such as halogenated or nitro compounds, readily form stable negative ions in the IMS. One of the major obstacles hindering the application of IMS instruments for monitoring chemicals in ambient air is the processing of the mobility spectra and their interpretation. As complex sequences of ion–molecule reactions, which are not always clearly understood, precede ion separation, interpretation of mobility spectra to derive quantitative information is generally not straightforward.

Typically, mobility spectra have relatively low signal-to-noise ratios, and contain a number of peaks, which are generally not very distinct from one another and their relative intensities change with time due to temporal concentration variations. When compared with chromatographic techniques, such as gas chromatography (GC) or liquid chromatography (LC), IMS shows quite a low resolution, typically on the order of 20–40, in terms of the ratio of the retention time to the full width at half maximum ($t/\mathrm{d}t$). As in GC and LC, compounds can be identified by IMS only by their retention time (or drift time) under given conditions, through use of a reference "library" of standards. To further complicate matters, two types of interferences appear in IMS. One is the result of the limited resolution of the instrument, namely, the proximity and overlapping of peaks due to ions of nearly similar drift times (mobilities), and the second is due to chemical interferences in the ion formation processes. Spectra processing methods cannot help to remove interferences of the second type, but may help to solve problems of the first type. A common spectra processing technique is averaging of multiple spectra, so the random noise is cancelled out. However, when applied to real-time tasks, this may extend the measurement and response time.

1.2. X-ray fluorescence

X-ray fluorescence is a non-destructive analytical technique that is used to simultaneously determine trace amounts of elements in a matrix [16]. In energy-dispersive XRF instruments, an x-ray source is used to excite the sample, and the resultant fluorescent x-rays of elements present in it are detected and analyzed according to their energy. Each excited element may emit radiation at a number of characteristic energies, which can be used to identify it. However, neighboring elements in the periodic table have similar energies. One such case is the group of platinum, iridium, osmium and rhenium, which emit x-rays of quite similar energies, as shown in Table 1. It is quite

Table 1
The characteristic energies and relative intensities of x-rays emitted from Re, Os, Ir and Pt

	Element				Relative intensity
	Re	Os	Ir	Pt	
$L\alpha_1$	8.650	8.910	9.173	9.441	100
$L\alpha_2$	8.585	8.840	9.099	9.361	10
$L\beta_1$	10.005	10.350	10.705	11.068	55
$L\beta_2$	10.275	10.595	10.919	11.249	20
$L\beta_3$	10.158	10.507	10.865	11.232	7
$L\beta_4$	9.846	10.174	10.510	10.853	4

easy to prepare calibration samples and determine the amount of each element separately in a polyethylene matrix. However, it is quite complicated to determine each element independently when the other three elements are also present in the matrix.

2. Experimental

2.1. Ion mobility spectrometry

The Rotem Industries prototype instrument PT-IMS was used in the present study. The instrument and its operating procedures were described previously [14], and will not be discussed here in detail. The PT-IMS was operated at 150° C, and ambient air, purified by a 13X molecular sieve trap, was used to provide the carrier and drift gas flows. Ammonia vapors emanating from a permeation tube were introduced into the carrier gas flow, in order to reduce interferences from chemicals that have proton affinities below 853 kJ mol^{-1} (see Table 2). The ammonia peak in the mobility spectrum also served as a means of normalizing the relative drift times (i.e. relative reduced mobilities). Introduction of samples into the IMS was done either by adsorbing vapors onto a syringe needle and desorbing them in the IMS, or by premixing the vapors and carrying them into the IMS. In both cases the vapors are carried by a stream of purified air into the reaction region of the IMS, where ions are formed through reactive ion–molecule processes. Under these conditions amines are readily protonated to form mainly the quasi molecular protonated molecule [13]. One thousand spectra were averaged to enhance the signal-to-noise ratio.

For demonstrating the ability of the NN to identify single chemical compounds under low signal-to-noise conditions, the mobility spectra of five compounds [benzophenone (BZ), diisobutylketone (DIK), dimethoxymethyl phosphonate (DMMP), dinitrotoluene (DNT) and pyrrole (PY)] were collected and averaged three and thousand times. A typical spectrum is shown in Fig. 1.

2.2. X-ray fluorescence

X-ray fluorescence measurements were carried out by an energy dispersive instrument, Model EX-6000, made by Jordan Valley Applied Radiation (Migdal Ha'emek, Israel). A Mo secondary target, which generates 17.44 keV almost monochromatic x-ray, was used. The excitation voltage was 40 kV. The samples were prepared by weighing appropriate amounts of Re, Os, Ir and Pt salts in powdered polyethylene and pressing the sample into a pellet after homogenization. The degree of homogenization was previously shown to be adequate for analytical purposes [17]. The composition of the samples used is shown in Table 3, and the counting time was 2400 s.

Table 2
The relevant properties of the amines studied

Compound	M.W. (a.m.u.)	P.A. [a] (kJ mol^{-1})	K_0 [b] (cm^2 V^{-1} s^{-1})	Number in Table 4
Ammonia	17	853.3	3.14	
Ethylamine	45	908	2.25	1
Dimethylamine	45	923	2.32	2
n-Propylamine	59	912	2.12	
Isopropylamine	59	915	2.16	3
sec-Butylamine	73	922	2.04	4
Di-*n*-propylamine	101	952	1.88	5
Triethylamine	101	972	1.94	6
2,4-Lutidine	107	951	1.95	

[a] P.A. = proton affinity; from Ref. 22. [b] From Ref. 13.

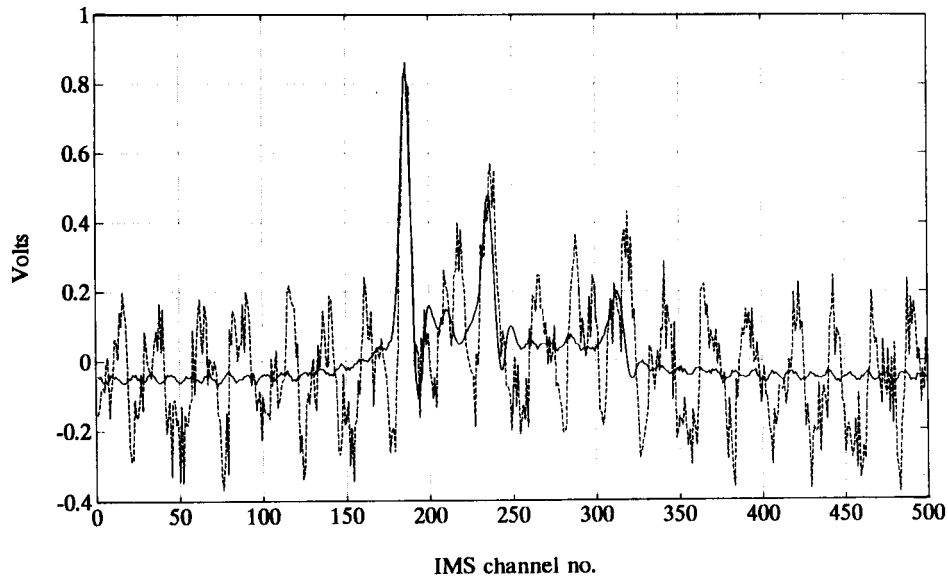

Fig. 1. The IMS spectra of dimethoxymethyl phosphonate (DMMP). Dashed line: spectrum obtained by averaging 3 spectra; solid line: spectrum obtained by averaging 1000 spectra.

2.3. The neural network

As a detailed review of NN theory and applications to chemistry is available [18], and the particular network used in this study has been described recently [11], only a very brief description of the neural network concepts will be given here.

In the computer simulation of artificial neural networks, processing "neural" nodes (neurodes) are linked to each other by variable-strength connections. The sum of all inputs to a neurode, if larger then a bias, activates the neurode. The neurode output, multiplied by connection weights, is transferred to all neurodes receiving inputs from this neurode. A neural architecture was

Table 3
The XRF sample composition (in ppm) and calculated concentrations of Re, Os, Ir and Pt in polyethylene matrix

Sample	Re		Os		Ir		Pt		Total	
	True	Calc.	True	Calc.	True	Calc.	True	Calc.	True	Calc.
1	11	10.5	20	24.9	30	26.5	40	40.4	101	102.3
2	40	35.0	10	11.4	20	14.8	30	37.1	100	98.3
3	30	28.5	40	38.2	10	9.8	20	23.0	100	99.5
4	20	18.3	29	31.2	40	36.5	23	13.2	112	99.2
5	39	39.2	28	31.8	19	16.8	10	15.1	96	102.9
6	30	33.0	20	18.4	10	11.1	40	34.5	100	97.0
7	19	14.5	10	14.0	38	37.7	33	36.9	100	103.9
8	10	14.7	40	39.1	30	31.3	20	24.0	100	109.1
r.m.s. error	3.2		2.9		2.7		5.5			

used in which the forward network included one input layer and two processing layers: the "hidden layer" and the output layer. The sigmoidal shaped activation equation used was:

$$y = 1/[1 + \exp(-x)]; \quad x = w \cdot y_p + b$$

where y_p are the outputs of the previous layer neurodes, w are the connection weights leading to a neurode with bias b, and y is the neurode output. The learning algorithm was the supervised error back-propagation algorithm, in which a data set of system inputs and outputs is presented to a neural net having initial connection weights. The difference between the network output and the known output is the network error, and the connection weights were modified by the conjugate gradient method to decrease the sum of the squared errors. The process was repeated, until the NN was considered to be "taught", as tested by a previously unseen data set which gave an acceptable small error.

An algorithm developed by Guterman [19] appears to solve the problem of extensive training time caused by use of random values for the initial connection weights, and heuristic-based choice of the number of hidden neurodes. Principle component analysis (PCA) calculation of the training data set estimated how many hidden nodes should be used, and further statistical analysis gave a good first guess for the values of the initial connection weights. A learning speed improvement by a factor of 20–50 over conventional learning is achieved by this algorithm, as it almost always converges to a global minimum in a relatively small number of dataset presentations during the learning process.

The procedure for IMS spectra analysis was described previously [11]. The training was done on an IBM 386/33 compatible machine, and up to several hundred presentations of the learning set (epochs) were needed to train each NN. The whole training and reduction session typically took less then an hour, using the non-optimized development version of the software. The proprietary NN algorithms are incorporated in a commercially available software package, operating in a Windows 3.1 environment [20].

3. Results and discussion

3.1. Ion mobility spectrometry

In a field application, the Rotem PT-IMS instrument was used to monitor amines in the ambient atmosphere in the vicinity of a chemical production plant. The presence of six aliphatic amines was anticipated: ethylamine, dimethylamine, isopropylamine, *sec*-butylamine, dipropylamine and triethylamine. All are readily protonated to form stable positive ions [13]. The relevant properties of these compounds, and of ammonia, are summarized in Table 2. The molecular weight affects the reduced mobility of the ion, as pointed out previously [21]. However, the proton affinity [22] plays an important role, as it determines the relative ionization efficiency of each of these compounds in the presence of the others. Ammonia is used as a reagent gas to increase selectivity and specificity of the IMS toward amines. The reagent is added directly into the carrier gas flow, and introduced into the reaction region at a concentration of about 25 ppm, thus forming NH_4^+ ions. These ions will transfer a proton only to compounds that have proton affinities above that of ammonia, while any interference by compounds with lower proton affinities will not affect the positive ion mobility spectrum. Proton transfer reactions from NH_4^+ to all the aliphatic amines are rapid and efficient.

The reduced mobilities of some of these protonated amines are close to one another, and in general it is quite impossible to separate all six when they are present simultaneously. Examples of spectra are shown in Fig. 2, in which it is evident that some of the compounds form ions that are not resolved in the IMS. Fig. 2b shows the mobility spectrum of a mixture of ammonia (the reagent gas) with a 5.36 ms drift time, dimethylamine (5.81 ms), isopropylamine (6.55 ms), *sec*-butylamine (6.94 ms) and dipropylamine (7.59 ms), which are quite readily separated. However, as seen in Figure 2a, a mixture of ammonia (5.40 ms) with ethylamine (5.96 ms) and *sec*-butylamine, triethylamine and dipropylamine (6.98, 7.31 and 7.59 ms, respectively) complicates

the spectrum, and the peaks are not fully resolved.

For air quality monitoring purposes, only measurement of the total amount of these amines was required. However, the use of NN techniques made it possible to derive more specific information on the contribution of individual amines to the total amine concentration.

First, mobility spectra of each compound and of two mixtures were measured. The spectra were aligned so that the drift time of the reagent ion (ammonia) peak coincided, and a range of 151 channels from these eight spectra was used to train the 151-4-6 NN. After completion of the training session, the mobility spectra of a number of mixtures were tested. Each of the six outputs

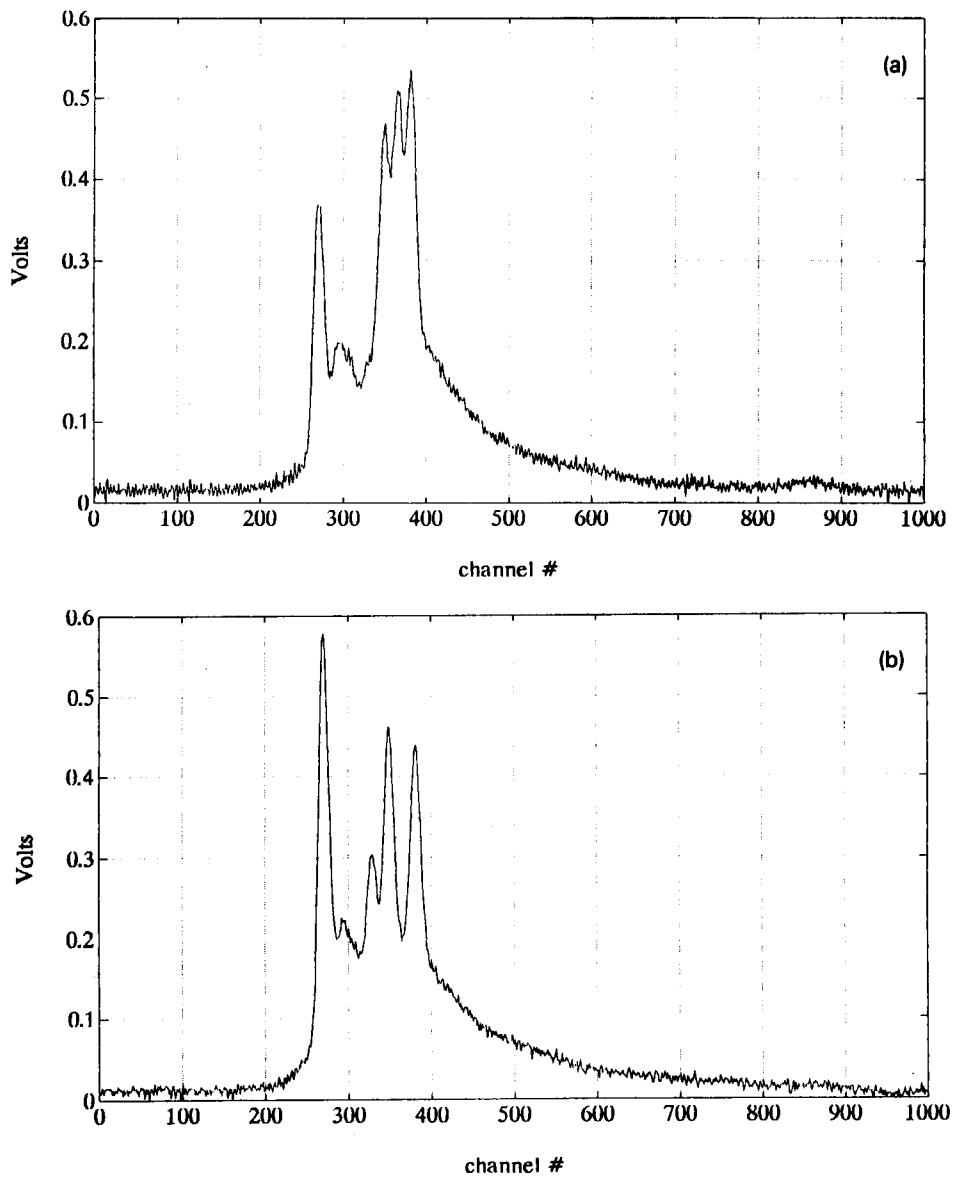

Fig. 2. The mobility spectra of aliphatic amines. (b) A mixture of ammonia, dimethylamine, isopropylamine, *sec*-butylamine and dipropylamine; (a) a mixture of ammonia, ethylamine, *sec*-butylamine, triethylamine and dipropylamine.

from the NN has values in the range 0.1–0.9. An output value above 0.7 was taken as positive identification of the compound, an output value below 0.3 was considered as negative (the compound not present), while output values in the range 0.3–0.5 were considered as uncertain negative and between 0.5 and 0.7 as uncertain positive. The results are summarized in the form of a truth table, and presented in Table 4. Thus, results may be true or false (T or F, respectively, in Table 4), depending on the actual presence of the components in the mixture. The ratio between the number of true and false outputs (shown in the last two columns of Table 4) is the test for evaluating the performance of the NN.

Table 4 shows that NN can be used with quite a high level of confidence for automatic identification of the individual components of a complex mixture of aliphatic amines.

The ability of the NN technique to operate successfully with noisy data was demonstrated by training a NN to recognize the 1000-times averaged spectra of five different compounds, and then testing it by the presentation of the 3-times averaged spectra of the same compounds. Out of the 501 available channels in the spectra, 200 contiguous channels (171–370) were presented to a NN with five outputs. Five hidden nodes were needed for the learning of the spectra. The results are given in Table 5, and it can be seen that the recognition of each compound was perfect, even with very noisy data, as shown in Fig. 1.

3.2. *X-ray fluorescence*

Although the XRF spectrum spans the energy range of 0–20 keV, only 100 channels, from 8.5 to 9.5 keV, were used in the present work. A typical XRF spectrum in this range is shown in Fig. 3, and evidently, it is quite noisy. The background XRF spectrum (pure polyethylene) was subtracted from each of the XRF spectra of the samples. The NN architecture was: 100 input channels, four hidden neurodes, four outputs, corresponding to the concentrations of the four elements: Re, Os, Ir and Pt. The criterion for

Table 4
Truth table of NN interpretation of the mobility spectra of mixtures of six aliphatic amines

Sample name	Compound number						Total	
	1	2	3	4	5	6	T	F
1 Ethyl	TP	TN	TN	TN	TN	TN	6	0
2 Dimetl	TN	TP	TN	TN	TN	TN	6	0
3 Iprop	UP	TN	TP	TN	TN	TN	6	0
4 Secbuta	TN	TN	TN	TP	TN	TN	6	0
5 Dipropa	TN	TN	TN	TN	TP	TN	6	0
6 Triethyl	TN	TN	TN	TN	TN	TP	6	0
7 456A	TN	TN	TN	TP	TP	TP	6	0
8 123	TP	TP	TP	TN	TN	TN	6	0
9 Secbut	TN	FN	TN	TP	TN	TN	5	1
10 Backg2	TN	TN	TN	TN	TN	TN	6	0
11 134	TP	FP	TP	FN	TN	TN	4	2
12 456B	TN	TN	TN	TP	TP	UP	6	0
13 UNK1	TN	TN	FN	TP	TN	FN	4	2
14 Lutagan	TN	TN	TN	TN	FP	FP	4	2
15 Ammonia	TN	TN	TN	TN	TN	TN	6	0
16 UNK2	UN	FN	TP	UN	FP	UN	1	5
17 UNK3	TN	TP	TN	TN	TN	TN	6	0

T = true; F = false; P = positive (output > 0.7); N = negative (output < 0.3): uncertain positive (0.5 < output < 0.7) and uncertain negative (0.3 < output < 0.5). Samples 1–8 were the training set, 9–17 the test set.

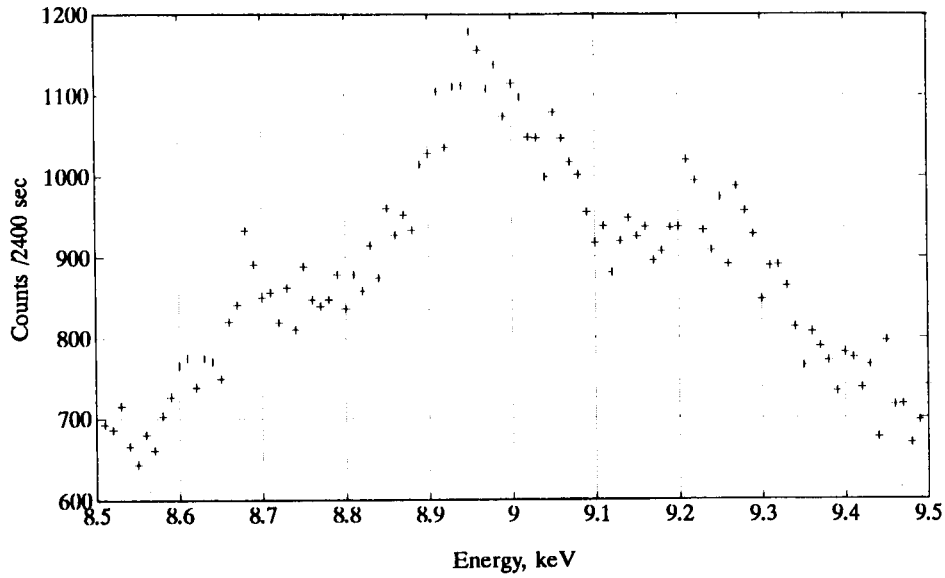

Fig. 3. XRF spectrum of polyethylene with 10, 40, 30 and 20 ppm of Re, Os, Ir and Pt, respectively, in the range 8.5–9.5 keV.

termination of the training was 0.02 for the sum of the squares of the errors. The training time on a PC 386/33 was typically 3–5 min.

Seven XRF spectra, of known composition (listed in Table 3), were used to train the network, while the eighth was taken as the test point. The training process was repeated eight times, with a different sample as the test point. The results are presented in Table 3, in which the calculated composition of the test samples is compared with their known composition. This method is recommended when the number of samples is smaller than the number of connections in the NN, to avoid the possibility of overfitting [23].

Table 5
Identification of 3-times averaged spectra by the 200-5-5 NN

Compound name	BZ	DIK	DNT	DMMP	PY
Benzophenone (BZ)	0.88	0.02	0.13	0.02	0.11
Diisobutylketone (DIK)	0.04	0.89	0.10	0.01	0.00
DNT	0.14	0.13	0.87	0.13	0.01
DMMP	0.00	0.02	0.11	0.97	0.03
Pyrrole (PY)	0.12	0.04	0.06	0.08	0.91

0.9 signifies presence, 0.1 signifies absence of the particular compound.

From these results it is evident that the lower the concentration of the metal in the sample, the larger the deviation between calculated and known concentrations. As seen from the root mean square error values, the agreement between the calculated and known concentrations of rhenium and platinum is not as good as it is for the osmium and iridium content, but most error values are only a few ppm. It is also interesting to compare the known total concentration of the metals with the calculated concentration, shown in the last two columns of Table 3. With a single exception, the deviations are less than 10%.

4. Conclusion

The advantage of using the neural network to interpret ion mobility spectra is that complete understanding (or for that matter any understanding) of the ion chemistry is not needed. Automatic identification of the components in a complex mixture of amines in air was also quite successfully accomplished with the NN.

The ability of NN to recognize known compounds even with noisy data was also demon-

strated. This ability is important, especially for real-time applications, where it can be coupled with NN hardware components, already available from several sources, and incorporated into portable or hand-held IMS instruments. Thus, a reliable tool to help meet environmental and chemical agents monitoring requirements may be provided.

The contribution of Re, Ir, Os and Pt to the x-ray fluorescence spectra of polyethylene samples doped with these metals, could be determined by use of a neural network. While conventional methods can, at best, be used to estimate the total concentration of these four elements, applying NN methods makes it possible to assess the individual contribution of each element.

Acknowledgement

We would like to thank Dr. Y. Soreq, Mr. Y. Nahmani and Mr. A. Hemi for the XRF data.

References

[1] J.R. Long, V.G. Gregoriou and P.J. Gemperline. Anal. Chem., 62 (1990) 1791.
[2] C. Borgaard and H.H. Thodberg, Anal. Chem., 64 (1992) 545.
[3] P. Olmos, J.C. Diaz, M. Perez, P. Gomez, V. Rodellar, P. Aguayo, A. Bru, G. Garcia-Belmonte and J.L. de Pablos, IEEE Trans. Nucl. Sci., 38 (1991) 971.
[4] M. Bos and H.T. Weber, Anal. Chim. Acta, 247 (1991) 97.
[5] J.B. Morris, R.A. Pesce-Rodriguez, R.A. Fifer, S.A. Libman, S.M. Lurcott, E.J. Levy, B. Skiffington and A. Sanders, Intell. Instrum. Comput., (1991) 167.
[6] A.L. Allanic, Y.J. Jezequel and J.C. Andre, Anal. Chem., 64 (1992) 2618.
[7] B.J. Wythoff, S.P. Levine and S.A. Tomellini, Anal. Chem., 62 (1990) 2702.
[8] K. Tanabe, T. Tamura and H. Uesaka, Appl. Spectrosc., 46 (1992) 807.
[9] M. Meyer and T. Weigelt, Anal. Chim. Acta, 265 (1992) 183.
[10] (a) Z. Boger, Israel Chem. Eng., 20 (1991) 6 (in hebrew); (b) Z. Boger, ISA Trans., 31 (1992) 25.
[11] (a) Z. Boger and Z. Karpas, J. Chem. Inf. Comput. Sci., in press.
(b) Z. Karpas and Z. Boger, Proceedings of the 1992 Workshop on Ion Mobility Spectrometry, Las Crusas, NM, 1992, p. 35.
[12] (a) R.J. Dam, in T.W. Carr Ed., Plasma Chromatography. Plenum Press, New York, 1984, Chap. 6.
(b) J.L. Brokenshire, V. Dharmarajan, L.B. Coyne and J. Keller, J. Cell. Plast., 29 (1990) 123.
[13] Z. Karpas, Anal. Chem., 61 (1989) 681.
[14] Z. Karpas and Y. Pollevoy, Anal. Chim. Acta, 259 (1992) 333.
[15] Z. Karpas, Int. J. Mass Spectrom. Ion Proc., 107 (1991) 435.
[16] R. Jenkins, X-Ray Fluorescence Spectroscopy, Wiley-Interscience, New York, 1988.
[17] Y. Soreq, personal communication.
[18] J. Zupan and J. Gasteiger, Anal. Chim. Acta, 248 (1991) 1.
[19] H. Guterman, Dept. of Computer and Electrical Engineering, Ben Gurion University, Be'er-Sheva, Israel, 1990, unpublished work.
[20] TURBO - NEURON, NEXSYS - Neural Expert System Ltd., Mishor Yamin, D.N. Arava, 86800 Israel.
[21] Z. Berant and Z. Karpas, J. Am. Chem. Soc., 111 (1989) 3819.
[22] S.G. Lias, J.F. Liebman and R.D. Levin, J. Phys. Chem. Ref. Data, 13 (1984) 695.
[23] M.A. Bos, A. Bos and W.E. van der Linden, Analyst, 118 (1993) 323.

ELSEVIER

Analytica Chimica Acta 292 (1994) 253–261

ANALYTICA CHIMICA ACTA

Selection of analytical variables to optimize laboratory efforts in future groundwater studies

J.M. Andrade [a], D. Prada *,[a], E. Alonso [a], P. López [a], S. Muniategui [a], P. de la Fuente [b], M.A. Quijano [b]

[a] *Dpto. Química Analítica, Universidad de La Coruña, La Zapateira s / n, 15071 La Coruña, Spain*
[b] *Instituto Tecnólogico Geominero, c / Río Rosas 23, 28003 Madrid, Spain*

(Received 10th March 1993; revised manuscript received 20th October 1993)

Abstract

The main objective of this work was to develop a way to select a subset of analytical variables from one initial broad study to monitor groundwater quality. The study was applied to one Spanish area. The work was focused on selecting actual physico-chemical variables rather than using typical multivariate techniques as a way to reduce costs, effort, necessities facility and staff workloads. Several chemometric multivariate techniques such as principal components analysis, factor analysis, singular value decomposition of raw data matrix and procrustes rotation were used as the mathematical means to achieve the objectives. Of the initial 29 variables analysed, six of them were selected to describe the system during five seasonal samplings and it is hoped that each season subset will allow the monitoring of groundwater quality during future seasons.

Key words: Optimization methods; Aquifers; Chemometrics; Factor analysis; Groundwater; Principal components analysis; Procrustes rotation; Singular value decomposition; Waters

1. Introduction

The natural composition of water can be altered by urban and industrial wastewater or by water from agricultural irrigation. This paper shows the evolution of the importance of some analytical variables to define the physico-chemical quality of one aquifer during one year.

The aquifer studied is located in southeast Spain and it is mainly used for human consumption and agricultural irrigation. Fourteen sample points were selected and 29 regulated features [1] were studied.

This study is part of a broad project to investigate groundwater quality. In these kinds of projects, questions such as the following can arise in analytical laboratories: are all the tests performed in the laboratory really necessary?; are all the features considered really important to describe the groundwater quality in this geographical area?; and what are the most important ones? Several chemometric techniques have been applied to answer questions similar to these. Two of the most popular techniques are principal compo-

* Corresponding author.

SSDI 0003-2670(94)00061-P

nent analysis (PCA) and factorial analysis (FA) [2–5].

Broadly, both techniques allow the combination of non-independent variables into linearly independent components. Those variables with a limited contribution to the system will appear either as variables with low communalities or as separate single-variable components as the number of retained factors is increased. Hence these techniques account for a decrease in the dimensionality of the original hyperspace of raw variables. Two main problems can be addressed with both methods and those related to them. The first is that the selection of the number of PCs is subjective and a topic not yet totally resolved [6,7]. The second problem is that principal components and even the factors are (strictly) obtained from a linear combination of the overall original variables, so the physical or chemical interpretation is not always easy. However, in fact, the use of PCs does not answer questions related to original variables or the problems of the selection of the "most important original variables" from the original ones [8,9] to characterize the aquifer.

Although a PCA aproximation decreases the space dimensionality, all the variables are still required for each PC definition. Therefore, this is not an optimum solution for our purposes, because our objective is to decrease the number of original variables while retaining the same (or nearly the same) confidence interval on the groundwater quality but using fewer tests.

If we were able to select a subset of variables from a greatest original set, several problems could be solved. Three of the main problems with analysis of the whole data set are the following [10]:

(1) Some of the variables may be totally irrelevant to the objectives of the study, and may mask any genuine effects that exist in the rest of the data.

(2) With a large number of variables presented, the sample size necessary to obtain realiable parameter estimates may be unrealistically high. This is one of our problems since, as was mentioned, we have only 14 wells and many regulated variables. Owing to several constraints, our work was restricted to 29 variables; nevertheless, suspicions can arise about the statistical significance of 29 variables measured in only 14 wells.

(3) A large number of variables will induce a large number of unknown parameters in the problem, and the larger the number of estimated parameters in any objective function, the more complications arise because of sampling variability.

In addition to these statistical considerations, there are others that are well known:

(4) On increasing the number of parameters to be tested, the sample size should also be increased. Problems related to transport, storage and manipulation arise.

(5) If more parameters are to be analysed, more money should be charged.

(6) When more parameters are considered, more amounts of reagents, time, staff workloads, delay time, equipment facility size, etc. should be take into account.

Our main objective in the chemometric studies considered have was to find some kind of solution that could address all of these problems. However, of course, the selection of variables must be performed in such a way that these "retained variables" will retain most of the information from the original data; in fact, these variables must be the "best subset" of variables that retain the main structure of the original data. If we were able to find a small subset of variables explaining most of the information captured by the greatest set, ideally we could apply it to monitor the aquifer system, saving a lot of effort and resources.

Clearly, statistical solutions must be complemented with a knowledge of the system [9] (pollution sources, agricultural and livestock uses, etc.). If, for example, the statistical results do not retain chemical oxygen demand (COD), NO_3^-, NO_2^- and NH_4^+ variables, it will be reasonable to keep one of them in the final subset to monitor easily "organic pollution characteristics".

As was correctly pointed out by one of the referees, the question arises as to the frequency with which contaminating species (e.g., Hg) appear. If the time between events is less than 1 year, then once a year may not be sufficiently

frequent, and if longer, then it may be too often given the resources needed to make all the analyses.

This problem is certainly very common, and we have no general solutions. In our opinion, a possible approach is that reported in this paper: we performed a 1-year study and can draw conclusions for each of the seasons. As a general rule of thumb, each sampling time data will represent the groundwater quality during each season. It should be stressed that these data are not "average quality data". Provided that all samplings are performed in the last month of the season (as we did), we shall obtain the "worst" situation of the groundwater quality in that season (in winter there will be a lot of water but there can also be a lot of organic matter; and in summer, there will be little water so the concentration of some analytes will be high).

We consider that one sampling per season is a good approximation to monitor the groundwater quality of this area (unpolluted area and fairly far from specific contamination sources). Certainly, if there is pollution due to a unique species, we shall not be able to select this particular contamination. However, such a contamination will only arise if some special source of pollution is present (e.g., industries, wastes). In this particular area, there are no factories and we pay attention to reports of accidents and public opinions about water quality. Because of the inherent characteristics of this area (i.e., agricultural and cattle uses), we only expect diffused and/or agricultural and cattle pollution. If other areas are studied and they include factories, one or more variables directly related to this typical industrial activity should be retained as important variables. If the values of the variables retained (i.e., those considered as important) suffer an anomalous increase, special and firm decisions would be taken.

2. Sampling

Fourteen existing wells were taken as sample points in an area in southeast Spain as the starting point for a broad project covering groundwater quality. In this area there are no more wells so we could not take more sampling points.

To reach a overview of the groundwater quality, two approaches were considered. The first was to select several sampling seasons spaced in time, pool the overall data set and draw conclusions. The second was to select one sampling per season, and draw conclusions for each season. One possible solution to the first approach could be the use of three-dimensional matrix analyses [11,12], because this kind of study will allow the manipulation of a hidden variable named "interseasonal changes with time". This "variable" is not directly measured with physico-chemical variables. We cannot apply this solution although it seems very appealing.

Five sampling seasons equally spaced during 1 year were selected and six data sets were considered: RESMU1 (winter), RESMU2 (spring), RESMU3 and RESMU4 (summer), RESMU5 (autumn) and RESMUM (average of the five sampling times). Two samplings were done in summer (June and September) because we were especially interested in studying parameter variations. The objective of RESUM was to compare

Table 1
Parameters included in statistical studies

Parameter	Range	Parameter	Range
pH	7.7–8.7	NO_3^-	0–102 mg l^{-1}
Conductivity	239–2420 μS cm^{-1}	Na	4–340 mg l^{-1}
COD	0.2–1.8 mg O_2	Mg	12–48 mg l^{-1}
Dry residue	120–2018 mg l^{-1}	Ca	23–105 mg l^{-1}
Cl^-	9–620 mg l^{-1}	K	0–11 mg l^{-1}
SO_4^{2-}	5–157 mg l^{-1}	SiO_2	0.6–19.4 mg l^{-1}
HCO_3^-	87–296 mg l^{-1}	Zn	0.0–0.51 mg l^{-1}
CO_3^{2-}	0–26 mg l^{-1}	Pb	0.0–0.17 mg l^{-1}

Table 2
Parameters not included in statistical studies

Parameter	Concentration range ($mg\ l^{-1}$)	Parameter	Concentration range ($mg\ l^{-1}$)
NO_2^-	< 0.010	Cr	< 0.001
NH_4^+	< 0.010	Cd	< 0.001
PO_4^{3-}	< 0.200	As	< 0.001
F^-	< 0.010	Se	< 0.001
Fe	< 0.010	CN^-	< 0.001
Mn	< 0.001	Hg	< 0.001
Cu	< 0.010		

its conclusions with those derived from the other sampling time.

3. Analytical techniques

Twenty-nine parameters were analysed in unfiltered samples. The features were tested according with current methods [1,13,14] and are detailed below.

Table 1 shows sixteen of these parameters with their concentration intervals and measurement units. Table 2 shows the remaining parameters present in all samples at concentrations lower than the limits of detection (LOD) indicated. These were not included in multivariate statistical studies because their standard deviation is zero.

3.1. Visible spectrometry

A Technicon SMA 12/60 flow-segmented autoanalyser was used. The determinations performed were for SiO_2, total alkalinity, Cl^-, SO_4^{2-}, PO_4^{3-}, NH_4^+, NO_3^-, NO_2^-, Ca and Mg, using standard methods [13].

3.2. Atomic absorption spectrometry

An IL 951 atomic absorption spectrometer was used, equipped with an IL 555 atomizer with pyrolytic graphite-coated graphite cuvettes and a FASTAC IL 254 automatic injector. Cd, Cr, Fe, Mn and Pb were determined by AAS with electrothermal atomization, Se and As by generating the hydrides and using flame AAS and Hg by the cold vapour technique, using $SnCl_2$ as reductant.

3.3. Potentiometry

A Metrohm E-632 potentiometer was used, equipped with an Ag/AgCl reference electrode. pH (glass membrane), fluoride (La_3F crystalline membrane) and cyanide (Ag_2S crystalline membrane) ion-selective electrodes were used. F^- and CN^- were determined.

4. Statistical techniques

In this following, bold capital letters will denote data matrices and bold lower-case letters will denote vectors; $\boldsymbol{v}'$ is the transposition of vector $\boldsymbol{v}$.

The main objective was to find a mathematical model that retains a subset of the original variables but with the condition that this subset should incorporate a large fraction of the initial system variance (if not all the variance). Moreover, it was attempted to optimize the extraction of information from the raw data matrix. The idea is to select those variables which account for most of the information in the data set and it is hoped that they will serve as indicators for monitoring the groundwater quality in the studied area. Variables not retained in the above-mentioned subset can be considered as having not very useful information.

The mathematical techniques and the algorithms used are well explained in [15–18]. Here only selected details are presented.

4.1. Selection of the best subset of variables

Selection of the best subset of variables can be considered as a technique of confirmatory factor analysis based on procrustes rotations and cross-validation.

As the final objective is to select redundant variables in raw data, this is equivalent to the identification of a subset of k variables which conveys the main structure of the raw data. The

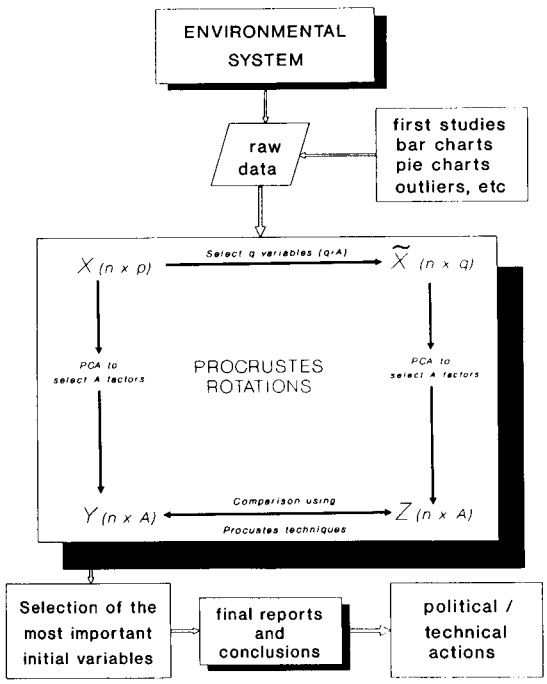

Scheme 1. Outline of the statistical technique employed.

k-variable subset is the one (among all k-variate subsets) that comprises the smallest predicted residual sum of squares (PRESS) (residues in the sense of least squares). Algorithms implemented by Eastman and Krzanowski [17–19] involve a very fast and easy calculation process allowing each variable to be deleted in turn across successive steps (using techniques such as cross-validation and jack-knifing) and both spaces, that considered as "true" and that without the deleted variable, to be compared. The spaces are compared by means of matching under translation, rotation and dilation [10]. If both spaces match, PRESS should be nearly or equal to zero. If we extract one "important variable", PRESS will be greatly increased, but it should not increase very much if that variable is "not important". An outline of the technique is showed in Scheme 1.

In Scheme 1, n, p and q have been defined above. PCA denotes a step where a principal component analysis is made using the SVD technique. $\boldsymbol{Y}$ will represent the "optimum representation of the raw data" using A principal components. $\boldsymbol{Z}$ will represent the "optimum representation" of the raw data set where only the "optimum" variables have been retained. $\boldsymbol{Y}$ and $\boldsymbol{Z}$ are compared using procrustes techniques. When the PRESS is minimum, $\boldsymbol{Z}$ will be the best possible representation of $\boldsymbol{Y}$ (i.e. $\boldsymbol{X}$) and this will allow us to select the optimum number of "q".

The main decissions have to be taken by the analyst. The first is to decide what is the true configuration. The second is to decide what is the minimum number of important variables. The two problems are closely related. The first and more intuitive approach for selecting the true configuration is to accept the one arising from a PCA of the raw data matrix. However, to avoid "noise data", we should choose an "optimum number of PCs". The true configuration will be the PC scores from the raw data matrix but using only, say, the first $\boldsymbol{K}$ components. As a practical approximation to select the optimum number of variables to be retained, Krzanowski [18] suggested $K+1$ variables. From this discussion, it is clear that selecting the optimum number of PC is a crucial point.

4.2. *Singular value decomposition (SVD) of raw data matrix. Selection of the optimum number of PCs.*

Data matrix decomposition using the SVD technique is the fastest and most exact way to determine the matrix-associated principal components. Another important advantage is that SVD is easily implementable in informatic software.

Let us suppose that p variables $(x_1,\ldots,x_p)$ are measured in each of the n cases (samples) $(n \leq p)$ and the resultant values are displayed in an $(n \times p)$ data matrix X. Principal component analysis provides p new variables $z_1,\ldots,z_p$ where $z_i = \sum_{j=1}^{p} v_{ij}x_j$. Taking $\boldsymbol{v}_i = (v_{i1},\ldots,v_{ip})^{\prime}$, $\boldsymbol{V} = (\boldsymbol{v}_1,\ldots,\boldsymbol{v}_p)$ and $\boldsymbol{L} = \mathrm{diag}(l_1,\ldots,l_p)$, where $l_1 \geq \cdots \geq l_p \geq 0$, we can obtain $\boldsymbol{V}$ and $\boldsymbol{L}$ from the spectral decomposition of $\boldsymbol{S}$ (where $\boldsymbol{S}$ is the variance–covariance matrix). The usual scaling adopted is such that $\boldsymbol{S} = \boldsymbol{VLV}'$ where $\boldsymbol{V}'\boldsymbol{V} = \boldsymbol{I}$ and the principal component scores are given by the $(n \times p)$ matrix $\boldsymbol{z} = \boldsymbol{XV}$.

All the required matrices can be obtained from the SVD decomposition of $\boldsymbol{X}$:

$$\boldsymbol{X} = \boldsymbol{UDV}' \quad (1)$$

where $\boldsymbol{U}'\boldsymbol{U} = \boldsymbol{I}_{p'}$, $\boldsymbol{VV}' = \boldsymbol{V}'\boldsymbol{V} = \boldsymbol{I}_p$ and $\boldsymbol{D} = \text{diag}(d_1, \ldots, d_p)$, with $d_1 \geq \cdots \geq d_p \geq 0$.

If the (i, j)th elements of the matrices $\boldsymbol{X}$ and $\boldsymbol{U}$ by x_{ij} and u_{ij}, respectively, decomposition 1 has the following elementwise representation:

$$x_{ij} = \sum_{t=1}^{p} u_{it} d_t v_{tj} \quad (2)$$

Thus, if the data structure is essentially m-dimensional, then variation in the remaining $(p - m)$ dimensions can be treated as random noise and we can postulate the system is described by Eq. 2 plus a residual error e_{ij}.

The optimum number of PCs can be obtained from the associated statistic [6,16–18]:

$$W_m = \frac{\text{PRESS}(m-1) - \text{PRESS}(m)}{DF_m} \Bigg/ \frac{\text{PRESS}(m)}{DF_r} \quad (3)$$

where W_m represents the increase in predictive information supplied by the mth component, divided by the average predictive information in each of the remaining components. Thus "important" components should yield values of W_m greater than unity.

W_m calculations make use of special algorithms to avoid typical problems associated with classical cross-validation techniques, e.g., that each point cannot be at the same time in the objective function and the adjustable matrix [16].

PRESS is named the "predicted residual sum of squares" and can be interpreted (in a gross way) like the sum of squares errors in typical linear regression. The lower the values in PRESS, the greater is the similarity between the two data spaces that are being compared. DF_r, and DF_m are the corresponding degrees of freedom [17,18].

5. Results and discussion

Because the data set was selected from normalized reports, some variables have standard deviations equal to zero because they have been reported as less than the LOD. Variables suffering from this fact are listed in Table 2; they were deleted from the statistical studies. These variables would not be selected as the most important ones and they are omitted from the studies by the software.

Only NO_2^- and NH_4^+ have values greater than the LODs in two wells with high COD and NO_3^- values, so the values associated with ammonium and nitrites are not given real independent information. These two variables were not included in the multivariate studies. If we find more values greater than the LOD, it would be better and useful to apply some kind of "filter" to evaluate if these truncated variables are or are not really important. Several techniques can be used, and some of them have recently been reviewed by Hesel [20]. We are most interested in the techniques described by Grimalt and co-workers [21–23]. The latter group followed a stepwise procedure involving identification of strongly censored variables, autoscaling, iterative FA, checks for outliers and iterative FA after outlier exclusion. However, they were not concerned with original variable selection. We did not apply such techniques because the LODs listed in Table 2 were not exceeded except in the two wells cited above.

According to Spanish Legislation for Drinking Water [1], several samples have shown parameter concentrations exceeding recommended values (Guide Values in Spanish and European Community legislation). High values have been observed for pH, Cl^-, NO_3^- and Pb. They could suggest that affected samples have suffered some kind of contamination.

The calcareous and semi-arid nature of the soil can explain the high alkalinity and chloride contents found in some samples. Soil solution and fertilizers can contribute to high nitrate concentrations. Usually this parameter is associated with other salinity factors in waters of poor quality. Most of the samples do not have significant Pb contents, although some of them show more than 0.100 mg l^{-1}. These contents are probably due to diffused external causes: home wastewaters, roadways, cowsheds, etc.

Every statistical study was applied to each of

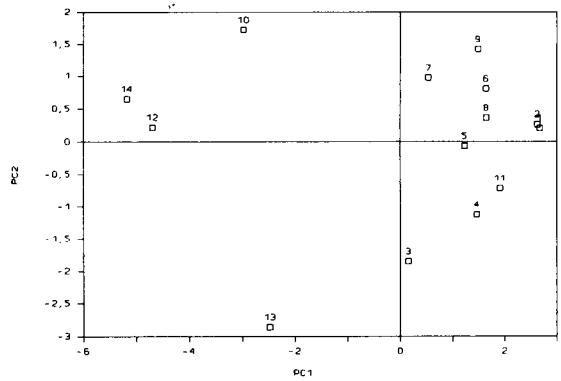

Fig. 1. Sample distribution in PC1–PC2 space (RESMUM data).

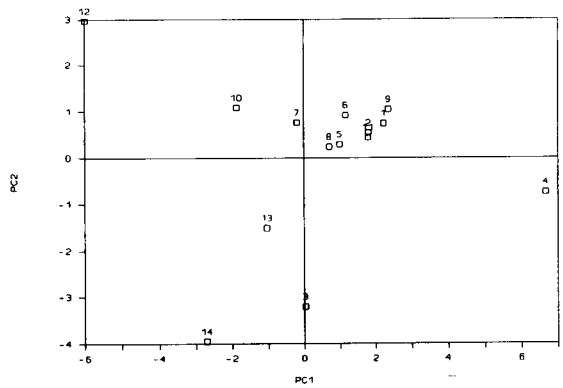

Fig. 3. Sample distribution in PC1–PC2 space (RESMU1 data).

the six data sets. In this way, water quality can be evaluated for each season, and possible changes in water composition during the year can be observed.

The following discussion is centred on these values, which are illustrated in Figs. 1 and 2. The discussion for each sampling time is analogous and is exemplified by Figs. 3 and 4; they correspond to the RESMU1 data set.

First, a principal component analysis was made using the SVD technique and the seasonal and average value data matrix. In the sample scores output, investigations were made to find and correct outlier data. Subsequently, an SVD was again performed and the optimum number of PCs was selected according to the W_m statistic.

For the RESUM data, the PCs selected were five and they explained about 88.5% of the variance. Fig. 1 shows the sample distribution in the sub-space PC1–PC2.

Once the number of PCs had been determined, it was used as the basis for the procrustes rotations. Krzanowski [18] recommended the selection of one more variable than the fixed number of PCs for a good characterization of the system, so the subset of selected variables will have six. Table 3 shows the selected subset for each data set.

To test the likelihood of the subsets selected, a final principal component determination was performed including data from the six selected variables. Fig. 2 shows the distribution of samples in this new (PC1′–PC2′) subspace.

Good agreement is observed between Figs. 1 and 2. The fact that samples 1, 2, 3 and 4 have

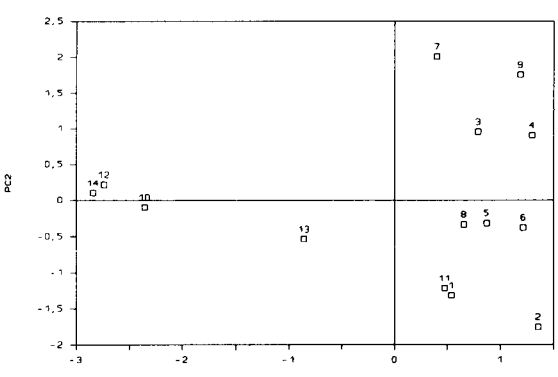

Fig. 2. Sample distribution in PC1′–PC2′ from retained variables (RESMUM data).

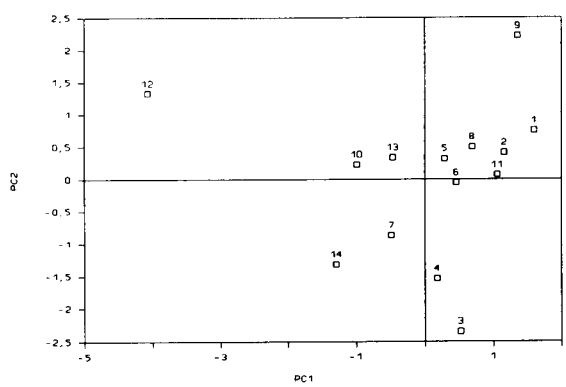

Fig. 4. Sample distribution in PC1′–PC2′ from retained variables (RESMU1 data).

Table 3
Selected variables for each data set

Data set	Selected variables					
RESMU1	COD	Cl^-	HCO_3^-	NO_3^-	Mg	Zn
RESMU2	COD	Cl^-	NO_3^-	Conductivity	Zn	Pb
RESMU3	COD	Cl^-	Na	Ca	Zn	Pb
RESMU4	SO_4^{2-}	HCO_3^-	CO_3^-	NO_3^-	K	Zn
RESMU5	HCO_3^-	NO_3^-	Mg	Dry residue	SiO_2	Pb
RESMUM	Cl^-	HCO_3^-	NO_3^-	Dry residue	Zn	Pb

changed their spatial locations (i.e., the sign of the scores) is attributed to the simplification of the dimensional space (i.e., the remaining variables have in fact information). In this case, the change in the score sign occurs in the second PC. Often, the change in the score sign between different studies of the same data is not considered important.

An interesting pattern observed in all the studies is that procrustes analyses conducts to groups of variables that, when a new PCA is performed on them, will define smaller sample clusters (intra-cluster distances). This is an interesting conclusion because it seems that "noise information" is avoided and the possible groups of samples are better "clustered". On the other hand, one possible disadvantage of this technique is that it seems that the inter-cluster distances are decreased (i.e. a small amount of information is lost). These facts were predicted as we are taking off variables (information) and minor differences are deleted (i.e., we are looking for major differences).

Neverthless, in our experience, the general patterns and even the main groups of samples are always retained and this is the most important fact because it indicates that these techniques work correctly.

To confirm this effect, and also the likelihood of the studies, Figs. 3 and 4, associated with RESMU1 values, are presented and it can be seen the above moving effect is not very important. Similar patterns can be obtained in the rest of the data sets (not shown here).

Hence the six selected variables (Table 3) in each of the seasonal samplings are acceptable subsets for monitoring the aquifer system under study. In the absence of unexpected contamination events (e.g., pesticide pollution), they can be considered as the groundwater quality variables to be measured in future sampling exercises.

The laboratory benefits of only having to measure six variables (e.g., COD, Cl^-, HCO_3^-, NO_3^-, Mg and Zn) instead of the initial 29 are obvious: decreases in workloads, analysis time, reagents costs, etc. These are important questions in governmental national surveillance departments or in independent laboratories. Such laboratories can save a lot of effort, money and time if they model several geographical areas (e.g., using some initial seasonal samplings) and subsequently analyse the selected variables.

We consider that only two major problems need to stressed: (i) if a contamination occurs in a parameter not selected (e.g., Hg), the pollution event will not be detected; this problem was discussed at the beginning of this paper; (ii) periodically (e.g., once a year) some Spanish national surveillance departments have to make "total water analyses" where the statistical studies cannot be applied. The latter problem is not really serious, in fact, the data obtained in the "total studies" will provide a very good opportunity to test our model (preferably selecting the most adequate predefined seasonal model).

5.1. Individual samplings

The results of the statistical studies are summarized in Table 3 and (as an example) in Figs. 3 and 4. For ease of comparison, a unification of the number of selected variables was performed. The number of retained variables was in all instances six. Interesting conclusions can be derived from Table 3.

In winter and spring samplings (RESMU1 and RESMU2), the common "important" variables are COD, Cl^- and NO_3^-. This may be a consequence of the decomposition of organic materials deposited in soils and water during the autumn period. It was assumed that organic matter came from agricultural and wild plants.

In summer samplings (RESMU3 and RESMU4 data), more geological influence is assigned to the great importance of HCO_3, dry residue, Mg and SO_4. A decreased water flow was observed in this season owing to the summer weather characteris-

tics. In the June sampling, beginning of the summer (RESMU3 data), it can be observed that there are similarities with RESMU2 data (spring). This could be predicted as RESMU2 was obtained in the latter part of April and RESMU3 in the middle of June. Hence, as expected, to characterize summer time, summer sampling will be done in September (RESMU4) rather than in June.

The influential presence of Zn and Pb during the entire year is attributed to external contamination sources (probably due to cattle-wastes) and the great variability in the experimental data they show.

A characteristic that must be emphasized is the different depths of the aquifer sampling points. This characteristic can be important in the interpretation of the different Zn and Pb values. The less deep are the wells, the less contamination can be observed. The most important identified sources of Pb were located near cities and highroads (they can both involve diffused contamination and disturb surface waters, e.g., rivers and brooks). An important source of Zn was not identified. Probably the most important source of Zn is in agricultural fertilizers (natural and synthetic) or some kind of unidentified waste waters.

As was suggested by one of the referees, a further step could be very interesting. The idea is to perform PLS to predict the variables that have been not retained. This approximation was not considered here because it was beyond the scope of our work as we were more interested in modelling the local area rather than predicting single values. In fact, the PLS problem is different from that studied here. In general, in environmental or even industrial product characterization, there does not exist a mathematical function that allows us to use PLS, discriminant functions, optimization techniques, etc.

6. Conclusions

Application of SVD techniques and the W_m statistic allows a fast and easy determination of the number of principal components. The need for the optimum selection of the PC number arises from its use to implement procrustes rotation techniques. Of the initial 29 variables, six were selected to describe the system during five seasonal samplings, one subset in each season.

Acknowledgement

The authors thank Professor W.J. Krzanowski, University of Exeter (UK), for his kind help and useful suggestions.

References

[1] Spanish Official Bulletin, BOE September 20th–4 (1990).
[2] T.W. Shattuck, M.S. Germani and P.R. Buseck, Anal. Chem., 63 (1991) 2646.
[3] R.C. Tabony, Meteorol. Mag., 115 (1986) 229.
[4] R. Tsao and K.J. Voorhees, Anal. Chem., 56 (1984) 368.
[5] P. Pistikopoulos, H.M. Wortham. L. Gomes, S. Masclet-Beyne, E. Bon Nguyen, P.A. Masclet and G. Mouvier, Atmos. Environ., 24A (1990) 2573.
[6] D.W. Osten, J. Chemometr., 2 (1988) 39.
[7] R.J. Harris, A Primer of Multivariate Statistics, Academic, London, 2nd edn., 1985.
[8] J.M. Deane and H.J.H. MacFie, J. Chemometr., 3 (1989) 477.
[9] J.M. Andrade, D. Prada, S. Muniategui, B. Gomez and M. Pan, J. Chemometr., 7 (1993) 427.
[10] W.J. Krzanowski, Principles of Multivariate Analysis; a User's Perspective, Oxford University Press, Oxford, 1990.
[11] P.J. Gemperline, K.H. Miller, T.L. West, J.E. Weinstein, J.C. Hamilton and J.T. Bray, Anal. Chem., 64 (1992) 523.
[12] S. Wold, P. Geladi, K. Esbensen and J. Öhman, J. Chemometr., 1 (1987) 41.
[13] Standard Methods for the Examination of Water and Wastewater, APHA, AWWA and WPCF, 18 edn., 1986.
[14] J. Rodier, Análisis de las Aguas, Omega, Barcelona, 1981.
[15] A. Lorber, L.E. Wangen and B.R. Kowalski, J. Chemometr., 1 (1987) 19.
[16] C.M. Cuadras, Métodos de Análisis and Multivariante, EUNIBAR, Barcelona, 1981.
[17] H.T. Eastman and W.J. Krzanowski, Technometrics, 24 (1982) 73.
[18] W.J. Krzanowski, Biometrics, 43 (1987) 575.
[19] W.J. Krzanowski, Appl. Stat., 36 (1987) 22.
[20] D.R. Hesel, Environ. Sci. Technol., 24 (1990) 1766.
[21] J.O. Grimalt and J. Olive, Anal. Chim. Acta, 278 (1993) 159.
[22] J.O. Grimalt, L. Canton and J. Olive, Chemometr. Intell. Lab. Syst., 18 (1993) 93.
[23] J.O. Grimalt, L. Canton and B. Alonso, Environ. Sci. Technol., 26 (1992) 2240.

ELSEVIER

Analytica Chimica Acta 292 (1994) 263–273

ANALYTICA CHIMICA ACTA

A lead-selective extraction chromatographic resin and its application to the isolation of lead from geological samples

E. Philip Horwitz [a,*], Mark L. Dietz [a], Susan Rhoads [a,1], Claudia Felinto [a,2], Noel H. Gale [b,*], Judith Houghton [b]

[a] *Chemistry Division, Argonne National Laboratory, Argonne, IL 60439, USA*
[b] *Isotrace Laboratory, University of Oxford, Oxford, UK*

(Received 13th December 1993; revised manuscript received 28th January 1994)

Abstract

A novel extraction chromatographic resin comprised of a 0.75 M solution of the macrocyclic polyether bis-4,4′(5′)-[*tert.*-butylcyclohexano]-18-crown-6 in isodecanol supported on an inert, polymeric substrate for the separation and preconcentration of lead from acidic media is described. The material is shown to retain lead efficiently and selectively over a wide range of nitric acid concentrations. Sorbed lead is readily recovered using any of a variety of complexing agents. The resin is demonstrated to be sufficiently stable to handle large sample volumes or to permit reuse. Application of the resin to the isolation of lead from geological samples for subsequent mass spectrometric determination of isotopic ratios is described.

Key words: Chromatography; Mass spectrometry; Extraction resin; Geological samples; Lead

1. Introduction

The potential adverse human health effects associated with exposure to lead have long been recognized [1–3]. Accordingly, there has been considerable interest in the development of methods for its determination in various biological and environmental samples [4–6]. The determination of individual lead isotopes or of isotopic ratios in various samples has also been of frequent interest. Lead-210 and its radioactive decay products (e.g., ^{210}Bi and ^{210}Po), for example, have served as valuable tracers for monitoring atmospheric, oceanic, and terrestrial processes [7]. Similarly, lead isotope ratio measurements (e.g., ^{206}Pb/^{207}Pb) have permitted the identification of the source of lead contamination in a variety of samples, ranging from household dust to the blood of children [8,9], and are of great interest in isotope geology [10], ore prospection [11], and archaeological science [12]. Although several extremely sensitive methods exist for lead quantitation (e.g., graphite furnace atomic absorption for total lead, thermal ionization mass spectrometry

* Corresponding author.

[1] Participant in the Summer 1992 Student Research Participation Program from Judson College, Elgin, IL, USA.

[2] Permanent address: Universidade de Sao Paulo, Instituto de Quimica, Sao Paulo, Brazil.

SSDI 0003-2670(94)00068-W

(TIMS) for individual isotopes), the complexity of many sample matrices can preclude their direct application. As a result, an important step in many lead determinations is an initial separation and/or preconcentration, both to free it from inert matrix constituents and to reduce the potential for interference.

A variety of methods have been proposed to effect this separation and preconcentration, among them solvent extraction [13], ion-exchange [14], extraction chromatography [15], precipitation [16] and combinations thereof [7]. In many instances, however, these methods suffer from one or more drawbacks which limit their utility. Solvent extraction, for example, is far too cumbersome for routine use on large numbers of samples. Similarly, the lack of selectivity of conventional ion exchange resins complicates separations. Moreover, these methods are typically ineffective for highly acidic samples.

Earlier work in this laboratory directed at the development of improved methods for the removal and recovery of strontium-89 and -90 from nuclear waste solutions has led to a novel extraction chromatographic material (Sr · Spec™) for the separation and preconcentration of radiostrontium from aqueous solutions containing a wide range of nitric acid concentrations (1–8 M). Recently, this material, which is comprised of a solution of a macrocyclic polyether in 1-octanol, has also been shown to exhibit extremely strong retention of lead under a wide range of solution conditions [17], too strong, in some instances, for convenient stripping. In an effort to develop an extraction chromatographic resin which exhibits satisfactory lead retention from nitric acid-containing aqueous phases yet which permits ready removal of sorbed lead, we have examined lead uptake by a modified version of the Sr · Spec™ resin based upon a higher molecular weight alcohol. In this report, we present a systematic evaluation of the selectivity of this new material for lead over selected elements and of the effect of macro levels of several elements on lead retention. In addition, we examine the elution behaviour of a variety of common metal ions on a column of this material and compare the effectiveness of various stripping agents for the removal of sorbed lead. Finally, we describe the application of this new material to the mass spectrometric determination of lead isotopes in geological samples.

2. Experimental

2.1. Reagents

The crown ether, bis-4,4′(5′)-[*tert.*-butylcyclohexano]-18-crown-6 (abbreviated as DtBuCH18C6), was obtained from Parish Chemical Co. (Orem, UT) and purified via recrystallization from methanol. Nitric acid was Ultrex II grade (J.T. Baker, Phillipsburg, NJ). All water was obtained from a Milli-Q2 system. Unless otherwise noted, all other reagents were A.C.S. reagent grade and were used as received.

2.2. Procedures

Preparation of extraction chromatographic resin

The extraction chromatographic material was prepared by impregnating Amberchrom™ CG-71md resin (Supelco, Bellefonte, PA) with a 0.75 M solution of DtBuCH18C6 in isodecanol using a procedure such as that described previously [18]. The resultant lead-selective chromatographic resin is now commercially available as Pb · Spec™ (for lead specific) from EIChroM Industries (Darien, IL).

Determination of weight distribution ratios and column characteristics

Radiochemical experiments were performed using the tracers and methods described in a previous report [17]. The activity levels employed (typically 10^4 to 10^6 cpm total) were chosen both to simplify handling of the radiotracers involved and to yield acceptable counting statistics in a reasonable time (< 30 min per sample). A detailed description of the measurement of weight distribution ratios, column capacity factors, and matrix effects has been given previously [17]. Column preparation and characterization were performed as outlined in an earlier report [17].

Elution behaviour of selected elements

The elution behaviour of a number of cations on the Pb · Spec™ resin was evaluated by introducing to a column of the material (bed volume = 1.0 ml; bed height = 2.5 cm) a 600 μl portion of a multi-element stock solution consisting of more than two dozen metal ions in 1 M nitric acid. (A detailed description of the solution composition can be found in Ref. 19.) The elements included were selected because of their presence in various environmental or biological samples or because of literature indicating their interaction with 18-crown-6-based macrocycles [20]. The sample was then eluted with 0.1 M nitric acid and the eluent collected in a series of 6.35 ml [ca. 10 free column volume (FCV)] aliquots until approximately 60 FCV had been gathered. The elutrient was then changed to 0.1 M ammonium oxalate and ca. 10 FCV were again collected. A portion of each of these fractions was then subjected to analysis by ICP-AES [21] or atomic absorption. The elution behaviour of various alkali and alkaline earth elements was similarly determined using a second stock solution containing only these elements. The composition of this solution was such as to permit ready detection of each element by ICP-AES or atomic absorption while not exceeding 5% of the column capacity (Table 1). Flow rates were maintained at 1–2 ml cm^{-2} min^{-1} throughout.

Table 1
Characteristics of lead-selective extraction chromatographic material and packed columns

Bulk material	
Stationary phase	0.75 M DtBuCH18C6 in isodecanol (p = 0.917 g/ml)
Support	Amberchrom™ CG-71
Particle size	50–100 μm
Extractant loading	40% (w/w)
Density of extractant-loaded beads	1.16 g/ml.
Packed columns	
V_s, ml/ml of bed	0.16
Bed density (g/ml)	0.37
V_m, ml/ml of bed (also FCV)	0.65 (Cs-137 breakthrough) 0.68 ($V_{bed} - V_{resin}$)
V_s / V_m	0.24
Capacity	
calculated, mg Pb/ml of bed	24.86
experimental, mg Pb/ml of bed	20.5

Stripping of sorbed lead

To compare the effectiveness of various stripping agents for the removal of lead from a Pb · Spec™ column, an aliquot of a ^{210}Pb tracer was applied to the column and the column rinsed with ca. 60 FCV of 0.1 M nitric acid to simulate removal of matrix constituents. The elutrient was then changed to any of a variety of stripping agents (e.g., 0.1 M ammonium oxalate solution) and a series of 0.5–1 FCV aliquots of column effluent were collected until either no appreciable lead was detected or 100 FCV had been reached.

Resin stability

To evaluate the stability of the Pb · Spec™ resin, the elution profile of a ^{85}Sr tracer (a convenient gamma-emitting stand-in for lead) was measured on a new Pb · Spec™ column using 1 M nitric acid as the elutrient. After elution was complete, the column was rinsed with a large volume (1000–2000 FCV) of deionized water and reconditioned with 1 M acid. The strontium elution profile was then remeasured. Changes in the location of the peak maximum and in peak width were taken as indications of a change in the condition of the column.

Blank minimization for geological samples

To achieve the sub-nanogram blanks required in the isolation of lead from geological samples for thermal ionization mass spectrometry, all experiments involving such samples were performed in better than Class 100 chemical workstations located inside a suite of Class 1000 overpressured clean rooms. For the same reason, all chemistry was carried out using Teflon–FEP™ ion-exchange columns and Teflon–PFA™ vessels (Savillex™, Minnetonka, MN). Ammonium carbonate was chosen for the removal of sorbed lead from the Pb · Spec™ columns (vide infra). Because the purest available form of this reagent (Normatom™ aqueous ammonium carbonate) was found to contain unacceptable levels of lead, however, a preliminary purification was carried

Table 2
Elution behaviour of various elements on the lead-selective resin [a]

	Percent of element found in FCV number						
	0.1 M HNO_3						0.1 M AOX [b]
Element	1–10	11–20	21–30	31–40	41–50	51–60	61–70
Li	100						
Na	96	< 1	< 1	1	< 1	< 1	< 1
K	100	–	–	–	–	–	–
Rb	100	–	–	–	–	–	–
Cs	100	–	–	–	–	–	–
Mg	100	–	–	–	–	–	–
Ca	100	–	–	–	–	–	–
Sr	100	–	–	–	–	–	–
Ba	100	–	–	–	–	–	–
Al	100	–	–	–	–	–	–
Cr	100	–	–	–	–	–	–
Mn	100	–	–	–	–	–	–
Fe	100	–	–	–	–	–	–
Co	100	–	–	–	–	–	–
Ni	100	–	–	–	–	–	–
Cu	100	–	–	–	–	–	–
Zn	100	–	–	–	–	–	–
Y	100	–	–	–	–	–	–
Zr	100	–	–	–	–	–	–
Mo	100	–	–	–	–	–	–
Ru	100	–	–	–	–	–	–
Rh	100	–	–	–	–	–	–
Pd	58	–	24	18	–	–	–
Ag	100	–	–	–	–	–	–
Cd	100	–	–	–	–	–	–
La–Eu	100	–	–	–	–	–	–

[a] Column parameters: particle size = 50–100 μm; bed volume = 1.0 ml; height = 2.5 cm; 1 FCV = 0.66 ml; load solution volume = 0.60 ml; load solution contained 0.1 M oxalic acid to solubilize zirconium.
[b] AOX = ammonium oxalate.

out using Diphonix™ (EIChroM Industries, Darien, IL), a new chelating cation exchange resin capable of selectively removing a wide range of transition and post-transition elements [including Pb(II)] from solutions containing high salt concentrations [22,23]. Briefly, a rigorously precleaned Teflon–FEP™ ion-exchange column (6 mm i.d.; 15 ml reservoir) was packed with Diphonix™ to a height of 27 cm (corresponding to a bed volume of ~ 7.63 ml). Traces of lead were removed from the column by passing through 95 ml of a 1 M solution of Ionquest-201 (Albright and Wilson, Richmond, VA) at a rate of 0.5 ml/min. The last 10 ml of solution were left in the column overnight. The column was then eluted with 83 ml of 3 M hydrochloric acid and rinsed with ~ 10 ml of water to pH 5. The column was then preconditioned with 14 ml of 2 M ammonium chloride, followed by 36 ml of 2 M isothermally distilled ammonia. Next, 14 ml of 1 M ammonium carbonate (Normatom™) were passed through the column and discarded. An additional 100 ml portion was then passed through and collected. From this purified material, a working solution of purified 0.2 M ammonium carbonate was prepared by dilution with Milli-Q water.

Purification of the Pb · Spec™ resin supplied by EIChroM (50–100 μm "Pb Spec SPS") to remove traces of lead was also found to be necessary to achieve the required blank levels. Advantage was taken of the ability of sulfuric acid to

strip lead from the resin (see Table 3), since this reagent can be obtained in a very pure state. Repeated batch cleaning of the resin was carried out with 0.2 M sulfuric acid (Romil/Seastar) in closed Teflon–PFA™ vessels, stirred with Teflon™–enclosed stirrer bars on a magnetic stirrer plate.

Lead determination in ore samples by TIMS

For the analysis of ore samples by TIMS, complete sample dissolution was achieved by treating a 1 g portion of each ore with nitric and hydrochloric acids in succession in closed Teflon–PFA™ vessels in a microwave oven (CEM™ Ltd., Buckingham) [24]. The solute was converted to the nitrate form by two successive evaporations with 0.5 ml portions of 3 M nitric acid. The residue was then dissolved in 3–6 M nitric acid.

For the isolation of lead from the dissolved ore samples, batch-cleaned Pb · Spec SPS™ was packed into a 0.24 cm i.d. Teflon–FEP™ ion-exchange column having a porous polyethylene frit and a 3 ml reservoir to yield a 0.14 ml bed. The resin was further cleaned by passing through 20 column volumes of 0.2 M sulfuric acid, then leaving the column to soak overnight in this reagent. The column was then washed with water (four 0.2 ml aliquots) to neutrality, then with 0.5 ml of 3 M nitric acid. The centrifuged sample solution (in 3–6 M nitric acid) was then loaded onto the column. The loaded resin was washed with five 0.5 ml aliquots of 3 M nitric acid to remove matrix constituents. This was followed by four water washes (0.2 ml each) to remove nitric acid and raise the pH of the column effluent to 4, thereby facilitating lead stripping. Sorbed lead was then removed from the column with three 1 ml portions of 0.2 M ammonium carbonate (~ 33 FCV) and the column effluent collected in a Teflon–PFA vessel. The strip solution was evaporated to dryness and the ammonium carbonate sublimed away by heating the vessel in a heating block maintained at 155°C. Upon completion of the sublimation, a drop of 8 M nitric acid was added to the vessel (still at 155°C) and the resultant solution taken to dryness to eliminate any trace of organic matter and to convert the sample to the nitrate form. If necessary, this treatment was repeated a second time. Finally, the sample was taken up in 4 μl of 0.1 M nitric acid and loaded with 1 μl of 1 M phosphoric acid and 2 μl of silica gel [25] onto the center of a zone-refined rhenium filament for mass spectrometry.

Table 3
Efficiency of lead stripping from a Pb·Spec™ column by selected reagents

Stripping agent [a]	Peak maximum (FCV)	Peak width [b] (FCV)	Total elution volume [c] (FCV)
Sulfuric acid	4.0	2.5	8.5
Ammonium oxalate (pH 6.4)	1.7	0.4	2.7
Ammonium sulfate (pH 6.0)	6.0	13	30
Ammonium tartrate (pH 6.7)	2.0	broad	–
Ammonium citrate (pH 5.1)	2.0	1.5	3.5
Ammonium carbonate (pH 9.1)	7.0	broad	–
EDTA (pH 7.5)	1.3	0.3	2.0
Glycine (pH 9.5)	2.0	0.5	4.0
DTPA (saturated; pH 7.5)	2.0	0.5	3.5

[a] 0.1 M solution unless otherwise noted.
[b] At $1/e$ of the peak maximum.
[c] At 1% of peak maximum.

The yield of this method was estimated using a synthetic ore sample containing 13% copper and 12% iron. Specifically, a 1 g sample of this synthetic mixture was spiked with 10 μg of the NIST Pb Isotopic Standard Reference Material (SRM) 981 and subjected to the above-described dissolution/separation procedures. The recovery of lead was evaluated via isotope dilution mass spectrometry after spiking the eluate from the Pb · Spec™ column with highly enriched ^{207}Pb.

2.3. Apparatus

For thermal ionization mass spectrometry, a modified VG Isotech (Middlewich) Isolab 54 computer-controlled three-stage (E–B–E) mass spectrometer equipped with seven Faraday collectors and a Daly ion counting detector system was used. The instrument was used in the static multicollector mode [26].

3. Results and discussion

3.1. Acid dependency of metal ion sorption / resin selectivity

In an earlier report [27], it was demonstrated that the extraction of strontium by dicyclohexano-18-crown-6 into any of a wide range of oxygenated, aliphatic solvents from nitric acid is directly related to the solubility of water in the solvent. For a given solvent family (e.g., alcohols), this solubility, in turn, was found to decrease with increasing solvent molecular weight. Thus, strontium extraction was found to decrease when, for example, *n*-hexanol was replaced by *n*-octanol as the organic solvent. If this correlation applies to the extraction of other metal ions by crown ethers, it would be expected that the sorption of lead by a crown ether-based extraction chromatographic resin could be reduced as desired simply by changing the solvent to one with a higher molecular weight. In fact, as anticipated, a resin prepared from a 0.75 M solution of DtBuCH18C6 in isodecanol yields D_w values for lead as much as four times lower than those obtained with Sr Spec™ [17], prepared using *n*-octanol as the diluent. Table 1 summarizes the essential features of this new resin.

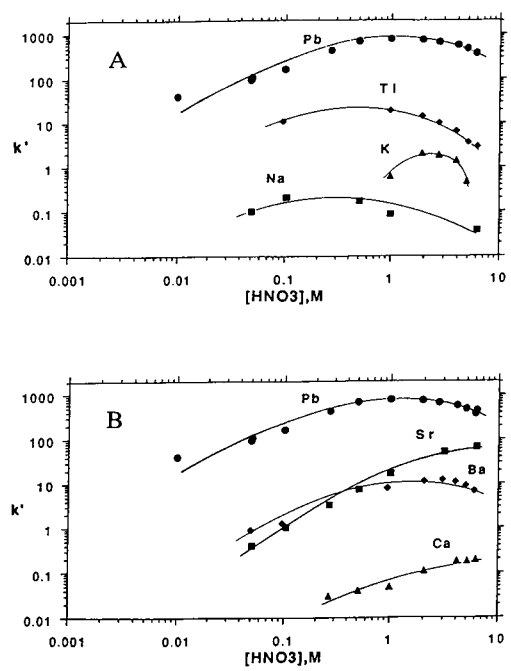

Fig. 1. Nitric acid dependency of k' for selected monovalent (A) and divalent (B) metal ions on Pb·Spec™ resin. (Cs^+ retention is not measureable under the experimental conditions.)

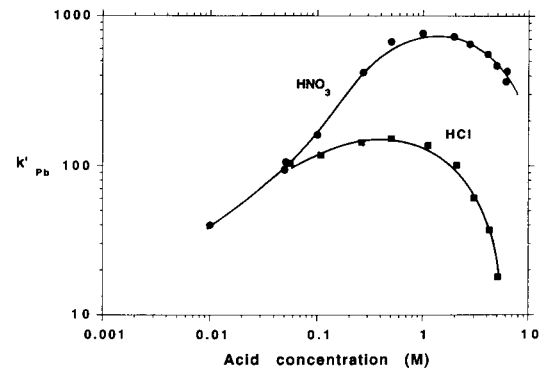

Fig. 2. Nitric acid and hydrochloric acid dependencies of k' for lead on Pb·Spec™ resin.

Fig. 1 shows the nitric acid dependence of the capacity factor, k', for selected metal ions on the Pb Spec™ resin. (These ions were chosen on the basis of literature data indicating the possibility of strong interaction with 18-crown-6-based macrocycles [20] or, as in the case of sodium, because of their presence in macro quantities in many biological and environmental samples.) As can be seen, k'_{Pb} exceeds that of each of the other metal ions by a wide margin over the entire range of acidities examined. In fact, in several instances, (e.g., Cs^+ and Na^+), the ion is essentially unretained under typical column loading conditions (0.1–3 M HNO_3). The excellent selectivity of the resin over sodium is especially significant given the ubiquitousness of this element. Also significant is the low capacity factor of the resin for calcium, an element present in substantial quantities in many biological and environmental samples.

Lead is also readily sorbed from hydrochloric acid solution (Fig. 2). Although the maximum k'_{Pb} observed is approximately a factor of five lower than that obtained from nitric acid, lead retention is still more than adequate for many purposes.

Table 2 summarizes the elution behaviour of a variety of different elements on a 1 cm^3 bed volume column packed with the Pb · Spec™ chromatographic resin. The data in this table indicate that the resin is quite selective for lead. In fact, under the load and rinse conditions, only lead exhibits significant retention. These results are consistent with the data presented in Fig. 1.

3.2. Matrix effects

It is well known that even elements which exhibit modest retention on an extraction chromatographic column may, if present in sufficiently large quantities (so as to approach the column capacity), reduce the sorption of a more strongly retained species. Sodium, potassium, calcium, iron, and aluminum are the major constituents of many environmental and biological samples [17]. The effect of increasing amounts of several of these matrix constituents on k'_{Pb} was therefore measured to establish the level of these constituents which could be tolerated without appreciably diminishing lead sorption. (Iron and aluminum were omitted because their extractability by DtBuCH18C6 has been shown to be less than that of sodium and calcium [28].) The results indicate that sodium and calcium concentrations of even 1 M produce no measurable effect upon k'_{Pb} from 1 M nitric acid. Concentrations of potassium ion exceeding 0.05 M, however, produce a significant decrease in lead sorption (Fig. 3). Nonetheless, even at 1 M K^+, more than 80 FCV of 1 M nitric acid are required to reach the peak maximum in lead elution. Note that these results parallel those observed for strontium on the Sr · Spec™ resin [17]. This fact, along with the results of our earlier studies of the effect of macro levels of ammonium ion on Sr · Spec™[17], suggests that high concentrations (> 0.1 M) of ammonium ion will also reduce lead sorption on the Pb · Spec™ resin, although not to the extent observed with potassium ion.

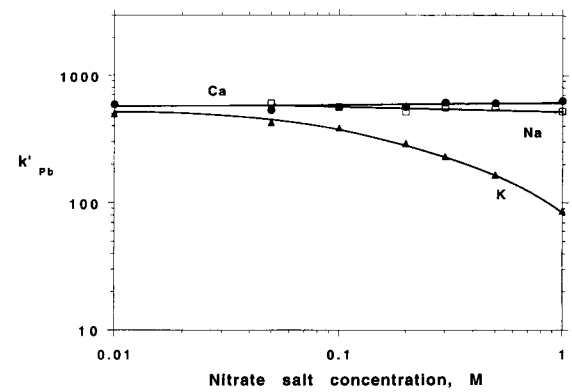

Fig. 3. Effect of matrix constituents on lead sorption by Pb·Spec™ resin.

3.3. Stripping of sorbed lead

It is clear from the data presented in Fig. 1 that sorbed lead will not be efficiently stripped from a Pb · Spec™ column simply by reducing the nitric acid concentration in the mobile phase, as lead is reasonably well retained from even 0.01 M nitric acid. A variety of reagents were therefore evaluated for possible use as stripping agents. Table 3 summarizes the results obtained with a number of these reagents, expressed as the number of free column volumes to the peak maximum (k') and the width of the peak at $1/e$ of the peak maximum, both indicators of the efficiency of lead removal. The results show that satisfactory stripping of sorbed lead can be achieved with any of several of them, including 0.1 M solutions of ammonium oxalate, ammonium citrate, or glycine. Of these, ammonium oxalate solution is especially useful, as in addition to providing efficient stripping, it can be readily removed via sublimation once the column effluent has been evaporated to dryness. Note however, that this reagent is only suitable for use with trace amounts of lead because of the low solubility of lead oxalate [29]. Note also that under certain circumstances, the use of ammonium carbonate is preferred, despite its poor performance relative to other stripping agents (see below). Removal of macro concentrations of lead is probably best accomplished using a solution of DTPA or ammonium citrate.

3.4. Resin stability

Fig. 4 summarizes the results of studies of the stability of the resin to prolonged water washing

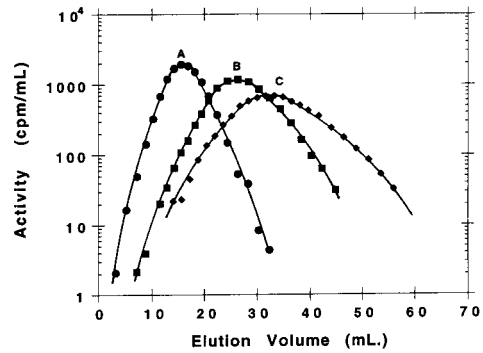

Fig. 4. Effect of column washing on strontium-85 elution on Pb·Spec™ resin.

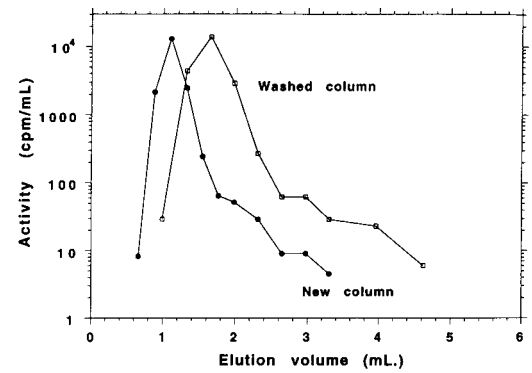

Fig. 5. Effect of column washing on lead stripping from Pb·Spec™ resin.

(i.e., large sample volumes). Curve A depicts the elution profile for a ^{85}Sr tracer on a new Pb Spec™ column, while curves B and C show the profiles obtained on the same column after ca. 1000 and 2000 FCV of water washing, respectively. As can be seen, column washing is accompanied by a pronounced shift in the peak maximum to higher elution volumes, an observation consistent with loss of diluent (here, isodecanol) and a concomitant increase in the concentration of the crown ether in the stationary phase. This shift is accompanied by an increase in peak width (Table 4). The column efficiency, however, as reflected in the number of theoretical plates present [30], is unaffected by 1000 FCV of washing and is reduced only slightly by more extensive washing. It is worth noting here that ~ 1000 FCV of washing leads to a significant (~ 33%) reduction in column efficiency for the analogous extraction chromatographic resin employing the more water-soluble 1-octanol as the diluent [31].

Table 4
Effect of column washing on the elution behaviour of ^{85}Sr on Pb·Spec resin [a]

Wash volume (FCV)	Peak maximum (ml)	Peak width [b] (ml)	N [c]
0	15.5	9.0	23.5
1000	26.4	15.4	23.5
2000	33.2	21.2	19.6

[a] Wash solution = deionized water; 1 FCV = 0.66 ml; ^{85}Sr tracer eluted with 1 M HNO_3; T = 23°C; flow rate = 1–2 ml cm^{-2} min^{-1}.
[b] At 1/e of the peak maximum.
[c] Calculated from $N = 8\,(V_{mr}/W)^2$, where V_{mr} is the elution volume to peak maximum and W is the peak width at $1/e$ of the peak maximum (from Ref. 30).

As a further check of the effect of column washing upon resin performance, the stripping of lead from a column of unused Pb Spec™ and from a column of the same resin washed with ~ 2000 FCV of water were compared. As shown in Fig. 5, stripping is only slightly more difficult from the washed column, with elution essentially complete by 5 ml. Taken together then, the results of these column washing studies demonstrate clearly that the Pb Spec™ resin possesses adequate stability to handle substantial sample volumes or to permit reuse of the column, provided of course, that the resin is washed carefully between runs to eliminate any possibility of cross-contamination.

3.5. Application of Pb Spec™ to the isolation of lead from geological samples for thermal ionization mass spectroscopy (TIMS)

Methods for the determination of either the concentration of lead or its precise isotopic composition in environmental, geological, or archaeological samples frequently require that a pure lead fraction (i.e., one free of interfering and extraneous matrix elements) be isolated from the sample for analysis. For example, in lead isotopic

analysis by thermal ionization mass spectrometry (including isotope dilution assays), chemical impurities must be removed from the lead because they may cause a severe reduction in ionization efficiency, variable isotope fractionation in the ion source, and instability in the measured ion beams. The isolation of lead from such samples can be particularly demanding because its concentration is frequently low (micrograms or less per gram of sample) and because the matrix composition is variable and often quite complex. Thus, an acceptable separation method must yield excellent decontamination from the macro constituents of typical samples and must perform satisfactorily despite variations in sample composition. The results presented in Fig. 1a and b and in Table 2 suggest that Pb · Spec™ should be well-suited to these demands.

The utility of Pb · Spec™ was evaluated by examining its performance in the isolation of lead from samples of one of the most difficult metallic ores we have encountered, a Cu–Ni–Fe–As–S ore containing tens of percent of each of these elements but only a few ppm lead. Although a number of procedures have been described for the isolation of lead from ordinary silicate rocks and minerals for TIMS, among them methods based on electrodeposition [32,33] or chromatography using conventional resins [34–36], these procedures yield unsatisfactory results (i.e., insufficient lead purity, low lead yields, and high blank values) for certain matrices, among them metal ores containing large amounts of iron, copper, arsenic and nickel. In contrast, application of the Pb · Spec™-based procedure described above to the isolation of lead from these ore samples yielded a lead fraction free of any traces of organic matter and without detectable quantities of copper, nickel, iron, arsenic, or sulfur, the chief constituents of these ores. In addition, lead recoveries were both high and remarkably consistent, ranging from 90 to 95%.

The blank levels associated with the procedure were also well within acceptable limits. Table 5 summarizes the lead contents of the reagents employed in the ore preparation and analysis. From these results, the blank associated with the dissolution of a 1 g ore sample can be estimated as 60–120 pg lead. The lead blank associated with the column separation step (including the final sublimation, evaporation, and TIMS filament loading steps) was measured using isotope dilution by substituting a small volume (6 ml) of ^{207}Pb-spiked 3 M nitric acid for the ore sample solution and following the procedure outlined above beginning with the loading of the sample onto the Pb · Spec™ column. The blank so obtained ranged from 240–380 pg lead. Of this, the acids, water, and strip solution used contribute, at most, 50 pg lead. (Some reduction in this contribution could, of course, be achieved by further purification of the acids and ammonium carbonate. A greater reduction, however, could probably be achieved by further purification of the Pb · Spec™ resin, perhaps by stripping the column with pre-purified EDTA, glycine, or ammonium oxalate. For smaller samples, lower blanks could be achieved simply by reducing the size of the column and the volumes of reagents used.) These results indicate that the total procedural blank for the method, as presently established, is less than 500 pg lead for a 1 g ore sample. If the sample actually contains 0.5 ppm

Table 5
Lead content of reagents used in the processing of geological samples

Reagent	Lead content (pg/g) [a]
Water, Milli-Q	7.2
Water, doubly distilled in Teflon–FEP™	4.4
Water, Ultrex II	9.5
Nitric acid, 8 M, doubly distilled in Teflon–FEP™	12.2
Hydrochloric acid, 6 M double distilled in Teflon–FEP™	12.7
Sulfuric acid, 97.5%, w/w (Romil/Seastar)	< 10
Ammonium carbonate, 1 M, Normatom™, unpurified	4765
Ammonium carbonate, 1 M, Normatom™, Diphonix treated	23

[a] From these values, lead concentrations of 7.3 pg/g and 8.1 pg/g, respectively, can be calculated for the 3 M nitric acid and the 0.2 M ammonium carbonate solution actually employed in the isolation of lead from ore samples.

lead, a procedural blank of this magnitude represents only a 0.1% contribution to the total measured lead concentration. For such a sample, the lead contributed by the blank would not cause any measurable alteration in the experimentally determined sample composition as measured by TIMS.

It is important to note that ammonium carbonate solution was chosen for the removal of sorbed lead from the Pb · Spec™ column for these runs, despite its poor performance relative to several other reagents in our earlier stripping experiments (Table 3). This choice was prompted by the ease with which ammonium carbonate can be purified and by the comparatively low temperature required for its sublimation following stripping (150°C). In contrast, ammonium oxalate cannot be sublimed away at a temperature below the melting point of Teflon–PFA™ [37]. Similarly, sulfuric acid cannot be used since the temperature required to evaporate it is outside of the working range of these vessels (< 260°C).

4. Conclusions

An extraction chromatographic resin comprised of a solution of bis-4,4′(5′)-[*tert.*-butylcyclohexano]-18-crown-6 in isodecanol supported on an inert polymeric substrate provides a simple and effective means for the separation and preconcentration of lead from acidic aqueous solution. Lead is efficiently sorbed by the resin from a wide range of either nitric or hydrochloric acid concentrations and its removal from the resin can be effected using any of a variety of stripping agents. Although several other ions (e.g., Sr^{2+}) are sorbed to varying degrees under certain conditions, the differences in the resin capacity factors for these ions are sufficient to permit isolation of only lead. Most commonly encountered cations (e.g., Ca^{2+}, Fe^{3+}, Na^{+}) are essentially unretained by the resin, making it well suited to the isolation of lead from a variety of sample types. In particular, it has been demonstrated that this new resin is highly efficacious for the isolation of purified lead from difficult geological matrices for thermal ionization mass spectrometry.

Acknowledgements

The authors thank E.A. Huff for ICP-AES analyses and Deborah Moshinsky for her assistance in the initial preparation and evaluation of the Pb · Spec™ resin. A portion of this work was performed under the auspices of the Office of Basic Energy Sciences, Division of Chemical Sciences, U.S. Department of Energy, under contract number W-31-109-ENG-38. The work in Oxford was performed under the auspices of research grant GR/G49265 from the U.K. Science and Engineering Research Council.

References

[1] D.G. Beevers, E. Erskine, M. Robertson, A.D. Beattie and A. Goldberg, Lancet, 2 (1976) 1.
[2] B.C. Campbell, A.D. Beattie, M.R. Moore, A. Goldberg and A.G. Reid, Br. Med. J., 1 (1977) 482.
[3] O. David, S. Hoffman, B. McGann, J. Sverd and J. Clark, Lancet, 2 (1976) 1376.
[4] M. Lerchi, E. Bakker, R. Rusterholz and W. Simon, Anal. Chem., 64 (1992) 1534.
[5] D. Noble, Anal. Chem., 65 (1993) 265A.
[6] D. To, Anal. Chem., 65 (1993) 2701.
[7] A.E. Nevissi, J. Radioanal. Nucl. Chem., 148 (1991) 121.
[8] R. Barnes, M. Viczian and A. Lasztity, J. Anal. At. Spectrom., 5 (1990) 293.
[9] E.S. Hall and E. Murphy, J. Radioanal. Nucl. Chem. Lett., 175 (1993) 129.
[10] G. Faure, Principles of Isotope Geology, Wiley, New York, 2nd edn., 1986.
[11] B.L. Gulson, Lead Isotopes in Mineral Exploration, Elsevier, Amsterdam, 1986.
[12] N.H. Gale and Z.A. Stos-Gale, in Archeological Chemistry IV, Advances in Chemistry, Volume 220, American Chemical Society, Washington, DC, 1989, pp. 159–198.
[13] Y.A. Zolotov, N.M. Kuz'min, O.M. Petrukhin and B.Y. Spivakov, Anal. Chim. Acta, 180 (1986) 137.
[14] H.F. Walton and R.D. Rocklin, Ion Exchange in Analytical Chemistry, CRC Press, Boston, MA, 1990, Chap. 9.
[15] F. Sebesta, in T. Braun and G. Ghersini (Eds.), Extraction Chromatography, Elsevier, New York, 1975, Chap. 11.
[16] Z.B. Alfassi, in Z.B. Alfassi and C.M. Wai (Eds.), Preconcentration Techniques for Trace Elements, CRC Press, Boston, MA, 1992.
[17] E.P. Horwitz, R. Chiarizia and M.L. Dietz, Solvent Extr. Ion Exch., 10 (1992) 313.
[18] E.P. Horwitz, M.L. Dietz and D.E. Fisher, Anal. Chem., 63 (1991) 522.
[19] E.P. Horwitz, M.L. Dietz and R. Chiarizia, J. Radioanal. Nucl. Chem., 161 (1992) 575.

[20] R.M. Izatt, K. Pawlak, J.S. Bradshaw and R.L. Bruening, Chem. Rev., 91 (1991) 1721.
[21] E.A. Huff and E.P. Horwitz, Spectrochim. Acta, 40B (1985) 279.
[22] E.P. Horwitz, R. Chiarizia, H. Diamond, R.C. Gatrone, S.D. Alexandratos, A.Q. Trochimczuk and D.W. Crick, Solvent Extr. Ion Exch., 11 (1993) 943.
[23] R. Chiarizia, E.P. Horwitz, R.C. Gatrone, S.D. Alexandratos, A.Q. Trochimczuk and D.W. Crick, Solvent Extr. Ion Exch., 11 (1993) 967.
[24] S.A. Matthes, in H.M. Kingston and L.B. Jassie, Introduction to Microwave Sample Preparation, American Chemical Society, Washington, DC, 1988, p. 48.
[25] J.W. Arden and N.H. Gale, Anal. Chem., 46 (1974) 2.
[26] G. Wagner, H. Rache and D. Tuttas, Variable Multicollection (Finnigan MAT Application Report No. 422), Finnigan MAT, Bremen, 1984.
[27] E.P. Horwitz, M.L. Dietz and D.E. Fisher, Solvent Extr. Ion Exch., 8 (1990) 199.
[28] E.P. Horwitz, M.L. Dietz and D.E. Fisher, Solvent Extr. Ion Exch., 9 (1991) 1.
[29] D.A. Skoog and D.M. West, Fundamentals of Analytical Chemistry, Holt, Rinehart and Winston, New York, 3rd edn., 1976.
[30] P. Markl and E.R. Schmid, in T. Braun and G. Ghersini (Eds.), Extraction Chromatography, Elsevier, New York, 1975, Chap. 3.
[31] M.L.Dietz and C. Felinto, Argonne National Laboratory, 1993, unpublished results.
[32] I.L. Barnes, T.J. Murphy, J.W. Gramlich and W.R. Shields, Anal. Chem., 45 (1973) 1881.
[33] F. Tera and G.J. Wasserburg, Earth Planet. Sci. Lett., 13 (1972) 457.
[34] J.H. Chen and G.J. Wasserburg, Geochim. Cosmochim. Acta, 47 (1983) 1725.
[35] G. Manhes, C.J. Allegre and A. Prevost, Geochim. Cosmochim. Acta, 48 (1984) 2247.
[36] P.E. Smith, R.M. Farquhar and R.G. Hancock, Earth Planet. Sci. Lett., 105 (1991) 474.
[37] H.M. Kingston and L.B. Jassie, Introduction to Microwave Sample Preparation, American Chemical Society, Washington, DC, 1988, p. 117.

ELSEVIER

Analytica Chimica Acta 292 (1994) 275–279

ANALYTICA CHIMICA ACTA

Effect of cyclodextrin as mobile phase additive on fluorescence intensity of dansylamino acids in microcolumn liquid chromatography

Toyohide Takeuchi *, Tomoo Miwa

Faculty of Engineering, Gifu University, 1-1 Yanagido, Gifu 501-11, Japan

(Received 9th November 1993; revised manuscript received 4th January 1994)

Abstract

The effects of cyclodextrin (CD) as mobile phase additive on the fluorescence intensity of dansylamino acids were investigated in microcolumn liquid chromatography. Signal enhancement was observed for β- and γ-CD, whereas no signal enhancement was observed for α-CD. The signal enhancement was pronounced for neutral dansylamino acids, and larger fluorescence enhancement was observed for mobile phases containing higher concentrations of CD.

Key words: Fluorimetry; Liquid chromatography; Amino acids; Cyclodextrins

1. Introduction

Cyclodextrins (CDs) are cyclic oligosaccharides with the ability to form inclusion complexes with different molecules, which leads to an improvement in the solubility or stability of the guest molecules. When a molecule is incorporated in the cavity of CDs, its UV–visible absorption, fluorescence, circular dichroism and nuclear magnetic resonance spectra often undergo alterations. Enhancement of fluorescence [1–9] and chemiluminescence [10–13] of guest molecules has been observed when they are incorporated in CDs. Frankewich et al. [9] reported an evaluation of the relative effectiveness of different water-soluble β-CD media to function as fluorescence enhancement agents.

Various micellar systems in the spectrofluorimetric determination of dansyl (Dns) amino acids, drugs and other compounds have been assessed [5–7,14]. It was shown that fluorescence enhancements with factors varying from 8 to 20 were achieved for dansylamino acids in comparison with that in water alone, leading to an improvement in sensitivity [5].

Armstrong et al. [15] reported the first known example of micellar enhanced fluorescence detection in liquid chromatography (LC). They demonstrated the separation of aromatic hydrocarbons with a micellar mobile phase and the benefits of micellar enhanced fluorescence detection in LC were discussed. In spite of the promising features of micellar or CD mobile phases, it seems there have been few papers reporting fluorescence en-

* Corresponding author.

SSDI 0003-2670(94)00071-S

hancement generated by CDs as mobile phase additives in LC.

When phenolphthalein is incorporated in β- and γ-CD in an alkaline medium, its absorption spectrum undergoes drastic variations at visible wavelengths [16]. This phenomenon could be applied to the indirect photometric detection of β- and γ-CD [17,18], in which the CDs were indirectly detected owing to a depression of the background maintained by phenolphthalein in the mobile phase.

This paper deals with effects of CDs as the mobile phase additive in LC on the fluorescence intensity of dansylamino acids.

2. Experimental

2.1. Apparatus

A microcolumn liquid chromatograph was assembled from an MF-2 microfeeder (Azumadenki Kogyo, Tokyo) equipped with a 0.5-ml MS-GAN050 gas-tight syringe (Ito, Fuji) as a pump, an ML-522 microvalve injector with an injection volume of 0.11 μl (Jasco, Tokyo), a 150 × 0.35 mm i.d. microcolumn, an 820-FP fluorimetric detector (Jasco) with a laboratory-made flow cell and a Chromatopac C-R4AX data processor (Shimadzu, Kyoto). The flow cell was prepared from fused-silica tubing of 0.32 mm i.d. (GL Science, Tokyo) [19]. The time constant of the fluorimetric detector was kept at 3.5 s. The microcolumn was prepared from fused-silica tubing of 0.35 mm i.d. (GL Science), as reported previously [20], and 5-μm Develosil ODS-5 octadecyl-bonded silica gel (Nomura Chemical, Seto) was employed as the packing material. The flow-rate of the eluent was 2.8 μl min^{-1}. Experiments were carried out at room temperature (ca. 25°C).

2.2. Reagents

Guaranteed reagent-grade solvents and reagents were obtained from Nacalai Tesque (Kyoto), unless indicated otherwise. These reagents were employed as received. HPLC-grade distilled water (Nacalai Tesque) was employed throughout. α- and β-CD were obtained from Tokyo Chemical Industry (Tokyo) and γ-CD from Wako (Osaka). Dns-L-amino acids and Dns-DL-Phe were purchased from Sigma (St. Louis, MO, USA). All standard solutions and eluents were prepared from distilled water and acetonitrile.

3. Results and discussion

3.1. Signal enhancement of dansylamino acids

Fluorescence enhancement was measured by using the FP-820 fluorimetric detector with a flow cell for conventional LC. Table 1 compares the wavelengths giving maximum fluorescence intensity and the enhancement factors, defined as the ratio of the fluorescence intensity observed in the presence of CD to that without CD. The analyte solution prepared was 40 μM Dns-L-Phe dissolved in 0.8% aqueous acetonitrile solution containing 1 mM of each CD. Signal enhancement was observed for β-and γ-CD, whereas no signal enhancement was observed for α-CD. The enhancement factors were 2.01 and 4.54 for β- and γ-CD, respectively. This result probably occurs because Dns-L-Phe can be incorporated in the cavity of β- and γ-CD, whereas the cavity of α-CD may be too small to incorporate Dns-L-Phe in the same orientation. In addition, the wavelength giving the maximum fluorescence intensity is slightly sifted to shorter wavelengths on addition of β- or γ-CD.

Table 2 compares the enhancement factors achieved for each Dns-L-amino acid in the presence of 1 mM γ-CD. It is found that the largest enhancement factor was achieved for Dns-L-Phe, i.e., 4.53. Enhancement factors between 2 and 3 were observed for aliphatic amino acids, whereas lower enhancement factors were observed for acidic and basic amino acids and for amino acids possessing a substituent group with a hydroxy group.

When β-CD was used as the mobile phase additive, the enhancement factors were 1.1–1.4 for the dansylamino acids listed in Table 2, except for Phe (2.01) and *N*-Hyp (1.01). The values were smaller than those achieved with γ-CD.

Table 1
Fluorescence enhancement of Dns-L-Phe via inclusion complexation with CD

Matrix	Emission wavelength (nm) [a]	Enhancement factor
No CD	535	–
1 mM α-CD	538	0.99
1 mM β-CD	529	2.01
1 mM γ-CD	529	4.54

Analyte solution, 40 μM Dns-L-Phe dissolved in 0.8% (v/v) aqueous acetonitrile solution containing 1 mM of each CD. Excitation wavelength, 335 nm.
[a] Wavelength giving maximum fluorescence intensity.

3.2. Effect of concentration of acetonitrile

The enhancement factor was strongly affected by the acetonitrile concentration. Fig. 1 shows the effect of acetonitrile concentration on the signal intensity and the signal enhancement of Dns-L-Leu. In the absence of γ-CD, the signal intensity increased with increasing acetonitrile concentration. This phenomenon probably results because water quenches the fluorescence of dansylamino acids [4]. On the other hand, the signal enhancement factor decreased with increasing acetonitrile concentration and reached almost 1 at ca. 20% (v/v). One of the reasons for this result is that the association constant decreases with increasing acetonitrile concentration. As the association constant between dansylamino acids and CD depends on the temperature and the composition of organic solvents, the signal intensity could be varied by changing these parameters.

3.3. Effect of CD concentration

The signal intensity is expected to increase with increasing CD concentration because the percentage of the analyte molecules incorporated in the cavity of CD increases with increasing CD concentration. Fig. 2 illustrates the enhancement factor of Dns-L-Phe as a function of γ-CD concentration at acetonitrile concentrations of 0.8 and 20.8% (v/v). In both instances the enhancement factor increases with increasing γ-CD concentration. The enhancement factor observed at 0.8% (v/v) acetonitrile was much larger than that at 20.8% (v/v), which is due to the difference in the association constants under these two different conditions.

In addition, in view of the sensitivity, γ-CD is favoured over β-CD for use as the mobile phase additive because of its higher solubility in water.

3.4. Separation of dansylamino acids

Fig. 3 demonstrates the separation of dansyl derivatives of L-Val, L-NVal and L-Phe, (A) in the presence and (B) in the absence of γ-CD in the mobile phase. The retention times of the analytes decreased with increasing acetonitrile and γ-CD concentrations. In the former instance, 25% (v/v)

Table 2
Fluorescence enhancement of Dns-L-amino acids via inclusion complexation with γ-CD

Dns-L-amino acid	Signal intensity (mV)		Enhancement factor
	Without γ-CD (535 nm)	With γ-CD (529 nm)	
Ala	2.84	5.45	1.92
αAB	3.08	6.50	2.11
NVal	3.12	6.87	2.20
Val	3.24	6.86	2.12
Leu	4.08	9.83	2.41
Ile	3.59	9.99	2.78
Phe	2.72	12.34	4.54
N^{α}-Trp [a]	2.48	3.83	1.54
Pro	1.77	5.15	2.91
Met	3.32	5.49	1.65
Ser	2.57	3.29	1.28
N-Thr [b]	3.04	4.44	1.46
N-Hyp [c]	2.26	3.03	1.34
Asp	2.75	3.40	1.24
Glu	3.01	3.70	1.23
Cysteic Acid	1.42	1.58	1.11
Asn	2.52	2.71	1.08
Gln	2.76	3.25	1.18
α-Arg [d]	3.18	3.77	1.19
N^{ϵ}-Lys [e]	3.05	4.78	1.57

Analyte solution, 40 μM Dns-L-amino acid dissolved in 0.8% (v/v) aqueous acetonitrile solution containing 1 mM γ-CD. Excitation wavelength, 335 nm.
[a] N^{α}-Dansyl-L-tryptophan.
[b] *N*-Dansyl-L-threonine.
[c] *N*-Dansyl-*trans*-4-hydroxy-L-proline.
[d] α-Dansyl-L-arginine.
[e] N^{ϵ}-Dansyl-L-lysine.

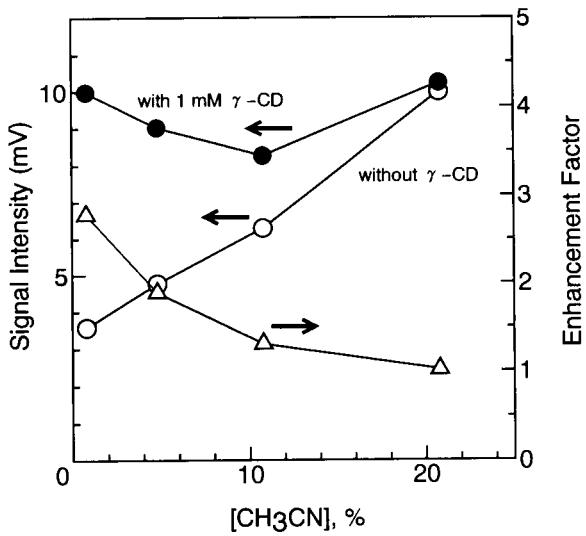

Fig. 1. Signal intensity and enhancement as a function of acetonitrile concentration. Analyte solutions, 40 μM Dns-L-Leu with or without γ-CD; excitation wavelength, 335 nm; emission wavelength, 529 nm (in the presence of 1 mM γ-CD) or 535 nm (in the absence of γ-CD); ● and ○ refer to the signal intensity observed with or without 1 mM γ-CD and △ refers to the signal enhancement.

acetonitrile solution containing 27 mM γ-CD was employed as the mobile phase, and in the latter 28% (v/v) acetonitrile solution without γ-CD was employed. The peak areas achieved in the former instance were 1.3–1.4 times larger than those in the latter, whereas the peak heights were higher in Fig. 3A by factors of 1.25, 1.12 and 1.80 for

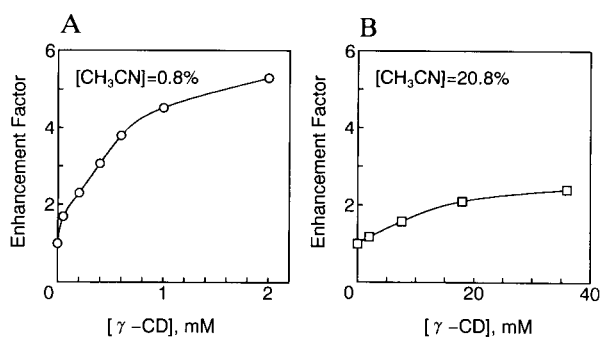

Fig. 2. Signal enhancement as a function of γ-CD concentration. Solutions, 40 μM Dns-L-Phe in (A) 0.8% and (B) 20.8% (v/v) acetonitrile; excitation wavelength, 335 nm; emission wavelength, 529 nm (in the presence of γ-CD) or 535 nm (in the absence of γ-CD).

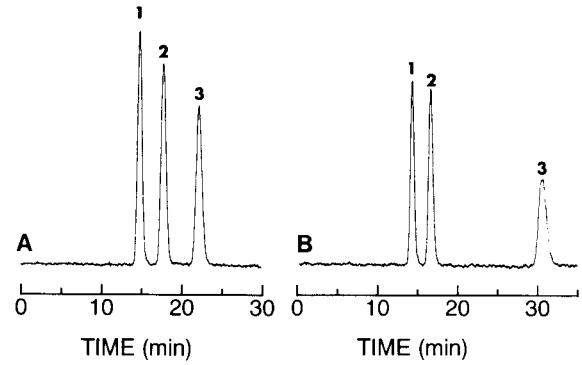

Fig. 3. Fluorimetric detection of dansylamino acids (A) with and (B) without γ-CD. Column, 150×0.35 mm i.d., packed with Develosil ODS-5; eluent, (A) 25% (v/v) acetonitrile in 40 mM ammonium acetate–27 mM γ-CD and (B) 28% acetonitrile in 40 mM ammonium acetate; flow-rate, 2.8 μl min^{-1}; excitation wavelength, 335 nm; emission wavelength, (A) 529 or (B) 535 nm; sample, 0.33 mM each of (1) Dns-L-Val, (2) Dns-L-NVal and (3) Dns-L-Phe.

dansyl derivatives of L-Val, L-NVal and L-Phe, respectively, compared with those in Fig. 3B. In addition, it is seen that the noise levels with both detection systems are nearly the same.

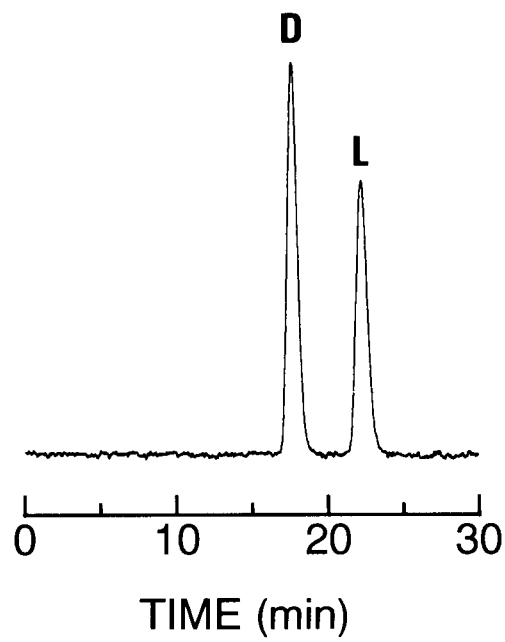

Fig. 4. Fluorimetric detection of racemic Dns-D-Phe and Dns-L-Phe in the presence of 27 mM γ-CD. Operating conditions as in Fig. 3A.

The separation of Dns-D-Phe and Dns-L-Phe is demonstrated in Fig. 4, where 25% (v/v) acetonitrile solution containing 27 mM γ-CD and 40 mM ammonium acetate was used as the mobile phase. The analytes were racemic mixtures, and the D-form gave a larger peak area than the L-form. The fact that the D-form elutes before the L-form suggests that the D-form is more favourably incorporated in γ-CD, resulting in an increase in the signal intensity. This phenomenon will allow the determination of the enantiomeric ratio by flow-injection analysis when the signal intensities can be carefully measured both in the presence and in the absence of γ-CD.

References

[1] T. Kinoshita, F. Iinuma and A. Tsuji, Biochem. Biophys. Res. Commun., 51 (1973) 666.
[2] T. Kinoshita, F. Iinuma and A. Tsuji, Chem. Pharm. Bull., 22 (1974) 2413.
[3] H. Kondo, N. Nakatani and K. Hiromi, J. Biochem., 79 (1976) 393.
[4] M. Hoshino, M. Imamura, K. Ikehara and Y. Hama, J. Phys. Chem., 85 (1981) 1820.
[5] H.N. Singh and W.L. Hinze, Analyst, 107 (1982) 1073.
[6] O. Jules, S. Scypinski and L.J. Cline Love, Anal. Chim. Acta, 169 (1985) 355.
[7] G. Patonay, M.E. Rollie and I.M. Warner, Anal. Chem., 57 (1985) 569.
[8] K.W. Street, Jr., J. Liq. Chromatogr., 10 (1987) 655.
[9] R.P. Frankewich, K.N. Thimmaiah and W.L. Hinze, Anal. Chem., 63 (1991) 2924.
[10] T.E. Riehl, C.L. Malehorn and W.L. Hinze, Analyst, 111 (1986) 931.
[11] T.E. Riehl, C.L. Malehorn and W.L. Hinze, Analyst, 111 (1986) 941.
[12] M.L. Grayeski and E.J. Woolf, J. Lumin., 33 (1985) 115.
[13] E.J. Woolf and M.L. Grayeski, J. Lumin., 39 (1987) 19.
[14] H. Singh and W.L. Hinze, Anal. Lett., 15 (1982) 221.
[15] D.W. Armstrong, W.L. Hinze, K.H. Bui and H.N. Singh, Anal. Lett., 14 (1981) 1659.
[16] Á. Buvári, L. Barcza and M. Kajtár, J. Chem. Soc., Perkin Trans. 2, (1988) 1687.
[17] H.W. Frijlink, J. Visser and B.F.H. Drenth, J. Chromatogr., 415 (1987) 225.
[18] T. Takeuchi, M. Murayama and D. Ishii, J. Chromatogr., 477 (1989) 147.
[19] T. Takeuchi, A. Asano and D. Ishii, J. Chromatogr., 471 (1989) 297.
[20] T. Takeuchi and D. Ishii, J. Chromatogr., 213 (1981) 25.

ELSEVIER

Analytica Chimica Acta 292 (1994) 281–295

ANALYTICA CHIMICA ACTA

An automated system for multichannel flow-injection analysis

U. Spohn *,[a], J. van der Pol [b], R. Eberhardt [b], B. Joksch [b], Ch. Wandrey [b]

[a] *Institut für Biotechnologie, Martin-Luther-Universität Halle, Weinbergweg 16a, D-06120 Halle / Saale, Germany*
[b] *Institut für Biotechnologie, Forschungszentrum Jülich GmbH, P.O. Box 1913, D-52428 Jülich, Germany*

(Received 24th May 1993; revised manuscript received 25th November 1993)

Abstract

An automated multi-channel flow-injection analyzer was developed both for new flow-injection analysis (FIA) procedures and for the process monitoring of animal and microbial cultivations. Up to six different analytes can be determined sequentially. The FIA set-up is working with up to six enzyme reactors configurated in parallel but with only one fluorescence detector and one pair of injection valves. By means of an automated sampling device the analyzer can be coupled on-line to a fermentation process. All active hardware components are computer controlled independently from each other guaranteeing a high flexibility. The software package, Flow Injection Analysis Control and Configuration (FIACCO), was developed for the hardware control, signal evaluation and long term recording of the on-line calculated results. Single and double step stopped flow procedures were developed to control the analyte conversion in packed bed enzyme reactors without an essential increase of the peak widths. Two carrier solutions are mixed to adjust the optimum pH for each applied enzyme also within one cycle of analysis. An enzymatic and a nonenzymatic procedure was developed to determine ammonia/ammonium after its gas dialytic separation from the sample solution. The application of the FIA set-up to the on-line process monitoring of an animal cell culture is demonstrated with respect to the five key components, glucose, ammonia, glutamine, glutamate and lactate.

Key words: Flow injection, Enzymatic determinations; Automation; Bioprocess analysis; Dialysis; Multicomponent analysis; Stopped flow FIA; On-line sampling

1. Introduction

Despite the wide acceptance of flow-injection analysis (FIA) and its obvious advantages one of the main drawbacks is the limited possibility to determine more than one or two components with the same FIA set-up. Typical solutions from food processing and fermentation media need to be analysed for more than two components. Some successful attempts to solve this problem have been published. Lazarol et al. [1] proposed the use of a diode array UV–visible detector. An alternative method is the arrangement of several detectors in serial or parallel configurations. A successful method is the arrangement of different ion sensitive electrodes [2–4]. For food and bioprocess analysis enzymatic assays are of particular interest. Renneberg et al. [5] proposed an

* Corresponding author.

SSDI 0003-2670(93)E0662-Q

arrangement with different biosensors for the simultaneous determination of glucose, glutamine and lactate in animal cell cultures. Hundeck et al. [6] described an enzyme thermistor with four parallel enzyme reactor cartridges in a FIA set-up. Ogbomo et al. [7] and Kittsteiner et al. [8] designed an FIA set-up with parallel enzyme reactors using reagent injection. A disadvantage of these multichannel systems is the restricted possibility to adjust the optimum reaction conditions for each enzymatic assay, whereas the FIA set-up with reagent injection also has a relatively high consumption of sample solutions. Nielsen et al. [9] and Nikolajsen et al. [10] combined up to 4 complete one-channel FIA set-ups to obtain a multicomponent analyzer. The relatively high costs per channel are justifiable in view of the successful on-line control of real processes.

The lack of suitable and reliable software and the insufficient reliability of the corresponding commercial hardware configurations are at present the main obstacles for a more general and flexible application of multichannel FIA set-ups especially in chemical process analysis.

The aim of our work was to develop a flexible, fully automated FIA analyzer for enzymatic multicomponent analysis. The flexibility should be especially extended to a wide range of automatically adjustable reaction conditions, for example reagent concentrations, pH values and residence times.

2. Experimental

2.1. Reagents and chemicals

Glucose dehydrogenase from *Bacillus megaterium* (GDH, EC 1.1.1.47, Merck, Darmstadt), lactate dehydrogenase from Rabbit muscle (LDH, EC 1.1.1.27, Sigma), glutamic–pyruvic transaminase from *E. Coli* (GPT, EC 2.6.1.2, Sigma), glutaminase from *E. coli* (GA, EC 3.5.1.2) and glutamate dehydrogenase from bovine liver (GlutDH; EC 1.4.1.3, Sigma), were used to prepare the corresponding enzyme immobilizates. All other chemicals were of analytical grade from Merck.

2.2. Enzyme reactors

With the exception of glutaminase the enzymes were immobilized and coimmobilized on aminopropylsilylated controlled pore glass (Schott, Mainz, Bioran G001/090/C/250, sieve fraction 180–200 μm, pore diameter 90 nm) according to Spohn et al. [11]. Glutaminase was immobilized analogously but without the borohydride reduction step and at pH 6.5 after the activation by glutardialdehyde. The immobilizates are packed into plexiglass tubes (inner diameter 3 mm) with inner threaded ends for the connecting fittings of the applied PTFE tubes. The length of the active packing is varied according to the specific enzyme activity. Polypropylene nets (20 μm hole diameter, Pharmacia, Bromma) were placed between the packing and the fittings.

2.3. Comparison methods

To control the on-line FIA measurements offline sampled solutions were taken. Glucose and lactate were measured with an amperometric two channel analyzer (Yellow Springs, YSI 2000, USA). Glutamine and glutamate were measured enzymatically according to Bergmeyer et al. [12]. Ammonium was measured photometrically during the reductive amination of α-oxoglutarate with NADH and glutamate dehydrogenase [13].

2.4. Instrumentation and system concept

The general system concept of the multichannel FIA system was developed on the basis of an earlier described FIA set-up [14,15]. The new FIA system is fully automated, more flexible and thermostated to 15°C. Table 1 summarizes the hardware components, which are computer controlled and can be easily exchanged. All active components can also be controlled manually from the PC-keyboard.

The configuration of the hardware components is adapted to a concrete analytical problem. The whole system is controlled by an IBM compatible personal computer (processor 80386, coprocessor 80387). The PC is equipped with a multifunction board (PC-74; Meilhaus, Puchheim), a reed relais board (PC-63; Meilhaus) and

Table 1
Hardware components

Active hardware components	Interface	Controllable variables and commands
4 piston pumps	RS 232(PC-31)	Pump rate selection, commands: Go, Stop, Refilling
Three channel peristaltic pump	Relais board (PC-63)	Two pump rates, stop and go
5 magnetic 3/2-way valves	Relais board (PC-63)	Flow channel selection and injection
2 injection valves	Relais board (PC-63)	Injection of sample and reagent solutions
2 six-way valves	Relais board (PC-63)	Positions for calling standards and flow reactors
Detector[a]	Relais board, RS 232, multifunction card(PC- 74)	Autozero, scaling, A/D conversion of the detector signal

[a] Fluorescence detector F1050, Merck-Hitachi.

an eightfold RS232 serial interface board (PC-31, Meilhaus).

The multifunction board consists of a 12 bit A/D converter with eight differential signal inputs. The reed relais board allows the independent control of up to 16 relais (24 VDC) setting six magnetic switching valves (Akzo, 3 way/2 position way valve, Type 368/1/3/24/30 and 4 way/2 position valve, Type 417/4/028/6/T/24V, Ratingen), two pneumatically actuated injection valves (9010, Rheodyne) and two 6 way valves (9060, Rheodyne). Other relais outputs allows the automatic selection of two pump rates of the peristaltic sampling pump (SP-GL 70, Meredos, Göttingen) preadjusted steplessly by two precision potentiometers and the time controlled on/off switch. Another output serves for the reed relais based switching of the detector auto zero.

The eightfold RS 232 serial interface card allows the automatic control of 4 precisely working piston pumps P1–P4 (Dosimat 665, Metrohm). The pumps are controlled independently from each other with respect to the flow rates $\dot{V}_{1-4}$ and to microprocessor commands GO, STOP, FILL and PUMP RATE. It is possible to switch over between four different carrier solutions synchronously with the corresponding pump stop/go commands. This enables a fast exchange of the carrier solution to be performed. The mixing ratios of the carrier solution pairs can be varied from 0.1 to 10.

The piston pumps are refilled after each determination to achieve the maximum stability of the flow rates. The pump command STOP allows the very flexible implementation of single and multiple stopped flow FIA procedures.

The pump rates are software controlled during the determination procedure and can be changed in 2 μl min^{-1} steps. For every 10 s another pump rate can be automatically adjusted. Up to eight different pump rates can be preadjusted and changed automatically during each time course and every 10 s with a time shift of 0.5 s.

All components are connected by PTFE tubes with an inner diameter of 0.5 mm (Latek, Heidelberg).

The primary process sampling device is a cross flow microfiltration module, which was described earlier [14].

Thin-layer dialysis cells with groove labyrinths of a groove width of 1.5 mm and a depth of 0.2 mm both on the donor and the acceptor side were used. The dialysis cell consists of two mirror symmetrical plexiglass plates with meander grooves. A regenerated cellulose membrane (cut off 10 000; Reichelt, Heidelberg) and a PTFE membrane (porosity 70–80%, mean pore size 0.2 μm, thickness 20 μm, Sartorius) were used as separation barriers between the donor and the acceptor side of the separation cell with an effective membrane exchange area of 504 mm^2.

The second six-way valve selects between six different flow reactors which are configurated in parallel. The sequential determination of six different samples is possible during one cycle of analysis. The sample plugs are loaded into the channels and analyzed after each other allowing a sixfold prolongation of the sample reaction time without an essential decrease of the sample throughput as proposed by Ruzicka and Hansen [16]. Only one detector is necessary for the sequentially implemented determinations. But it is

also possible to combine six different detectors in series and in parallel.

The software package, Flow Injection Analysis Control and Configuration (FIACCO), allows the automatic control of all active hardware components and the online signal evaluation. All valve positions and the state of the piston pumps are checked automatically and can be announced ensuring a high degree of reliability and selfdiagnosis. Malfunction is promptly indicated. Nearly all common FIA configurations [16] for normal FIA, merging zone FIA and FIA with reagent injection and stopped flow regimes can be implemented. The exact timing and the highly constant flow rates of the piston pumps allows also kinetic measurements especially with respect to measurements of enzyme activities [17].

The data logging rate is one measuring point per 100 ms. The programm is written in C.

For every FIA procedure an optimized timetable of commands is preadjusted, which is executed in a repeated manner. For every active hardware component a separate time course is defined for the switching states. The time resolution of all switching commands including the sample and reagent injection times is 0.5 s.

The sampling time is adapted to the necessary rinsing and residence times in the FIA channel system and to the allowed maximum response time for a required minimum measurability [18,19]. Up to 6 different sampling procedures can be preprogrammed enabling the automatic adaptation to the currently working assay.

The detector signal is scanned and saved during the complete determination cycle. The baseline is calculated by linear regression before and after the signal peak.

The position of the time windows for the baseline, peak evaluation and signal recording allows, in connection with the automatic autozero, to circumvent regular disturbances. Such disturbances can be caused by the restarting of the piston pumps, by the injection events or the switching over between different carrier solutions.

The preselected limits of the signal-to-noise ratio (S/N) determine the minimal signal height, which will be evaluated. The selected lower S_{min} and the upper relative peak height level S_{max} predetermine which peak signals of an injection series is ignored. The arithmetic average of the peak values S_{av} in an injection series is the 100% reference value. The limit of recalibration is defined by an upper and a lower peak signal level of a preselected recalibration standard. During the recalibration two selected standard signals are compared with the corresponding precalculated signals. The frequency of the recalibration is programmed in dependence on the long term stability of the determination channels. After exceeding or falling below the corresponding level the complete calibration procedure with up to six standards is repeated automatically.

The calibration graph is fitted with polynomials of up to the seventh order.

The time cycle, ANALYSIS, is repeated up to the next preadjusted recalibration time.

The time required for the development of a new determination procedure is reduced by generating a configuration file containing the names of the activated hardware components. The user then selects the necessary components. Complete FIA methods with their different time courses and parameters can be copied and recalled.

2.5. Animal cell culture

Cells of a mouse/mouse hybridoma strain were cultivated continuously to produce Ig2a antibodies. The cells were immobilized on porous microcarriers (Siran R glass, Schott, Mainz) according to Luellau et al. [20]. A fluidized bed reactor was inserted in a circulation loop. The total reactor volume was 170 ml. The dilution rate was varied between 0 and 0.45 l/h. The medium was a 3:1 volumetric ratio mixture of DMEM and Ham's F-12 (GIBCO, Eggenheim) [21].

3. Results and discussion

3.1. Application of flow rate control programs in packed bed enzyme reactors and in the dialysis cell

The possibility of flow rate changes when the sample substance enters the enzyme reactors was

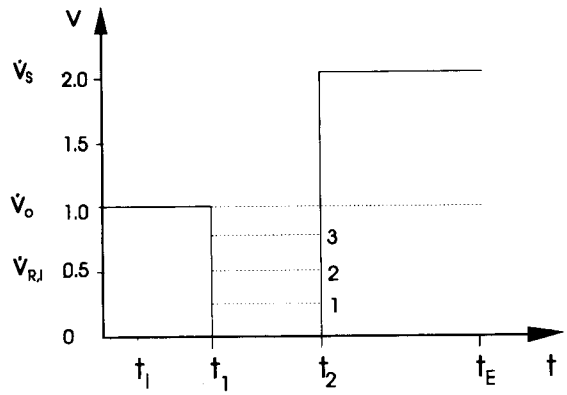

Fig. 1. Flow rate control in the FIA set-up shown in Fig. 2 without the mixing coil MC_2 and the enzyme reactor INV/MUT, $\dot{V}_O$ = the starting flow rate, $\dot{V}_{Ri}$ = the flow rate during the substrate conversion in the enzyme reactor and $\dot{V}_S$ = the flow rate of buffer rinsing.

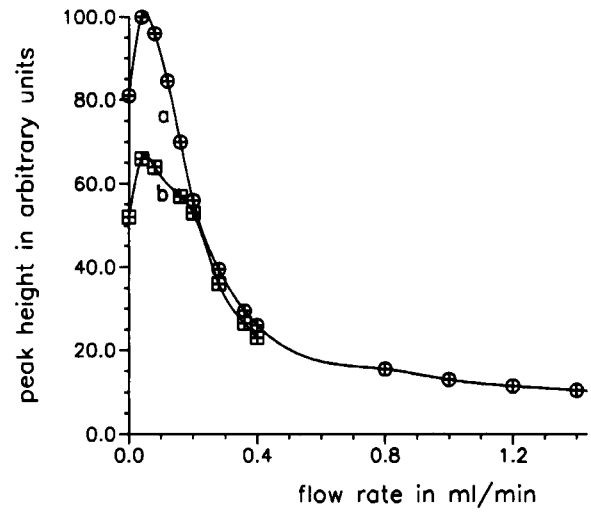

Fig. 3. Dependence of the peak height on the flow rate during the conversion time in the enzyme reactor, stop time/time of decreased flow rate: a = 40 s, b = 20 s.

used to control the degree of substrate conversion.

Fig. 1 shows the principle of the flow rate control in the case of the enzymatic glucose determination implemented with the set-up shown in Fig. 2 but without the mixing coil MC2 and without the invertase reactor INV/MUT. The injected glucose solution is transported to the enzyme reactor GDH. After an operational time of 4 months the GDH reactor still had a conversion of 20% of the initial value for 20 μl injections of 0.25 mM glucose. Then the flow rate $\dot{V}$ is decreased to $\dot{V}_{R,i}$ to prolong the residence time in the reactor. To shorten the peak width the flow rate is increased to $\dot{V}_S$ to accelerate the rinsing of the sample plug. Fig. 3 shows the dependence of the peak height on the flow rate $\dot{V}_{Ri}$ for a 20 and 40 s period of decreased flow rate respectively. The flow rate V_{Ri} is adjusted automatically just in that moment, when the sample/reagent plug enters the enzyme reactor. It is noticed that flow rates smaller than 0.08 ml min^{-1} cause higher peaks than a stop period of the same time length probably because of the additional convective mass transfer. Obviously long stop and low flow rate periods increase the signal height. The advantage of the automatic flow rate control is also that no essential change of the dispersion factor D is necessary to adapt the sensitivity to different concentration ranges.

In a sequential two step enzymatic assay working with separated invertase/mutarotase and glucose dehydrogenase reactors (Fig. 2) the sample concentration profile, resulting from a 5 μl injection, can be stopped for different times in both enzyme reactors. For example: In the first reactor the saccharose is completely hydrolyzed to α-glu-

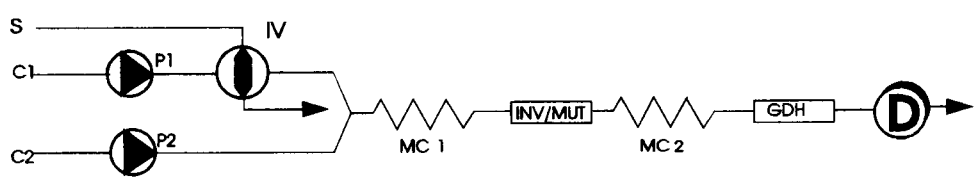

Fig. 2. FIA set-up for the enzymatic determination of glucose and saccharose, INV/MUT = enzyme reactor with immobilized invertase and mutarotase, GDH = enzyme reactor with immobilized glucose dehydrogenase, IV = injection valve, S = sample, C1 and C2 = carrier solutions, P1 and P2 = piston pumps, MC1 and MC2 = mixing coils, D = detector.

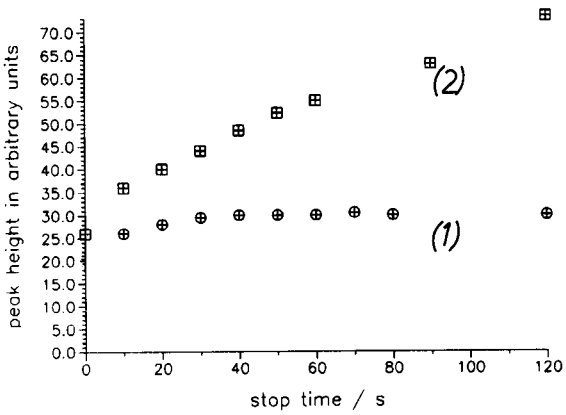

Fig. 4. Peak height dependence on the stop times in the enzyme reactors; curve $1 = T_1$ ($T_2 = 10$ s), curve $2 = T_2$ ($T_1 = 0$).

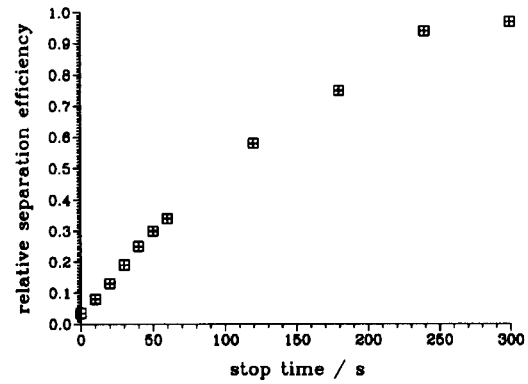

Fig. 5. Dependence of the relative separation efficiency on the stop time in the dialysis cell for a 2 mM glucose solution flowing through the donor cell chamber with 2 ml min^{-1}, acceptor flow rate 2 ml min^{-1}.

cose and fructose. The α-D-glucose/ β-D-glucose equilibrium is catalyzed by co-immobilized mutarotase. In the other reactor glucose dehydrogenase catalyzes the oxidation of β-D-glucose with NAD^+. For example the sample plug is stopped in the INV/MUT reactor for 10 s ($T_1 = t_2 - t_1$) and in the GDH reactor for 30 s ($T_2 = t_4 - t_3$). Fig. 4 shows the dependence of the peak height on the first stop time T_1 and on the second stop time T_2. Obviously the enzyme loading of the first reactor, INV/MUT, is so high that the residence time plays no significant role. But the enzyme activity of the GDH reactor is too low to provide signals which are independent of the residence time up to a stop time > 210 s.

According to Johansson et al. [22] the complete analyte conversion in enzymatic flow reactors has the advantage of being relatively independent of enzyme effector concentrations, temperature and flow rate drift. Extended linear determination ranges are achieved. Complete analyte conversions are implemented with packed bed enzyme reactors in some FIA procedures described by Johansson and co-workers [23,24]. The flow rate control could prolong the opera-

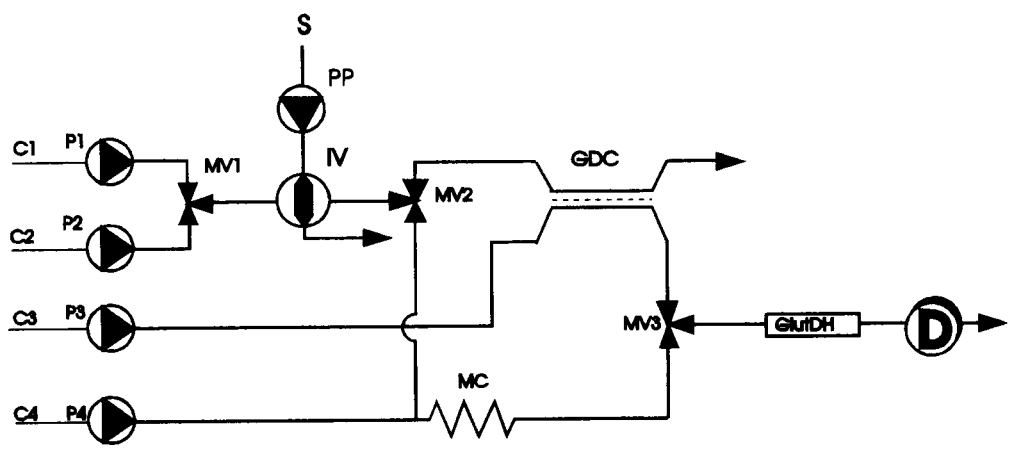

Fig. 6. FIA set-up for the enzymatic determination of ammonia and glutamate, PP = peristaltic pump, GDC = gas dialysis cell, GlutDH = glutamate dehydrogenase reactor, MV1-3 = 3 way/2 position magnetic valves, other symbols with the same meaning as in Fig. 2.

tional time during which such reactors are working with 100% substrate conversion. Only the stop times or the periods with decreased flow rates have to be prolonged according to the enzyme deactivation.

The stopped flow technique can also be used to control the efficiency of the dialytic separation cells. Fig. 5 shows the separation efficiency of a continuously working dialysis cell for 2 mM glucose in dependence on the stop time. The dialysis cell was placed upstream to the injection valve IV. The flow rates were 2 ml min^{-1} both in the donor and in the acceptor stream. The efficiency was measured by the timed injection of that dialysate, which was obtained during the stopped flow period, into the described enzymatic glucose FIA set-up. The efficiency was calculated from the peak height ratio between the injection of the dialysate and the non-dialyzed sample solution.

3.2. *Sequential enzymatic determination of a volatile and a nonvolatile analyte*

The combination of a gas dialytic separation step with enzymatic assays can be used to determine volatile and nonvolatile substances simultaneously with improved selectivities.

The simultaneous determination of ammonia and glutamate was implemented according to the measuring set-up shown in Fig. 6 demonstrating the selectivity enhancement by a gas dialysis step. A glutamate dehydrogenase reactor is used for both determinations. The active bed length of the enzyme reactor was 3 cm. 10 mg glutamate dehydrogenase were immobilized on 200 mg aminopropylsilylated controlled pore glass.

The sample is injected into the carrier C1 containing 0.1 M NaOH causing the conversion of ammonium to ammonia with a conversion degree $> 99.9\%$. Ammonia is separated from the glutamate in the thin layer gas dialysis cell into the carrier C3 containing 0.1 M Tris, 20 mM α-oxoglutarate and 0.2 mM NADH adjusted to pH 8.0. Ammonia/ammonium is consumed in the reductive amination of α-oxoglutarate according to

$$\alpha\text{-oxoglutarate} + \mathrm{NADH} + \mathrm{NH_4^+} \rightleftharpoons \text{L-glutamate} + \mathrm{NAD^+} \quad (1)$$

catalyzed by immobilized glutamate dehydrogenase in the enzyme reactor GlutDH. The resulting negative NADH peaks are detected fluorimetrically.

Ammonium can be determined in the range from $c = 0.002$ to 1 mM using the gas dialysis meander cell described above and working with the microporous PTFE membrane. The regression line

$$y = (1.01 \pm 0.07)\mathrm{l/mmol} \times c + (0.06 \pm 0.05) \quad (2)$$

with the level of insignificance $\alpha = 0.05$, $n = 5$ and $r^2 = 0.996$ was determined. 1 mM ammonia corresponds to the normalized detector signal $y = 1$. Glutamate concentrations of up to 20 mM in the sample solution have no significant influence.

After switching over the 3/2 way valves MV1, MV2 and MV3 the carrier solutions C1 and C3 are replaced for the solutions C2 and C4, respectively. The corresponding pairs of the pumps P1, P3 and P2, P4 are synchronously switched off and on, respectively. Now the sample solution is injected into C2 containing 0.1 M Tris and 0.1 M Na_2SO_4 adjusted to pH 9.5. The carrier C2 is mixed with carrier C4 containing 2.5 mM NAD^+ and 25 mM $(NH_4)_2SO_4$ in 0.1 M Tris buffer with pH 6.5. The relatively high ammonium concentration is used to level out small ammonium amounts injected together with the glutamate to be determined.

According to the backreaction of (1) L-glutamate is deaminated to α-oxoglutarate producing NADH.

The least squares calibration equation was

$$y = (2.00 \pm 0.04)\mathrm{l/mmol} \times c + (0.07 \pm 0.03) \quad (3)$$

where y is the peak height and c the glutamate concentration. The correlation coefficient is $r^2 = 0.997$ (eight data points, $\alpha = 0.05$, $n = 4$) for the range from 0.05 to 0.5 mM L-glutamate. The detector output signal is taken as 1 for 0.5 mM L-glutamate. The calibration equation

$$y = (1.99 \pm 0.05)\mathrm{l/mmol} \times c + (0.03 \pm 0.03) \quad (4)$$

with $r^2 = 0.997$, $\alpha = 0.05$, $n = 4$ was obtained in the presence of 1 mM ammonia in the injected sample. The injection volume was 10 μl in both cases. Up to 1.5 mM ammonium can be tolerated.

Table 2
Glucose, glutamine, glutamate and L-lactate reactions

glucose +	$NAD^+ \longrightarrow$ gluconate + H^+ + NADH	(5)
glutamine +	$H_2O \longrightarrow$ glutamate + NH_3	(6)
glutamate +	$NAD^+ \rightleftharpoons \alpha$-oxoglutarate + NADH	(7)
lactate +	$NAD^+ \rightleftharpoons$ pyruvate + NADH	(8)
pyruvate + glutamate	$\rightleftharpoons$ L-alanine + α-oxoglutarate	(9)

3.3. Sequential determination of five analytes

To monitor the animal cell culture ammonia has to be determined quasi-simultaneously with glucose, glutamine, glutamate and L-lactate, which can be determined enzymatically by means of immobilized dehydrogenases according to reactions 5–9 summarized in Table 2. The advantage of the dehydrogenases is the independence of the oxygen concentration in comparison to the also applicable oxydases.

The enzymatic ammonia FIA determination (1) provides negative peaks. The instability of NADH solutions and their costs were the reason to develop a nonenzymatic procedure.

Several authors [25–27] applied the reaction of ammonia with *o*-phthaldialdehyde in the presence of mercaptoethanol in a partial nonaqueous

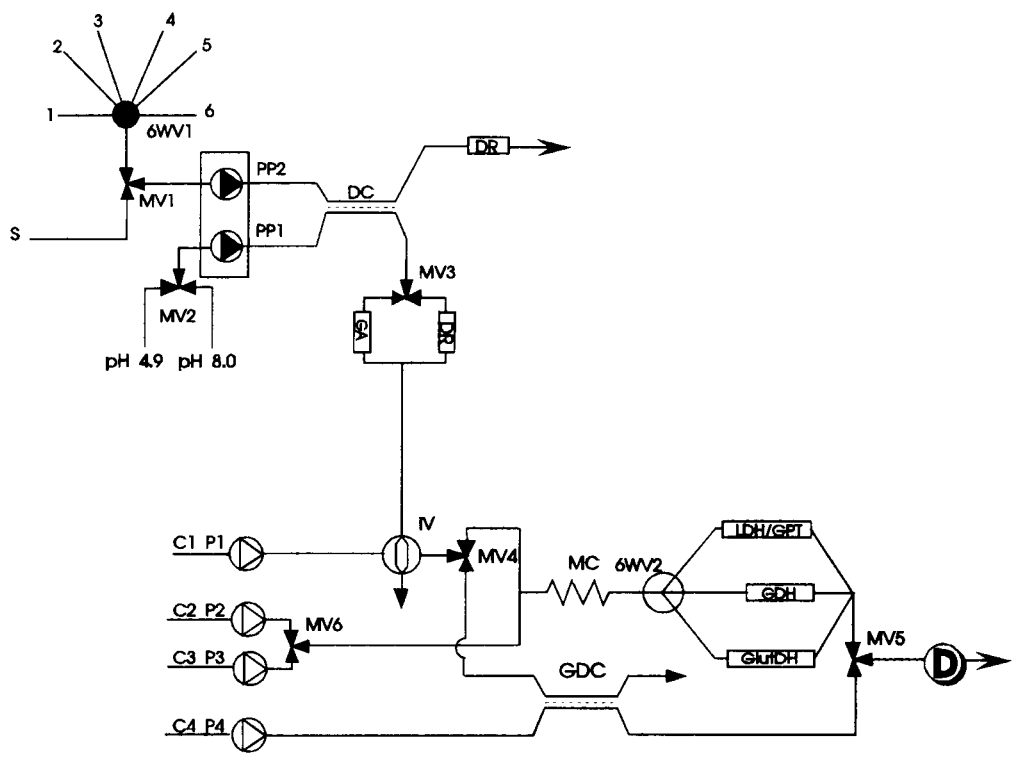

Fig. 7. FIA set-up for the automatic determination of ammonia, glucose, lactate, glutamine and glutamate, 6WV1 and 6WV2 = six way valves, GA, LDH/GPT, GDH, GlutDH = enzyme reactors, DR = blank reactors, DC = dialysis cell, GDC = gas dialysis cell, W = waste, PP1 + 2 = channels of the peristaltic pump, other symbols as in Figs. 2 and 6.

solution. Amino acids interfere in most cases. This problem can be solved by the gas dialytic transfer of ammonia into the acceptor solution. But the gas dialysis separation and the OPA reaction can not be performed simultaneously in the gas dialysis cell because the microporous separation membrane would be wetted by the organic solvents. Therefore an aqueous OPA reagent was developed.

Replacing the mercaptoethanol for thioglycolic acid allows to prepare a totally aqueous OPA reagent with an acceptable stability of around 14 days. The reagent contains 7.5 mM *o*-phthaldialdehyde and 28.7 mM thioglycolate in 0.4 M borate buffer and is adjusted to pH 10.4. The isoindol derivate, which is produced according to

$$NH_3 + OPA + \text{thioglycolate} \rightleftharpoons \text{isoindolderivative} \quad (5)$$

is measured fluorimetrically with an excitation wavelength of 340 nm and an emission wavelength of 440 nm. The enzymatically produced NADH is detected at the same wavelengths. First the sequential determination of glucose and ammonia was implemented in the corresponding FIA set-up shown in Fig. 7. The aqueous standard solutions were directly injected into the 0.1 M Tris, 20 mM Na_2SO_4 carrier solution with pH 10.6 (C1: 1 ml min^{-1}). Then the sample flows through the gas dialysis cell GDC. At the acceptor side the OPA reagent is propelled with $\dot{V}_4 = 1$ ml min^{-1}. The separated ammonia is absorbed and chemically trapped by the OPA. Ammonia can be determined in the range from 1.2 μM to 4.0 mM. The regression line is represented by

$$y_{NH4+} = (2.695 \pm 0.046)\text{l/mmol} \times c + (0.187 \pm 0.095) \quad (6)$$

with $\alpha = 0.05$, $n = 5$ and $r^2 = 0.998$, and was calculated in the range from 0.1 to 2.0 mM. To determine glucose the magnetic valves MV4 and MV5 are switched. MV5 prevent the back transport of the OPA reagent into the enzyme reactors. The pumps P2 and P4 are switched synchronously on and off, respectively. Now the carrier solutions C1 and C2 (2.5 mM NAD^+, 0.1 M TRIS) with pH 1.6 are mixed in the coil MC establishing the optimum pH 7.3 for the GDH.

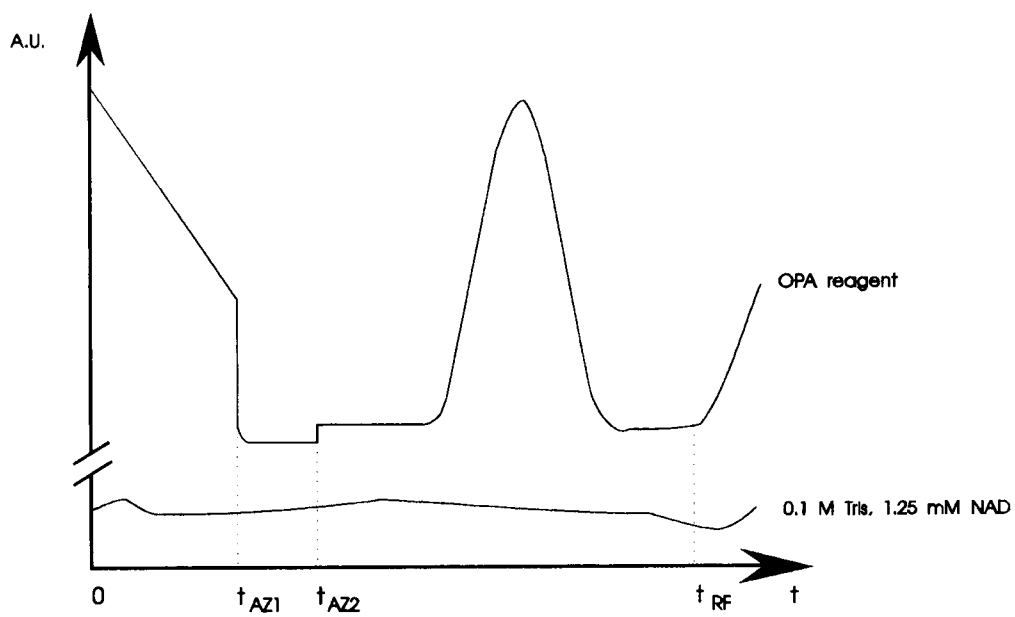

Fig. 8. Detector signal courses in arbitrary units (A.U.) after starting the pumps and sample injection for the fluorimetric ammonia determination with the OPA method in comparison to the basis line of the NAD^+ reagent solution; t_{AZ1}, t_{AZ2} = moments of the first and the second autozero time, t_{RF} = begin of refilling.

The low pH value allows the NAD^+ solution to be stored and used for more than 8 weeks. It was found that sodium ions activate glucose dehydrogenase in Tris buffer solutions. Glucose can be determined in the range from 0.2 to 1.5 mM on the basis of the regression line:

$$y_{gluc} = (3.136 \pm 0.062)\text{l/mmol} \times c + (1.05 \pm 2.53) \quad (7)$$

with $\alpha = 0.05$, $n = 5$, $r^2 = 0.999$. To implement these determination procedures in the same detector range and with one and the same parameter set, automatically a wide range autozero is necessary because of the high basis signal of the OPA reagent in comparison with NAD^+. After switching from the enzymatic to the nonenzymatic assay the detector baseline shifts out of range caused by the high fluorescence of the OPA reagent alone. The autozero scales the fluorescence signal back to the primary scale. Fig. 8 demonstrates the effect of a twofold recall of the autozero for the fluorimetric determination of ammonia. Also during the refilling of the piston pumps the background fluorescence is increasing considerably. The first autozero call sets the base line to its original level. After a further 10 s the autozero is repeated. The lower line represent the fluorescence signal of the mixture C1 + C2.

All determination procedures can work with the same fluorimetric detection. Easily oxydizable substances, e.g. ascorbic acid, uric acid and iron(II) did not disturb the proposed determination procedures. However even the different optimum reaction conditions of the enzymatic assays are not compatible with each other.

Fig. 9 shows the pH dependence on the flow rate ratio. The pH was monitored with a glass

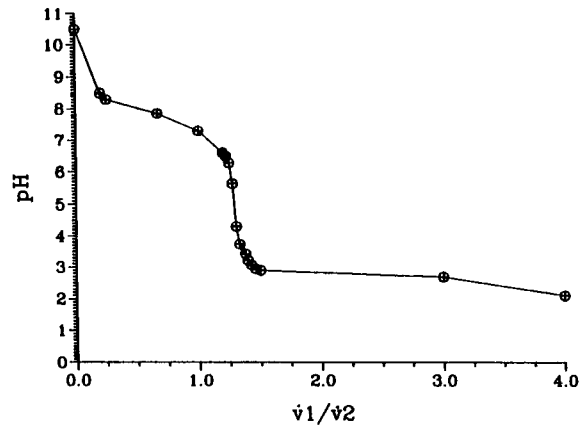

Fig. 9. pH-working curve for mixing the buffer solutions 1 = 0.1 M Tris with 2.5 mM NAD^+ adjusted to pH 1.6 and 2 = 0.1 M Tris, pH 10.6; $\dot{v}_1$ and $\dot{v}_2$ = the corresponding flow rates.

electrode in the outlet of the mixing coil MC1. The pH can be precisely adjusted between 6.5 and 8.5 allowing the optimum pH values for each enzymatic assay to be adjusted during the analytical cycle of the five channel set-up.

The immobilized glutaminase has its activity maximum around pH 4.9 and is stable between pH 4.5 and 6.0. Therefore the glutamine has to be determined in two steps at pH 4.9 for Eq. 6 and at pH 8.4 for Eq. 7 (Table 2).

The sample solution is dialyzed against a 0.05 M sodium acetate buffer with pH 4.9. Sample and acceptor solution are pumped with $\dot{V} = 1$ ml min^{-1}. The glutamine is hydrolyzed continuously in the glutaminase reactor GA. The MV3 valve switches between this reactor and a blank reactor, which have nearly the same dispersion D. This configuration opens up a way to determine

Table 3
Parameters of the determination channels in the FIA set-up shown in Fig. 4

	Flow C1, pH 1.6 (ml min^{-1})	Flow of the second carrier pH 10.6 (ml min^{-1})	Stop time in the reactor (s)	Stop time in the dialysis cell (s)
Glucose	1.5	C2 = 1.5	0	0
Lactate	0.5	C2 = 1.5	0	10
Glutamine	0.25	C2 = 0.75	20	30
Glutamate	0.25	C2 = 0.75	20	30
Ammonium	0.5	C4 = 0.5	/	30

glutamate and glutamine sequentially by means of a difference measurement of the resulting peak areas. Then the preconditioned sample solution is injected into the carrier C1 which is mixed with carrier C2 to adjust the pH optimum 8.4. For all other determinations the sample solution is dialyzed against a 0.1 M Tris buffer, pH 8.0, which is selected by MV2.

The six way valve 6WV2 selects the corresponding enzyme reactors enabling the sequential determination of glucose, lactate and glutamine/glutamate to be performed.

To implement the lactate determination according to Eqs. 8 and 9 (Table 2) an additional carrier solution C3 is necessary, which is mixed with the carrier C1 to adjust the optimum pH value of 8.0. The composition of C3 was 0.1 M Tris, 1 M NaCl, 5 mM NAD^+ and 30 mM sodium glutamate with pH 1.6. Up to 30 lactate determinations per hour are possible for a reactor flow rate of 2 ml min^{-1}.

Table 3 gives the summary of the preadjusted optimum parameters for the five determination procedures.

The adaptation of all determination procedures to the same fluorescence detector range was achieved by the adjustment of the corresponding residence times in the dialysis cell, the gas dialysis cell and the enzyme reactors.

The FIA system was applied for the fast sequential determination of glucose, L-lactate, L-glutamine, L-glutamate and ammonia in mixed standard solutions, which were adapted to the real cell culture media with respect to the expected concentration ranges and the protein content. Table 4 summarizes the determination ranges, the regression line equations and the maximum injection rates.

The reliability and the robustness of this five-channel configuration was proved during several 120-h runs. Table 5 shows the measured peak height stabilities of the enzyme reactors. All enzyme reactors appeared to be stable enough for the monitoring of animal cell cultures for more than 5 days. The stability of the lactate channel is determined by the stability of the immobilized glutamate pyruvic transaminase. Lactate can also be determined with immobilized lactate dehydrogenase alone in the desired concentration range from 0.1 to 20 mM, which allows a threefold increase of the sampling frequency. In this case a parabolic calibration graph is obtained, which, however, allows precise lactate determinations to be performed with relative standard deviations between 1.1 and 2.3% ($n = 4$, $\alpha = 0.05$).

The sampling system is a considerable source of error and disturbances, which are especially caused by the slowly increasing fouling of the dialysis membrane in the presence of proteins. Despite the long response time of more than 2 min is not critical for the investigated process analytical problem, it is generally desirable to minimize the response time. Additionally it was also found that the glutaminase reactor is more stable in the pulsed FIA mode.

Table 4
Five-channel FIA; $m = 6$; $n = 4$; $\alpha = 0.05$

Glucose

$y_1 = (1.008 \pm 0.012)$l/mmol $\times x_1 + (0.015 \pm 0.019)$
$y_1 = 1$ for $c_1 = 50$ mmol/l with $x_1 = c_1/(50$ mmol/l)
range: $x_1 = < 0.1; 50 >$ mmol/l
$r^2 = 0.999$; maximum injection rate: 100/h

L-Lactate [a]

$y_2 = (0.992 \pm 0.015)$l/mmol $\times x_2 + (0.024 \pm 0.020)$
$y_2 = 1$ for $c_2 = 20$ mmol/l with $x_2 = c_2/(20$ mmol/l)
range: $x_2 = < 0.1; 20 >$ mmol/l
$r^2 = 0.996$; maximum injection rate: 20/h

L-Glutamine

$y_3 = (0.994 \pm 0.011)$l/mmol $\times x_3 + (0.009 \pm 0.019)$
$y_3 = 1$ for $c_3 = 5$ mmol/l with $x_3 = c_3/(5$ mmol/l)
range: $x_3 = < 0.1; 5 >$ mmol/l
$r^2 = 0.998$; maximum injection rate: 50/h

L-Glutamate

$y_4 = (0.999 \pm 0.012)$l/mmol $\times x_4 + (0.010 \pm 0.018)$
$y_4 = 1$ for $c_4 = 5$ mmol/l with $x_4 = c_4/(5$ mmol/l)
range: $x_4 = < 0.1; 5 >$ mmol/l
$r^2 = 0.999$; maximum injection rate: 50/h

Ammonium

$y_5 = (1.005 \pm 0.016)$l/mmol $\times x_5 + (0.034 \pm 0.021)$
$y_5 = 1$ for $c_5 = 20$ mmol/l with $x_5 = c_5/(20$ mmol/l)
range: $x_5 = < 0.1; 20 >$ mmol/l
$r^2 = 0.992$; maximum injection rate: 60/h

[a] With co-immobilized GPT/LDH.

Table 5
Stability of the enzyme reactors and of the OPA reagent, $T = 15°C$, with FIA set-up in Fig. 9

Reactor/reagent	Analyte concentration mM	Relative sensitivity (%) after	
		48 h	120 h
Glutaminase[a]	3	98	70
GlutDH	3	97	72
GDH	5	85	70
LDH/GPT	2.5	90	55
OPA	2.5	99	97

[a] OPA fluorimetric detection of the released ammonia, GlutDH = glutamate dehydrogenase, GDH = glucose dehydrogenase, LDH/GPT = lactate dehydrogenase/glutamate pyruvic transaminase.

Therefore the FIA set-up was modified according to Van der Pol et al. [28] to that shown in Fig. 10 which was used in the following investigations. The dialysis cell DC is inserted between the injection valve IV and the magnetic valve MV3. The switching over between the nonenzymatic ammonia determination and the three channel enzymatic analyzer is implemented as in the set-up shown in Fig. 7. The automatic pH adjustment is implemented by the 4/2 way valve MV4/2 and the two 3/2 way valves MV3 and MV4. During the determination sequence the flow rate ratio between pump P2(C2) and pump P3(C3) is selected automatically to adapt the pH value to the pH optimum for the enzyme reactors.

The sampling time is considerably decreased. Because of the pulsed dialysis the sensitivities of the determination channels are around 10-fold lower than in the set-up shown in Fig. 7.

Fig. 11 shows the on-line monitored concentrations of ammonia, glutamine, glutamate, lactate and glucose during the start phase of an animal cell culture. All determination procedures were performed without stopped flow steps. At the beginning of the process monitoring glutamate was determined by subtracting the peak areas, which are measured without from those measured with the glutaminase reactor. But no significant glutamate concentration could be detected during this experiment. Therefore the glutamate channel was switched off. The measurement of the remaining 4 components by double injections including a washing step of 5 min after each completed analysis cycle took 42 min. The sampling tube is rinsed with 0.2 M sulphuric acid between MV2 and the injection valve.

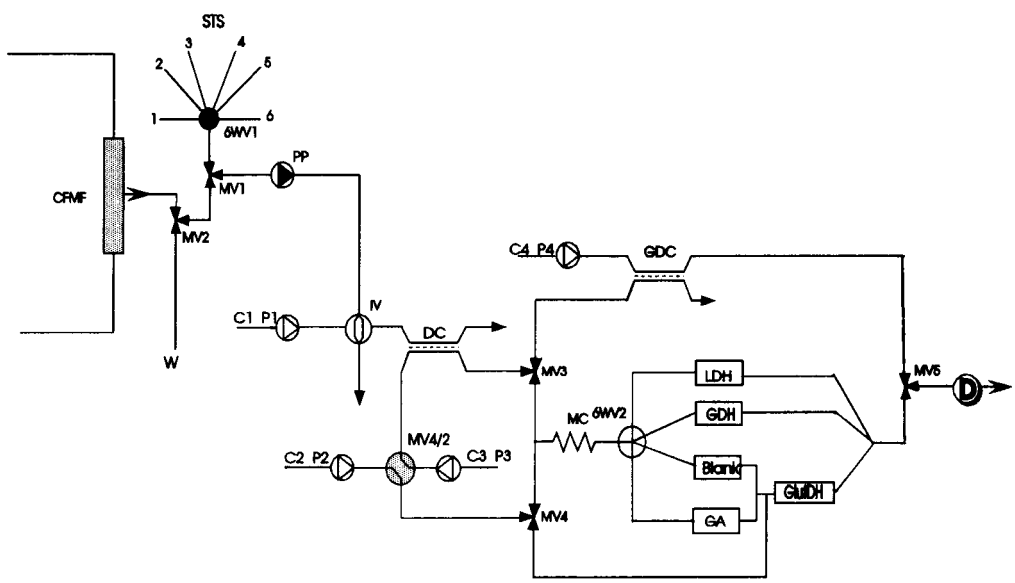

Fig. 10. FIA set-up for the long-term on-line monitoring of animal cell cultures, STS = standard solutions, MV 4/2 way/position valve, CFMF = cross flow microfiltration module, other symbols as in Fig. 9, see text for explanation.

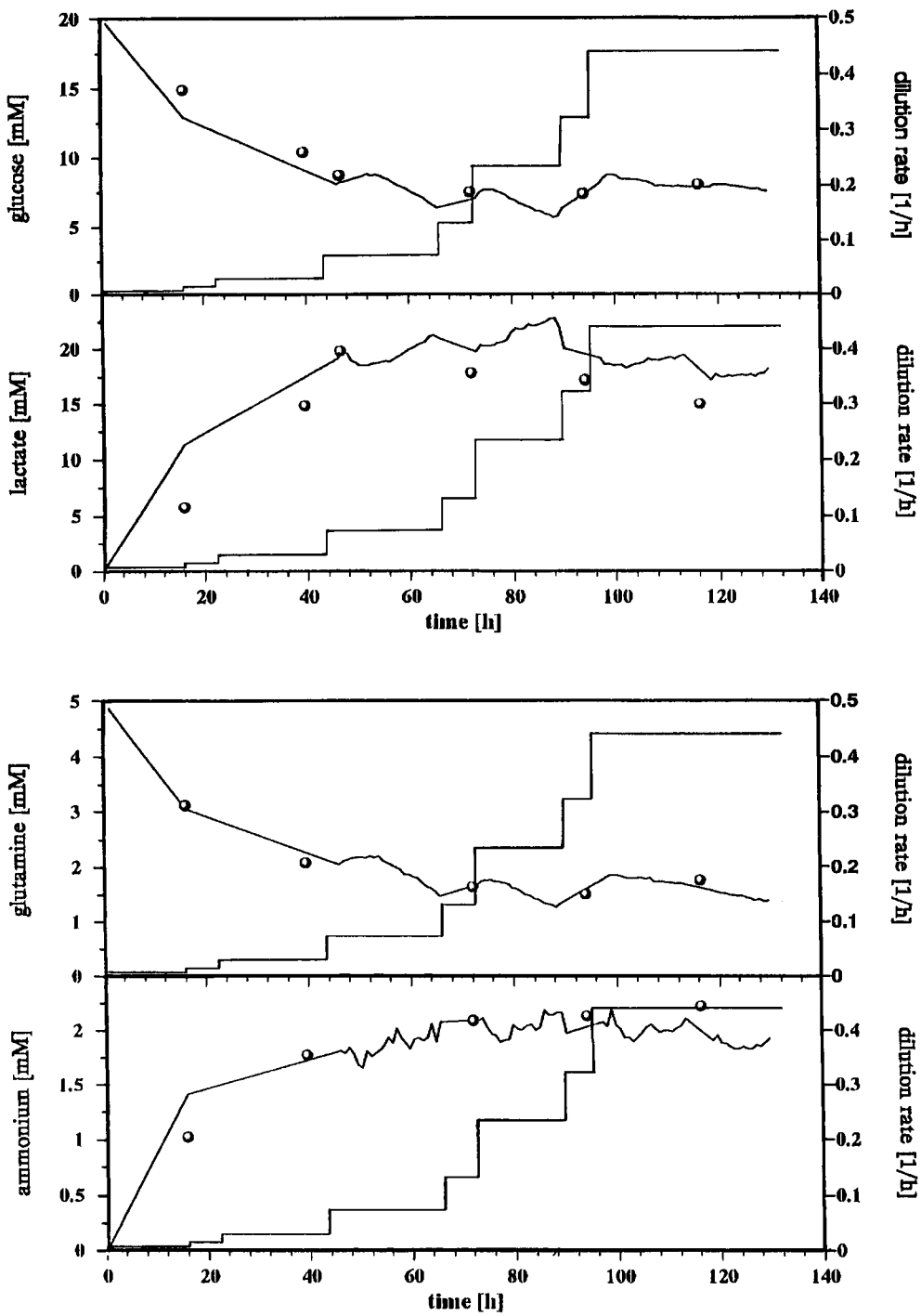

Fig. 11. On-line monitored concentrations during the start phase of a continuous animal cell culture, ○ = off-line measured values, a = glucose and lactate, b = glutamine and ammonia/ammonium, see text for explanation.

Table 6 summarizes the composition of the carrier flows and their pH values. To improve the robustness of the modified FIA set-up in comparison to that shown in Fig. 7, 0.2 M Tris buffer solutions of pH 5 and 9 are mixed to adjust the optimum pH value. Because sodium azide does not inhibit the enzymes significantly it is used to prevent microbial growth in the carrier and standard solutions. The standard solutions were prepared in the cell culture medium.

The animal cell cultivation was monitored on-line without interruptions during the first 130 h. One complete analysis with two injections for glucose and lactate and three injections for glutamine and ammonia took around 25 min. The sampling line was washed 5 min after such a complete analysis cycle. The off-line and the on-line measured concentration values agreed well for glucose, glutamine and ammonia. The on-line monitored lactate values were significantly higher than the off-line values, which were measured by the amperometric lactate sensor.

The long-term stability of the enzymatic assays was tested under process conditions for 55 days in a separate experiment. Fig. 12 shows the measured peak stability for the injection of 340 mg l^{-1} glutamine, 1.8 g l^{-1} glucose and 1.8 g l^{-1} lactate under the conditions of the on-line process monitoring. The glutamine channel did not show any decrease of the peak height in the first two weeks. The conversion degree of the glucose reactor decreased by only 16% in the first two weeks. The peak heights of the lactate channel increased surprisingly in the first two weeks. Up to 3000 injections for the lactate and the glucose channel and 4500 injections for the glutamine channel could be performed under process conditions without an exchange of the enzyme reactors. The long term stability of the FIA system may be improved further by two equal enzyme reactors for the most frequently used determination channels.

Table 6
Carrier solutions for the on-line monitoring of the animal cell cultivation

C1	0.2 M Tris, 0.2 M Na_2SO_4, 0.02% NaN_3	pH 7.15
C2	0.2 M Tris, 0.2 M Na_2SO_4, 0.02% NaN_3	pH 9.0
C3	0.2 M Tris, 2.5 mM NAD^+, 0.02% NaN_3	pH 5.0
C4	OPA reagent	pH 10.4

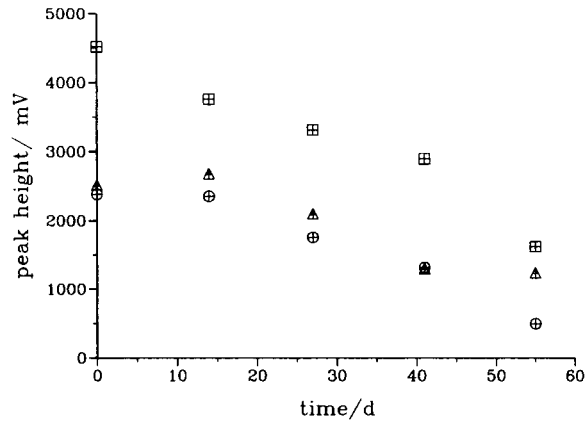

Fig. 12. Peak height stability of the four active determination channels during the on-line monitoring of the animal cell culture, □ = glucose, △ = L-lactate and ○ = glutamine.

Other and more detailed FIA investigations of the animal cell cultivation are described by Van der Pol et al. [28]. Attempts to use the proposed FIA set-up to automatically control the glucose and the glutamine concentration during a continuous cell cultivation will be reported later.

4. Conclusions

By means of a robust and highly flexible software control and the corresponding modular hardware very different FIA procedures can be implemented as well as some new procedures. Because all switching times and time courses of the FIA components can be freely programmed and independently controlled from each other a highly flexible flow analytical system is realizable.

The use of precisely working pumps and highly reliable injection valves together with a robust hardware in all parts of the measuring set-up is of essential importance for successful longterm runs of a multichannel FIA set-up. An advantage of the described FIA set-up is the relative high precision of all measurements.

A developed and fully automated FIA set-up including the on-line sampling and the in-line sample conditioning can be applied for the on-line process monitoring of biotechnological processes like, for example, the continuous animal cell culture.

Reagents and analytes can be stopped in the enzyme reactors to implement one step and two step stopped flow methods. Such FIA stopped flow methods open up a way to control the analyte conversion and to optimize multistep enzymatic assays.

The optimum conditions for up to six different determination reactions can be automatically adjusted on-line. Precisely controlled sample preconditioning and separation steps and finely tuned residence times enables a nearly optimum adaptation to also very different determination ranges and the necessary reaction conditions. During a multicomponent analysis the residence times and the reaction conditions can be automatically controlled in wide ranges and changed during the assay procedures.

Detailed information about the software FIACCO and the corresponding licence can be requested from R. Eberhardt.

References

[1] F. Lazaro, A. Rios, M.D. Luque de Castro and M. Valcarcel, Anal. Chim. Acta, 179 (1986) 279.

[2] K. Cammann, Fresenius' Z. Anal. Chem., 329 (1988) 691.

[3] T.J. Cardwell, R.W. Cattrall, P.C. Hauser and I.C. Hamilton, Anal. Chim. Acta, 214 (1988) 359.

[4] M. Bos, A. Bos and W.E. van der Linden, Anal. Chim. Acta, 233 (1990) 31.

[5] R. Renneberg, G. Trott-Kriegeskorte, M. Lucki-Lange, M. Pawlowa, A. Warsinke, V. Jäger, R. Wagner, K. Löster, G. Kaiser, F. Noll, U. Wollenberger, R.D. Schmid and F.W. Scheller, GBF Monograph, Vol. 14, Flow Injection Analysis (FIA) based on Enzymes or Antibodies, VCH, Weinheim, 1991, p. 67.

[6] H.-G. Hundeck, A. Sauerbrei, U. Hübner, T. Scheper, K. Schügerl, R. Koch and G. Antranikian, Anal. Chim. Acta, 238 (1990) 211.

[7] I. Ogbomo, R. Kittsteiner-Eberle, U. Englbrecht, U. Prinzing, U. Danzer and H.-L. Schmidt, Anal. Chim. Acta, 249 (1991) 137.

[8] R. Kittsteiner-Eberle, I. Ogbomo and H.- L. Schmidt, Biosensors, 4 (1989) 75.

[9] J. Nielsen, K. Nikolajsen, S. Benthin and J. Villadsen, Anal. Chim. Acta, 237 (1990) 165.

[10] K. Nikolajsen, J. Nielsen and J. Villadsen, Anal. Chim. Acta, 214 (1988) 137.

[11] U. Spohn, K.H. Mohr, K. Reichwald and I. Rapthel, Anal. Chim. Acta, 252 (1991) 145.

[12] H.U. Bergmeyer, J. Bergmeyer and M. Graβl (Eds.), Methods of Enzymatic Analysis, Vol. 8, VCH, Weinheim, 3rd edn., 1985, p. 357.

[13] H.U. Bergmeyer, J. Bergmeyer and M. Graβl (Eds.), Methods of Enzymatic Analysis, Vol. 8, VCH, Weinheim, 3rd edn., 1985, p. 454.

[14] U. Spohn, R. Eberhardt, B. Joksch, R. Wichmann, Ch. Wandrey and H. Voβ, in R. Schmid (Ed.), Flow Injection Analysis (FIA) Based on Enzymes or Antibodies, GBF Monograph, Vol. 14, VCH, Weinheim, 1991, p. 51.

[15] B. Joksch, R. Eberhardt, U. Spohn and Ch. Wandrey, in R. Schmid (Ed.), Flow Injection Analysis (FIA) Based on Enzymes or Antibodies, GBF Monograph, Vol. 14, VCH, Weinheim, 1991, p. 63.

[16] J. Ruzicka and E.H. Hansen, Flow Injection Analysis, Wiley, New York, 2nd edn., 1988

[17] K. Steube and U. Spohn, Anal. Chim. Acta, (1994) in press.

[18] D.L. Massart, A. Dijkstra and L. Kaufman, Evaluation and Optimization of Laboratory Methods and Analytical Procedures, Elsevier, Amsterdam, 1978, p. 543.

[19] W.E. van der Linden, Anal. Chim. Acta, 179 (1986) 91.

[20] E. Luellau, G. Dreisbach, A. Grogg, M. Biselli and Ch. Wandrey, in R.E. Spear, J.B. Griffiths and C. MacDonalds (Eds.), Animal Cell Technology: Developments, Processes and Products, Butterworth-Heineman, Oxford, p. 469.

[21] J. Thömmes, J. Gätgens, M. Biselli, R.W. Rundstadtler and Ch. Wandrey, Cytotechnology, (1993) in press.

[22] G. Johansson, L. Ögren and B. Olsson, Anal. Chim. Acta, 145 (1983) 71.

[23] B. Olsson and G. Johansson, Anal. Chim. Acta, 145 (1983) 87.

[24] B. Olsson, B. Stalbom and G. Johansson, Anal. Chim. Acta, 179 (1986) 203.

[25] M. Roth, Anal. Chem., 43 (1971) 880.

[26] T. Aoki, S. Uemura and M. Munemori, Anal. Chem., 55 (1983) 1620.

[27] M.C. Garcia Alvarez-Coque, M.J. Medina-Hernandez, R.M. Villanueva Camanas and C. Mongay Fernandez, Anal. Biochem., 178 (1989) 1.

[28] J. van der Pol, U. Spohn, R. Eberhardt, J. Gaetgens, M. Biselli, Ch. Wandrey and J. Tramper, Biotechnol. Bioeng., (1994) in press.

ELSEVIER

Analytica Chimica Acta 292 (1994) 297–304

ANALYTICA CHIMICA ACTA

Description of a three-dimensional polarograph

F. David [a], H. Ouguenoune [a], A. Bolyos *[,a,1], N. Papadopoulos [b,*]

[a] *Laboratoire de Radiochimie, Institut de Physique Nucléaire, Bat. 100, 91406 Orsay Cedex, France*
[b] *Section of Physical, Analytical and Environmental Chemistry, Department of Chemistry, Aristotle University, 54006 Thessaloniki, Greece*

(Received 21st April 1993; revised manuscript received 27th July 1993)

Abstract

All the mechanistic and kinetic information for an electrochemical reaction lies on the i–E–t surface. The collection of all these data is almost impossible without a computerized polarograph. This paper describes the construction of such an instrument. For the creation of the software that controls a three-dimensional polarograph, Labview, a special programming language for data flow programming, was used. In this language the programmer designs the block diagram of the control program and this block diagram is the actual program. In this way the programming work is considerably simplified. In order to test the instrument, the electrochemical oxidation of the iodide ion on mercury was studied.

Key words: Polarography; Computerized polarograph; Three-dimensional polarograph

1. Introduction

An essential condition for the successful application of all electroanalytical methods is an understanding of the course of the electrode process. Only when the mechanism of the electrolytic process is understood is it possible to interpret unexpected changes in electroanalytical measurements and predict interferences. Polarography possesses a favoured position among electroanalytical methods because of the relative simplicity of its theory and use. Essential advantages are the well controlled and defined transport of the electroactive species to the electrode surface, the virtually potentiostatic conditions of the electrolysis in which the products formed at one potential cannot affect the process at another potential and the fresh, clean surface of every drop virtually unaffected by previous electrolysis. In addition, the polarographic response is convenient for quantitative measurements because current plateaux are obtained in the mass transfer-limited region. However, the information obtainable from classical d.c. polarography provides a limited basis for the characterization of the nature of a

* Corresponding author.
[1] Permanent address and corresponding author: Laboratory of Isotopic Research, Institute of Chemistry and Physics, University of Debrecen, Debrecen, Hungary.

SSDI 0003-2670(94)00062-Q

charge-transfer process because polarography is considered as a method with a very restricted time window [1].

Usually electrochemists use cyclic voltammetry [2] to acquire a reasonable understanding of the system with which they are working. However, cyclic voltammetry as a technique for studying an electrochemical reaction has several serious drawbacks which arise from the fact that the experimental variables are changing with time and with potential. We believe that a better way to elucidate an electrochemical reaction is to use a step potential perturbation. When a potential step perturbation is applied there is only the element of time to consider, as all potential-dependent quantities will be constant. We have demonstrated recently that electrochemical reactions can be studied with the use of three-dimensional (3D) voltammetry. [3,4] The method relies on the principle that the complete electrochemical behaviour of a system can be obtained through a series of steps to different potentials with recording of the current–time curves to yield a three-dimensional surface [5]. Intersections of this three-dimensional surface with planes vertically oriented to the t axis produce polarographic-type i–E curves for different times. The validity of this methodology does not lie, of course, in the display of the i–E–t surface in the 3D space, but in the information that the reconstructed i–E curves can provide. The latter have the advantages of a chronoamperometric technique, i.e., potentiostatic conditions and an extended time window together with those of voltammetric techniques, i.e., a clear picture of the dependence of the electrochemical reaction on potential. The only prerequisite for the application of this method for the elucidation of an electrochemical reaction is for the working electrode to have an easily renewable and constant surface. If we use as the working electrode a static mercury drop electrode [6], three-dimensional voltammetry can be considered as a kind of a polarography with a wide and finely resolved time window.

Up to now this technique has not found widespread use, probably because the analysis and accumulation of the data to construct the i–E–t surface are virtually impossible without a computerized electrochemical system. The application of on-line computers to electrochemistry developed only slowly owing to the early problems associated with interfacing. Minicomputers were first used for on-line control of electrochemical experiments in the early 1970s and on reading the early papers it is seen that considerable expertise in both analog and digital electronics was required to interface the computer with the electrochemical cell. Now the situation has changed. Today it is possible to purchase "off-the-shelf", at reasonable cost, very satisfactory interface cards for several of the most popular personal computers. The first instrument that could produce such an i–E–t three-dimensional surface was constructed by Bond and Anderson [7,8]. Their instrument was based on a Motorola 6800 D2 microprocessor "kit" equipped with an additional 8 K of RAM and an input–output board. Much of the small memory of this microcomputer was used for programming steps, leaving minimal capacity for data manipulation. The software for this microcomputer had to be written in assembly and offered very limited flexibility. Machine language uses up less of the memory capacity than the much easier to use higher level languages. Modern microcomputers have much more memory than their ancestors and permit the use of a high-level language.

Recently we have interfaced an IBM-compatible computer to a PAR 170 electrochemistry system using Turbo basic as the programming language for the interface and the analysis of the experimental data [3]. Using this electrochemical data acquisition and analysis system, we have demonstrated that three-dimensional voltammetry can provide the means to examine the pathway of an electrochemical reaction in detail. The time-scale of the experiment can be varied to investigate whether there are other processes coupled to the one of interest. However, the instrument manipulation is still difficult and requires technical knowledge about the hardware, the programming language and the operating system.

The objective of this paper is to describe the construction of a "user-friendly" 3D polarograph. Such an instrument gives electrochemists who are

not specialists in computers the possibility to operate it.

2. Experimental and results

In this work we interfaced a Macintosh II FX personal computer with a PAR Model 373 potentiostat and a Tacussel type EGMA polarographic stand that consists of a static mercury drop electrode (SMDE), an electromagnetic hammer for the dislodgement of the drop, a magnetic stirrer and an electromagnetic valve that controls the flow of the inert gas for the deoxygenation of the solution. All the operations with this polarographic stand can be controlled either manually or by means of external TTL signals. For the interface we used the NB-M10-16 multifunction card supplied by National Instruments. This card contains a 12-bit A/D converter with 16 analog inputs, two 12-bit D/A converters, eight lines of TTL compatible digital input output and three 16-bit counter timers for timing. The use of Labview, a language based on data flow programming [9] specially designed by National Instruments for building high-performance instrumentation and analysis applications, helped enormously in the construction of a user-friendly 3D polarograph. This application software package gives all the necessary tools to control an electrochemical instrument [10].

The digital-to-analog converter (DAC) in the NB-M10-16 multifunction card serves as a programmable function generator, supplying voltages to the electrochemical system. The analog-to-digital converter, provided by the same plug-in board, acquires the current. Labview provides the software drivers to configure and control the various functions of the card in the form of icons.

In order to run a 3D polarographic experiment, a series of potential step experiments are needed. First the mercury drop is formed at a potential where no faradaic process occurs; after allowing a 3-s rest time for the solution in the drop neighbourhood to equilibrate, a potential step is applied at the working electrode and the current is recorded. Then the mercury drop is dislodged, the solution is stirred with a magnetic stirrer and purged with nitrogen for 1 s and a new drop is formed.

For the timing of the experiment the timer of the NB-M10-16 multifunction card was used.

All chemicals used were of analytical-reagent grade.

2.1. Principles of program development

Traditional instrumentation systems consist of individual instruments that are physically interconnected. Each instrument has a front panel with its own combination of indicators, knobs and switches. Modern instrumentation systems include computers, which provide more efficient control of instruments, automatic data acquisition and extensive data analysis capabilities. The modern systems, however, are expensive to implement and maintain because of the amount of programming required.

Scientists and engineers usually use a block diagram to explain an application program. The block diagram shows the major components and their relationships. Then this block diagram is converted into code using a conventional programming language. With Labview the block diagram is the executable program and in this way the programming work is extremely simplified. The Labview software system is designed to simplify scientific programming. Labview is a complete scientific language and provides all the tools needed for data acquisition, data analysis data management and presentation. Labview uses data flow concepts, traditional program control structures and an instruction set consisting of graphical elements. All the arithmetic operations and control structures found in a conventional language are also found in Labview in the form of icons that can be selected from a functions menu. Any computation possible with a conventional language is also possible with Labview.

A data flow program is represented graphically. The syntactic items of this language are icons that perform various functions. The block diagram is created by choosing these graphical items and wiring them together. The user develops an application program in this environment by building a "virtual instrument" (VI). A VI is

simply a software program that looks and acts like a real-world instrument. A VI like a real-world instrument, possesses a front panel and the operator can control the VI from this panel. The front panel defines the inputs and the outputs of a VI. As the front panel of a VI is much like a hardware front panel, the inputs are referred to as controls and the outputs are as indicators. The front panel contains all the controls that allow the manipulation of the VI and the indicators and the graphs where the data are displayed. In Labview, inputs to the program can take the form of switches, knobs and buttons while outputs can be indicators graphs and meters. Thus the real world can be represented in the computer's world and the information is displayed in a manner that is readily assimilated by the human eye and mind. The front panel of a VI is its interactive interface to the program operator. It is the means by which the operator adjusts parameters and executes the program. If it is desired to use a VI programmatically, that is, to call it from another VI like a subroutine, then an icon is designed for the sub-VI and this icon is "wired" into the block diagram of the VI in the higher program. Each icon has a set of connecting terminals that define the points of the icon that receive input and provide output. In a block diagram various lower level VI can be combined by graphically wiring them together. Their function is similar to the role of a subroutine in a classical programming language.

The diagram specifies the operations to be performed to convert the input to the correct output just as one would do when writing source code. The icons perform these functions and wires pass the necessary parameters from controls to icons, from icons to icons and from icons to indicators Wires in the diagram are different

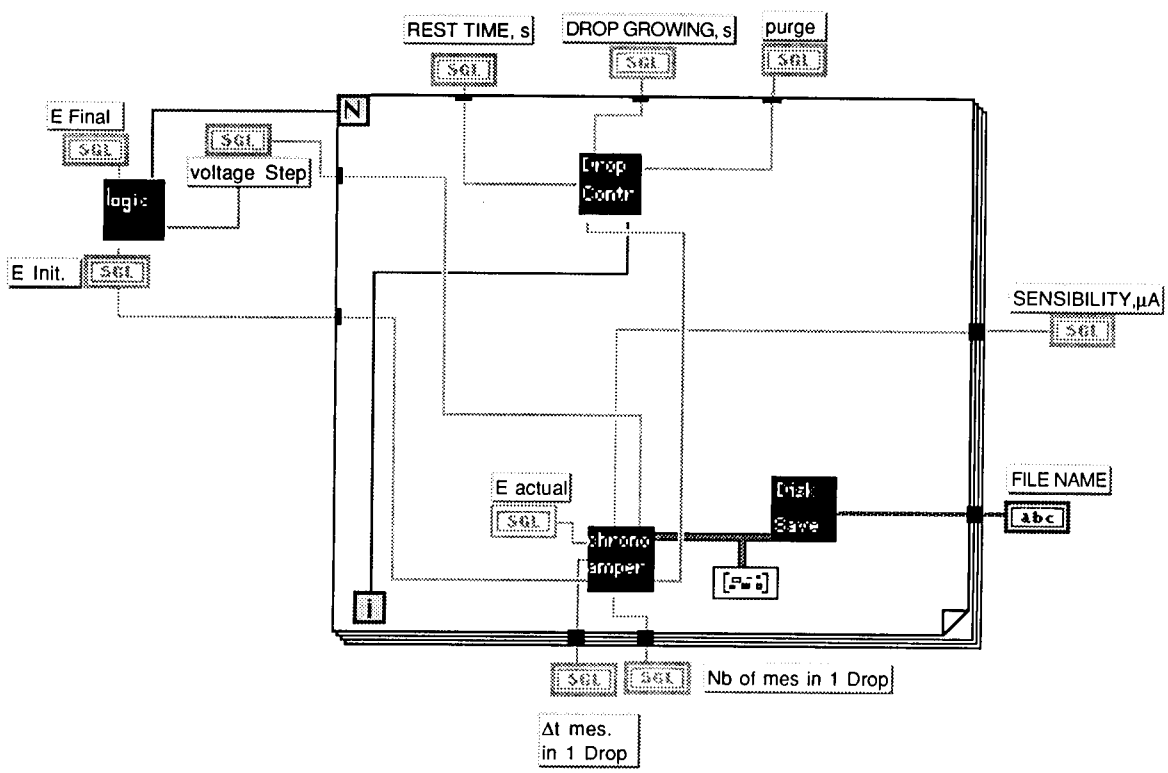

Fig. 1. Block diagram of the 3D polarograph. This diagram is the actual software program that controls the polarograph.

styles for different data types. (single-precision, double-precision, integer, binary, string, array, etc.)

It is very tedious and almost impossible to run a 3D experiment with direct manipulation. A series of chronoamperometric experiments are required. Data must be acquired and saved for each experiment. Then the data collected from all these chronoamerometric experiments must be analysed and presented. For this application we designed two virtual instruments: the 3D polarography VI and the 3D analysis VI.

Fig. 1 shows the block diagram of the 3D polarography VI. In order to simplify this software program, we designed four sub-VI: (a) the "logic" VI, which receives input from initial voltage, final voltage and voltage step controls and produces as output the number of chronoamperograms needed to complete a 3D polarography experiment; (b) the "drop control" VI, which controls the SMDE; (c) the "chronoamperometry" VI, which applies the voltage to the potentiostat and reads the current during the drop's life, this VI also displays, during the experiment, the applied voltage at an indicator, and at the end of each chronoamperometric experiment it displays the chronoamperometric curve at a graph indicator and sends the data to the "disk save" VI; and (d) the "disk save" VI, which saves the data to the disk.

In Fig. 2, the front panel of a 3D polarography VI is shown. On the front panel the operator is able to select the initial and final potentials, the voltage increment, the birth potential of the drop, the drop life and the number of current acquisitions that will be performed during the drop's life. When the user requests the execution of the program, data written in the controls pass through the wires into the icons.

The "drop control" VI, the "chronoamperometry" VI and the "disk save" VI are inside a for-next loop. N is the limit terminal of a for-next loop, while i is the counter value of the for-next loop. Each time that the loop is executed, this

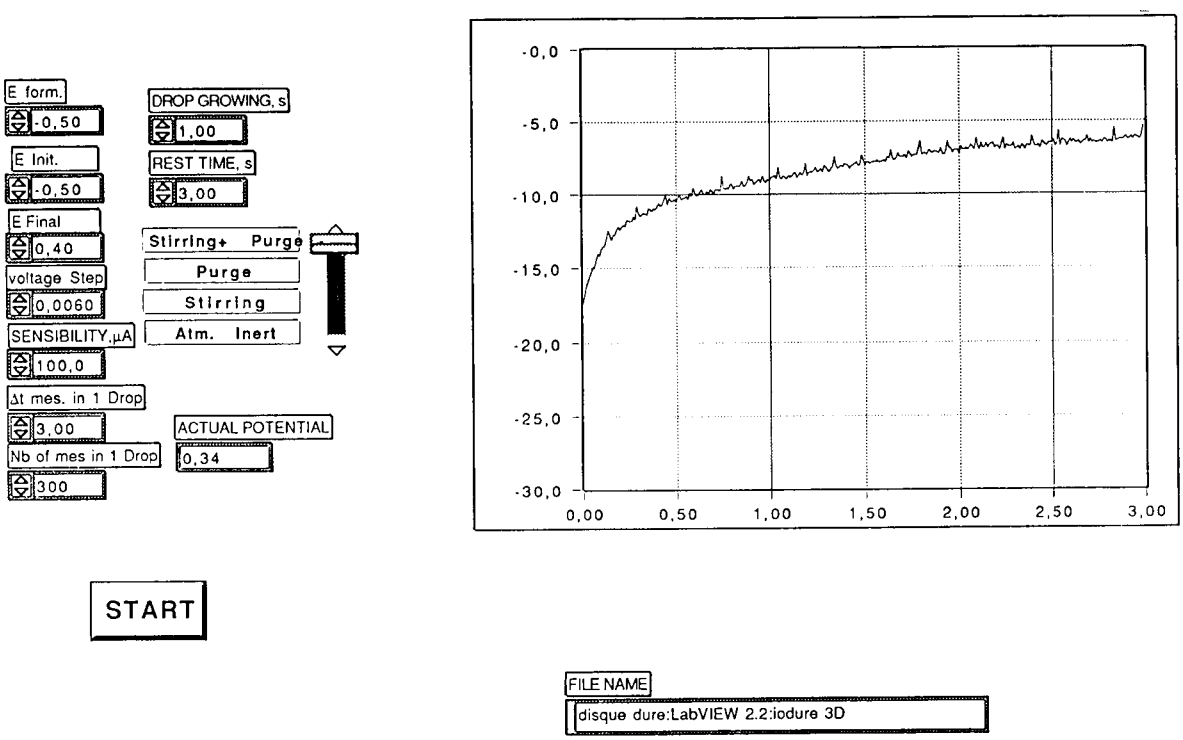

Fig. 2. Front panel of the 3D polarograph.

value is incremented. The "logic" VI computes the numbers of iterations for this loop and passes this value to the N terminal. The execution of this for-next loop begins. The value of the counter is passed to the "drop control" VI; the old drop is dislodged and a new one is formed as described earlier. When the execution of this module is completed, a dummy parameter is passed to the "chronoamperometry" VI and the operation of this virtual instrument begins. The potential is calculated and applied to the cell and the i–t transient is shown on the front panel. At the end of each chronoamperometric experiment, the potential is returned to the initial value E, the data are sent to the "disk save" VI and this VI saves the data in the disk, in a file with the polarogram's name.

For the analysis of the 3D polarographic data we designed a 3D analysis VI. With this instrument the treatment of 3D polarographic data is possible. The operator selects the name of the 3D polarogram to be evaluated, selects the sampling time and the E–i curve for the desired sampling time is shown on the screen. The E–i curves in Fig. 3 were produced with the help of this virtual instrument. In addition, the $E_{1/2}$, i_d and the slope of the $\log(i/i_d - i)$ versus potential plot can be calculated and the log-plot can be displayed on the screen. More details are available from the authors on request.

2.2. Test of the instrument

In order to test the 3D polarograph, we studied the polarographic behaviour of the iodide ion in the concentration range 3×10^{-4}–1×10^{-2} M. The potential steps covered the whole +0.6 to −0.6 V vs. SCE range in 4-mV intervals. The sampling rate was set to 10 ms per sample and 300 points were stored in digital form for each curve. Fig. 3 shows i–E curves sampled at 20, 50, 100, 200 and 500 ms and from 3D polarographic experiments at different concentrations.

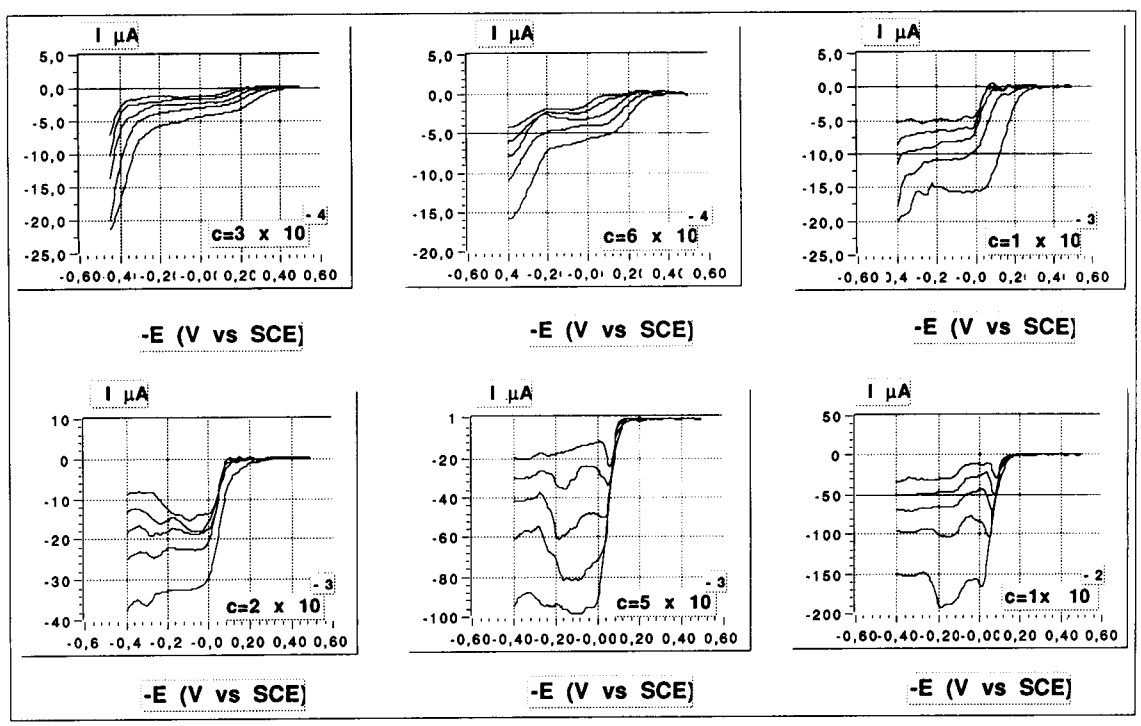

Fig. 3. i–E curves sampled at 20, 50, 100, 200 and 500 ms. These curves were produced with the 3D analysis virtual instrument designed for the analysis of 3D polarographic data. Concentrations (c) in M.

3. Discussion

Anodic polarographic oxidation, as a result of the formation of insoluble reaction products on the electrode surface, is subjected to a phenomenon that inhibits the response of a dropping mercury electrode (DME). The d.c. polarographic behaviour of iodide was investigated by Kolthoff and Miller [11], who used a DME with a drop time of 3–4. They observed that the waves are well defined when the concentration of I^- is lower than 2.5×10^{-4} M. For higher concentrations, the diffusion current is ill-defined and changes in a highly irregular way with increasing positive potential; the current in the diffusion region is determined by the electrode film characteristics rather than by the rate of diffusion of material to the electrode surface. Canterford et al. [12] showed that short drop times (rapid polarography) improve the analytical usefulness of waves complicated by film formation. A paper by Turner et al. [13] on anodic processes involving mercury compound formation illustrates that similar improvements are also obtained in the normal but not differential-pulse polarographic response. The improvement is attributed to the decreased time-scale and equally short electrolysis times of both short drop time or pulse methods. All these results accumulated from various researchers at different times can be collected in a single 3D polarographic experiment.

Three-dimensional voltammetry allows the study of the electrochemical process to be carried out with respect to both potential and time under strictly potentiostatic conditions. We observe that the $E_{1/2}$ value shifts to more positive potential for the curves that correspond to longer sampling times because of an HgI_2 film on the surface. For our study we used an SMDE. The conventional DME exhibits a continuously increasing area until drop dislodgement. In the SMDE the drop is expanded to a given area, which is then maintained constant. This feature enables the current measurement to be made on an electrode with a static area. The DME sometimes produces artifacts that can mislead the experimenter [12]. With a DME, even when using short, controlled drop times, the oxidation wave of iodine shows a pre-step. A possible explanation is the continuous growth of the drop on the DME, which results in a continuous increase in the area occupied by the surface film. We did not observe any pre-wave in our voltammograms. Since the introduction of polarography, many instrumental modifications have been developed to improve the form of the polarogram and to increase the sensitivity and the resolution [14–16]. However, the limitations in polarography are not introduced by the electronics but by the DME. Owing to the increasing surface area, a component of charging current always exists that distorts the form of the polarographic wave, especially at low concentrations. Christie and Osteryoung [17] have shown that the small charging current that produces the mercury drop growth limits the sensitivity of the pulse polarographic method. Bond and Jones [18] found that sampled d.c. polarography using an SMDE is comparable to the performance of differential-pulse polarography with a normal DME.

Different polarographic techniques involve different time domains and measure different responses of the electrode process. With 3D polarography, the time evolution of a process can be followed continuously. In our experiment, the electrochemical process is controlled by diffusion and by film-formation kinetics. Koryta's equation [19] can give an estimation of the diffusion effect:

$$t = 1.85 \times 10^6 \Gamma^2 / C^2 D$$

where Γ = the maximum adsorbate surface concentration, C = the adsorbate bulk concentration, D = the adsorbate diffusion coefficient and t = the time needed to cover completely the surface of the electrode.

Using this equation, the time needed to cover completely the surface with a film of iodine molecules is about 4 for a concentration of 3×10^{-4} M and about 16 ms for a concentration of 5×10^{-3} M. We observed that the polarographic waves are well defined for all the curves that correspond to sampling times shorter than the time needed for a monomolecular film to be created on the mercury surface. For the curves that correspond to higher sampling times we observed that the anodic limiting current fluctuates irregularly and is poorly defined.

4. Conclusions

A computerized electrochemical system and an SMDE permit all the instrumentation difficulties to be overcome and extend polarography to a third dimension, time, and thus render the polarographic technique suitable for mechanism diagnosis. With the use of an on-line microcomputer for the acquisition, storage and analysis of the data, it is possible to give the polarographic technique a very wide time window, limited only by the *RC* constant of the cell, the rise time of the potentiostat and that of the current measuring system. Hence in a 3D polarographic experiment, in the time needed to run a classical polarographic experiment information for many time domains is recorded.

The cost of the hardware components has decreased considerably in recent years and with Labview the creation of sophisticated software is no longer expensive proposition. The most difficult part in an application program written in a conventional language is to create a user-friendly interface, that is, a user interface that is readily identifiable and easy to understand. In Labview, the front panel concept, with its knobs, switches graphs and displays, provides a user-friendly interface for operating the program. Labview simplifies computer interfacing because it includes icons that provide voltage output and data collection capabilities. These are software modules that can drive the NB-M10-16 multifunction card. The programmer does not need to know the details of the hardware but simply wires the suitable icons for an input–output operation in the block diagram. The weak point of Labview is that it does not accept code directly. Tasks that require a great deal of data manipulation or calculation are more easily implemented with a conventional language than in the graphic language of Labview. Although it gives the opportunity to integrate code written in C or Pascal, this code must be written and tested using an external compiler and then integrated into a Labview program. These operations are not simple.

Acknowledgement

This work was supported by the Greek–French "Platon" scientific cooperation program.

References

[1] A.J. Bard and L.R. Faulkner, Electrochemical Methods: Fundamentals and Applications, J. Wiley, New York, 1980.
[2] B.W. Rossiter and J.F. Hamilton (Eds.), Physical Methods of Chemistry, Vol. II: Electrochemical Methods, J. Wiley, New York, 1986.
[3] N. Papadopoulos, C. Hasiotis, G. Kokkinidis and G. Papanastasiou, J. Electroanal. Chem., 308 (1991) 83.
[4] N. Papadopoulos, C. Hasiotis, G. Kokkinidis and G. Papanastasiou, Electroanalysis, 5 (1993) 99.
[5] W.H. Reinmuth, Anal Chem., 32 (1960) 1509.
[6] Z. Galus, in P.T. Kissinger and W.R. Heineman (Eds.), Laboratory Techniques in Electroanalytical Chemistry, Dekker, New York, 1984.
[7] J.E. Anderson and A.M. Bond, Anal. Chem., 3 (1981) 5048.
[8] J.E. Anderson and A.M. Bond, Electroanal. Chem., 145 (1983) 21.
[9] M. Anderson, Data Flow Programming with Labview, Application Note PN320117-01, National Instruments, 1988.
[10] F. David and N. Papadopoulos, Electroanalysis, 3 (1991) 72.
[11] I.M. Kolthoff and C.S. Miller, J. Am. Chem. Soc. 63 (1941) 1405.
[12] D.R. Canterford, A.S. Buchanan and A.M. Bond, Anal. Chem., 45 (1973) 1327.
[13] J. Turner, R.H. Abel and R.A. Osteryoung, Anal. Chem., 7 (1975) 1343.
[14] G.C. Barker, in Proceedings of Congress on Analytical Chemistry in Industry, St. Andrews, 1957, p. 199.
[15] G.C. Barker and A.W. Gardner, Fresenius' Z. Anal. Chem., 173 (1960) 79.
[16] R.E. Cover and J.G. Connery, Anal. Chem., 41 (1969) 918.
[17] J.H. Christie and R.A. Osteryoung, J. Electroanal. Chem., 49 (1974) 301.
[18] A.M. Bond and R.D. Jones, Anal. Chim. Acta, 121 (1980) 1.
[19] J. Koryta, Collect. Czech. Chem. Commun., 18 (1953) 206.

ELSEVIER

Analytica Chimica Acta 292 (1994) 305–310

ANALYTICA CHIMICA ACTA

Response of polyacrylamide-benzo-15-crown-5 coated platinum electrode to calcium ion and some other cations in propylene carbonate and its thermodynamic application

Toshio Nakamura *, Chiharu Hayashi, Kosuke Izutsu

Department of Chemistry, Faculty of Science, Shinshu University, Asahi, Matsumoto 390, Japan

(Received 16th November 1993; revised manuscript received 28th January 1994)

Abstract

The response of an ion sensor consisting of polyacrylamide (PAA) coupled to benzo-15-crown-5 (B15C5) to sodium, potassium, magnesium, calcium and barium ions in propylene carbonate (PC) were investigated. The PAA–B15C5 electrode showed a Nernstian response to sodium and calcium ions in PC. The electrode was applied to obtain the successive complex formation constants of the calcium ion in PC with such basic aprotic solvents, D, as *N*,*N*-dimethylformamide, *N*-methylpyrrolidinone, *N*,*N*-dimethylacetamide, dimethyl sulfoxide, and hexamethylphosphoric triamide. From the constants obtained in PC-rich solutions, the Gibbs energies of transfer of the calcium ion from PC to D and PC–D mixtures were calculated. The electrode was also used to obtain directly the Gibbs energies of transfer of the calcium ion from PC to PC–D mixtures. The successive complex formation constants of the sodium ion in PC with D and the Gibbs energies of transfer of the sodium ion from PC to D and to PC–D mixtures were also obtained to certify the developed electrode.

Key words: Ion selective electrodes; Potentiometry; Aprotic solvents; Calcium; Complex formation; Crown ethers; Ion transfer

1. Introduction

Ion-selective electrodes have been widely used for both thermodynamic and analytical studies in non-aqueous solutions [1]. Some of them have been successfully applied to the study of ionic solvation. Recently some new types of ion-selective electrodes for use in aprotic solvents based on a polymer coupled to ionophores or metal phthalocyanine complexes were developed and one of them was used to obtain the successive complex formation constants of magnesium and barium ions in acetonitrile (AN) and propylene carbonate (PC) with some basic aprotic solvents, D, and the Gibbs energies of transfer from PC to PC–D mixtures [2,3].

Here we report on the potentiometric responses to alkali and alkaline earth metal cations in PC of an electrode prepared by coating a platinum disk with a membrane of polyacryl-

* Corresponding author.

SSDI 0003-2670(94)00051-M

amide (PAA) coupled to benzo-15-crown-5 (B15 C5) and the application of the electrode to obtaining the complex formation constants of the calcium and sodium ions in PC with such other solvents D as *N*,*N*-dimethylformamide (DMF). *N*-methylpyrrolidinone (NMP). *N*,*N*-dimethylacetamide (DMA), dimethyl sulfoxide (DMSO) and hexamethylphosphoric triamide (HMPA). From the constants obtained in PC-rich solutions, the Gibbs energies of transfer of the calcium and sodium ions from PC to D and to PC–D mixtures were calculated. The electrode was also used to obtain directly the energies of transfer of the calcium and sodium ions from PC to PC–D mixtures.

2. Experimental

2.1. Apparatus

Both the construction and the preparation of the electrode and the potentiometric measuring system were similar to those mentioned previously [2,3].

2.2. Reagents

4-Nitrobenzo-15-crown-5 was a product of Tokyo Kasei Kogyo. *N*,*N*′-dicyclohexylcarbodiimide was purchased from Wako. Raney Nickel was a product of Nakarai. Calcium trifluoromethanesulfonate [$Ca(CF_3SO_3)_2$] was prepared from calcium hydroxide and trifluoromethanesulfonic acid purchased from Wako. The calcium salt was recrystallized from ethanol and dried under high vacuum and the purity was confirmed by an EDTA titration. All other chemicals were the same as those mentioned in the previous paper [2,3].

2.3. Preparation of PAA–B15C5 conjugate

The crown ether, 4-nitrobenzo-15-crown-5, was conjugated at the carboxyl group of the carboxyl-modified polyacrylamide by the same procedure as that described in the previous report [4].

2.4. Measurement of the electrode potential

The response of the electrode was tested in the following cell I:

$Ag/10\ mM\ AgClO_4$
$+ 10\ mM\ Et_4NClO_4[PC + 2\%(v/v)AN]$
$//50\ mM\ Et_4NClO_4(PC)$
$//C\ MX_x + 10\ mM\ Et_4NClO_4(PC)$
/PAA–B15C5/Pt (Cell I)

where MX_x stands for such salts as $NaClO_4$, $KClO_4$, $Mg(ClO_4)_2$, $Ca(CF_3SO_3)_2$ and $Ba(ClO_4)_2$ to be tested.

All the solutions were freshly prepared daily. To obtain calibration graphs, the concentration, C (mol dm^{-3}), was usually increased by the standard addition method with a microburette. Other conditions were the same as mentioned in the previous paper [3].

2.5. Determination of complex formation constants and Gibbs energies of transfer

The e.m.f.'s of the following cell II were measured:

$Ag/10\ mM\ AgClO_4$
$+ 10\ mM\ Et_4NClO_4[PC + 2\%(v/v)AN]$
$//50\ mM\ Et_4NClO_4(PC)$
$//5 \times 10^{-4}\ M\ Ca(CF_3SO_3)_2$
$+ 10\ mM\ Et_4NClO_4(PC + D)$
/PAA–B15C5/Pt (Cell II)

In order to determine the complex formation constants of calcium ion in PC with other solvents, D was added stepwise to the cell. Analyses of the potentiometric data were carried out with an NEC PC9801-UX personal computer.

3. Results and discussion

3.1. Responses of the electrode

The responses of the polymer membrane electrode (PAA–B15C5) to sodium, potassium, mag-

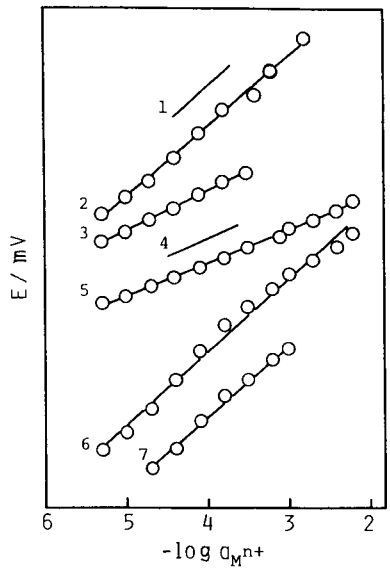

Fig. 1. Calibration graphs for various cations in propylene carbonate for the PAA–B15C5 electrode (25° C). Lines 1 and 4: theoretical slope for singly charged cations (59.2 mV/log a_{M^+}) and doubly charged cations (29.6 mV/log $a_{N^{2+}}$), respectively: (2) Na^+; (3) K^+; (5) Ca^{2+}; (6) Mg^{2+}; (7) Ba^{2+}.

nesium, calcium and barium ions in PC were investigated. Usually the electrode reached a steady state potential within 5 min after changes in the ion concentrations. The response was faster than that of the same electrode used in AN [5]. Some typical calibration graphs obtained with the electrode in PC are shown in Fig. 1. The activity of the metal ion, $a_{M^{n+}}$, was calculated using the same method as described in the previous report [3]. The electrode responded in a Nernstian manner to sodium and calcium ion activities in the concentration ranges of 6.0×10^{-6} M–1.8×10^{-3} M and 6.0×10^{-6} M–8.0×10^{-3} M with a slope of 58.6 mV/log a_{Na^+} and 28.6 mV/log $a_{Ca^{2+}}$, respectively. Although the E–log a_{K^+} relationship was linear for the potassium ion, the slope was lower than the theoretical one, whereas the responses for the magnesium and barium ions were super-Nernstian as shown in Fig. 1. It is interesting that the slopes for the doubly charged cations were very close to the one for the singly charged cations, but the reason for obtaining such slopes cannot be elucidated at this stage.

3.2. Successive complex formation constants of calcium ion

The electrode developed here was applied to study the complexation of calcium ion in PC with solvents D such as DMF, NMP, DMA, DMSO and HMPA. Prior to the experiment the electrode was conditioned in 0.5 mmol l^{-1} $Ca(CF_3SO_3)_2$–PC solution for two days. From the e.m.f. change obtained by the stepwise addition of D to Cell II the complex formation constants, β_i, of the calcium ion were obtained. The electrode usually reached a steady state potential within 3 min after addition of D. The change in the liquid junction potential between the sample solution and the salt bridge on addition of D is considered to be small based on an experimental study on the liquid junction potential [6]. The complex formation constant is defined in the same manner as described in Refs. 2 and 7.

Examples of the relationships between R_i (i = 1 and 2) and [DMA] are shown in Fig. 2. From

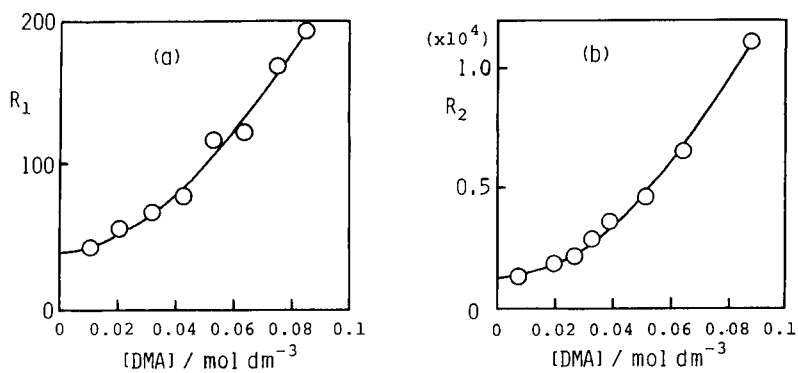

Fig. 2. Relationships between (a) R_1 and [DMA], and (b) between R_2 and [DMA] for the calcium ion in propylene carbonate.

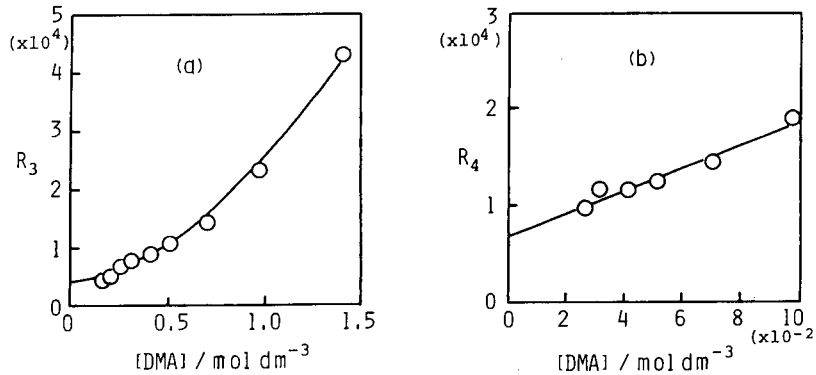

Fig. 3. Relationships between (a) R_3 and [DMA] and (b) between R_4 and [DMA] for the calcium ion in propylene carbonate.

the intercepts with the ordinates of Fig. 2a and 2b the values of β_1 and β_2, respectively, could be obtained. Fig. 3 shows the relationships between R_i ($i = 3$ and 4) and [DMA]. The values of β_3 and β_4 could be obtained from the intercepts with the ordinates of Fig. 3a and 3b, respectively. The

Table 1
Complex formation constants of calcium ion in PC with some basic aprotic solvents, D, and Gibbs energies of transfer (ΔG_{tr}) [a] of calcium ion from PC to D and to PC–D mixtures at 25° C

D = DMF	(log β_1 = 1.47, log β_2 = 1.80, log β_3 = 1.93, log β_4 = 2.3, log β_5 = 3.0)										
ϕ (DMF)	0.001	0.006	0.015	0.024	0.038	0.065	0.091	0.167	0.231	0.286	0.333
$-\Delta G_{tr(1)}$	0.20	0.78	1.38	1.92	2.70	4.00	4.96	6.93	8.11	8.95	9.61
$-\Delta G_{tr(3)}$	0.13	0.65	1.20	1.86	2.65	3.82	4.69	6.60	7.84	8.71	9.09
$-\Delta G_{tr(2)} = 11.6$											
D = NMP	(log β_1 = 1.56, log β_2 = 3.68, log β_3 = 4.30, log β_4 = 4.3, log β_5 = 4.5)										
ϕ (NMP)	0.001	0.006	0.015	0.024	0.038	0.065	0.091	0.167	0.231	0.286	0.333
$-\Delta G_{tr(1)}$	0.38	1.95	3.17	3.96	4.78	5.92	6.74	8.53	9.65	10.47	
$-\Delta G_{tr(3)}$	0.34	1.93	2.90	3.80	4.72	5.80	6.55	8.02	8.64	9.16	
$-\Delta G_{tr(2)} = 13.10$											
D = DMA	(log β_1 = 1.60, log β_2 = 3.06, log β_3 = 3.62, log β_4 = 3.8, log β_5 = 4.1)										
ϕ (DMA)	0.001	0.006	0.015	0.024	0.038	0.065	0.091	0.167	0.231	0.286	0.333
$-\Delta G_{tr(1)}$	0.27	1.34	2.43	3.22	4.07	5.29	6.16	8.00	9.14	9.96	10.60
$-\Delta G_{tr(3)}$	0.22	1.28	2.34	3.17	3.95	5.11	5.94	7.71	8.71	9.51	9.87
$-\Delta G_{tr(2)} = 12.59$											
D = DMSO	(log β_1 = 1.86, log β_2 = 3.50, log β_3 = 4.25, log β_4 = 4.8, log β_5 = 5.3)										
ϕ (DMSO)	0.001	0.006	0.015	0.024	0.038	0.065	0.091	0.167	0.231	0.286	0.333
$-\Delta G_{tr(1)}$	0.59	2.24	3.71	4.77	5.89	7.37	8.35	10.33	11.50	12.35	13.00
$-\Delta G_{tr(3)}$	0.35	2.19	3.62	4.80	5.86	7.13	7.98	9.72	10.82	11.55	12.16
$-\Delta G_{tr(2)} = 15.02$											
D = HMPA	(log β_1 = 2.78, log β_2 = 4.48, log β_3 = 6.00, log β_4 = 7.9, log β_5 = 10.2)										
ϕ (HMPA)	0.001	0.006	0.015	0.024	0.038	0.065	0.091	0.167	0.231		
$-\Delta G_{tr(1)}$	1.04	4.02	6.62	8.12	9.50	11.15	12.21	14.26	15.46		
$-\Delta G_{tr(3)}$	0.83	3.95	6.45	8.04	9.60	11.49	12.77	14.63	15.59		
$-\Delta G_{tr(2)} = 19.02$											

[a] $\Delta G_{tr(1, 2, 3)}$ in kcal mol^{-1}.

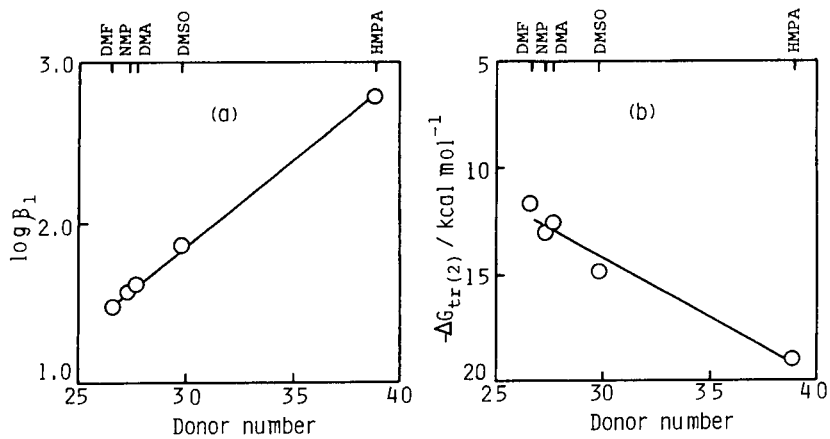

Fig. 4. Relationships between (a) log β_1 and donor number and (b) between $\Delta G_{tr(2)}$ and donor number for the calcium ion in propylene carbonate.

value of β_5 was equal to that of the slope obtained from the linear relationship in Fig. 3b. The values of β_i ($i = 1$–5) obtained in the experiment are summarized in Table 1. In Fig. 4a and b relationships between the donor number of D and log β_1, and $\Delta G_{tr(2)}$ are plotted. The linear correlations shows that the complexing ability of the calcium ion in PC increases with the donor number of D.

3.3. The Gibbs energies of transfer for calcium ion

The Gibbs energies of transfer, $\Delta G_{tr(3)}$, of calcium ion from PC to PC–D mixtures were obtained by the general thermodynamic equation $\Delta G = -2F\Delta E$, where ΔE is the difference between the potentials obtained for PC and PC–D in Cell II. The equations proposed by Clune et al. [3,8] were used for calculating $\Delta G_{tr(1)}$, $\Delta G_{tr(2)}$ and $\Delta G_{tr(3)}$. The relations between $\Delta G_{tr(3)}$ and ϕ_{DMA} are shown in Fig. 5. The solid line in Fig. 5 is $\Delta G_{tr(1)}$ obtained by using the successive formation constants shown in Table 1. Fig. 5 also shows the values of $\Delta G_{tr(2)}$ [ϕ(DMA) = 1.0]. The results, $\Delta G_{tr(2)}$, obtained in solvents such as DMF, NMP, DMA, DMSO and HMPA are also listed in Table 1.

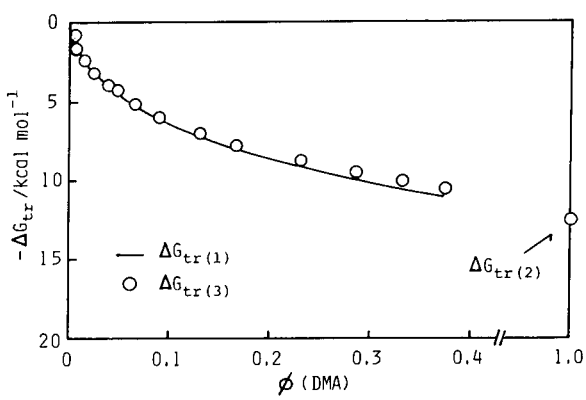

Fig. 5. Relationships between $\Delta G_{tr(1,2,3)}$ and ϕ(DMA) for the calcium ion in propylene carbonate.

3.4. Successive complex formation constants and Gibbs energies of transfer for sodium ion

For the verification of the PAA–B15C5 electrode the complex formation constants of the sodium ion in PC with DMF, NMP, DMA and

Table 2
Complex formation constants of sodium ion in PC with some basic aprotic solvents, D, and Gibbs energies of transfer of sodium ion from PC to D at 25° C

D	log β_1	log β_2	log β_3	log β_4	$-\Delta G_{tr(2)}$
DMF	0.40	0.59	0.49	−0.64	5.2
NMP	0.52	0.72	0.41	−0.05	5.5
DMA	0.61	0.58	0.87	0.17	5.8
	(0.57)	(0.86)	(0.6)	(0.3) [b]	(6.0) [b]
DMSO	0.78	0.94	0.92	0.82	7.4
	(0.74)	(0.92)	(0.9)	(0.8) [c]	(7.3) [c]

[a] $\Delta G_{tr(2)}$ in kcal mol^{-1}.
[b,c] See Ref. 8.

DMSO were obtained by using the electrode. The results are summarized in Table 2. The values are comparable to the values obtained in AN in previous work [7]. The Gibbs energies of transfer of the sodium ion were also calculated from log β_i by the same method as that used for the calcium ion and the results are listed in Table 2. The values of $\Delta G_{tr(1)}$ and $\Delta G_{tr(3)}$ of sodium ion in PC agree well each other. The relationship between the donor number of D and the $\Delta G_{tr(2)}$ of the sodium ion showed a linear correlation ($r^2 = 0.9863$). In Table 2 the values obtained previously by Clune et al. [8] with the cation-sensitive glass electrode according to the proposed method [7] are listed in parentheses. The results obtained with different electrodes agree well with each other as shown in Table 2. The reliability of the values of log β_1 in Tables 1 and 2 seem to be within 10% error.

4. Conclusions

Thermodynamic data concerning calcium–solvent interactions are very rare. The results in this experiment suggest that the PAA–B15C5 electrode may be considered to work satisfactorily both in PC and in PC–D mixtures as an indicator electrode for variation in the solvation energy of the calcium ion. As a result the electrode can be used to obtain such thermodynamic parameters as successive complex formation constants of the calcium ion with several dipolar aprotic solvent molecules and Gibbs energies of transfer of the calcium ion from PC to D and PC–D mixtures. The successful development of the calcium ion-selective electrode which can be used in aprotic solvents seems to be the first case.

Acknowledgement

This work was supported in part by a grant-in-aid for Scientific Research from the Ministry of Education, Science and Culture of Japan.

References

[1] J.F. Coetzee, B.K. Deshmukh and C.-C. Liao, Chem. Rev., 90 (1990) 827.
[2] T. Nakamura, H. Higuchi and K. Izutsu, Bull. Chem. Soc. Jpn., 61 (1988) 1020.
[3] T. Nakamura, M. Komai, S. Hosono and K. Izutsu, Anal. Chim. Acta, 238 (1990) 351.
[4] T. Nakamura and G.A. Rechnitz, Anal. Chem., 57 (1985) 393.
[5] T. Nakamura et al., unpublished results.
[6] K. Izutsu, T. Nakamura and Y. Aoki, J. Electroanal. Chem., 334 (1992) 213.
[7] K. Izutsu, T. Nakamura and K. Iwata, Anal. Chim. Acta, 117 (1980) 329.
[8] G. Clune, W.E. Waghorne and B.G. Cox, J. Chem. Soc. Faraday Trans. I, 72 (1976) 1294; B.G. Cox, W.E. Waghorne and C.K. Pigott, J. Chem. Soc., Faraday Trans. I, 75 (1979) 227.

ELSEVIER

Analytica Chimica Acta 292 (1994) 311–315

ANALYTICA CHIMICA ACTA

Pyrenebutyric acid fibre-optic chemical sensor for metronidazole in serum

Bin Zhu *, Xinyi Zhang, Jian Chen

Department of Pharmacy, Xinjiang Medical College, Urumqi 830054, Xinjiang, China

(Received 10th October 1993; revised manuscript received 24th January 1994)

Abstract

A pyrenebutyric acide fibre-optic chemical sensor based on fluorescence quenching was developed for the measurement of the serum concentration of metronidazole. A fluorescent membrane that was prepared by solvent casting from dioxane to incorporate pyrenebutyric acid into the polymer with plasticizer was used for the immobilized reagent phase of this optical sensor, obtaining limits of detection of 2.6 μg ml^{-1} for metronidazole in rabbit serum. No pretreatment of the serum samples was required. The pharmacokinetic parameters for the proposed method were in good agreement with a liquid chromatographic method.

Key words: Fluorimetry; Sensors; Fibre-optic sensors; Metronidazole; Pharmaceuticals; Pyrenebutyric acid; Serum

1. Introduction

The rapid determination at very low levels of pharmaceutical compounds in biological samples, e.g., blood, serum, plasma and urine, is very important in clinical therapeutics. Recently, fibre-optic chemical sensors (FOCS) have expanded rapidly in this field, mainly based on absorption, chemi- and bioluminescence, fluorescence, etc. [1,2]. Only a few of them deal with fluorescence quenching, e.g., for potassium [3] and halide ions [4].

In this work, a pyrenebutyric acid fibre-optic chemical sensor (PBA sensor) for metronidazole based on fluorescence quenching was developed. Quenching of fluorescence obeys the Stern–Volmer law, provided that the quenching is exclusively dynamic. The relationship between quencher concentration [Q] and measured fluorescence intensity F is given by

$$F_0/F = 1 + K_{SV}[Q]$$

where F_0 being the fluorescence intensity of the indicator in the absence of any quencher and K_{SV} the Stern–Volmer quenching constant.

Because of the complexity of biological samples, it is a challenge to use FOCS for the direct measurement of a component in a biological sample. Sepaniak et al. [5] developed a single fibre-optic fluoroprobe for the in vivo determination of the antitumour drug doxorubicin. In this work, a FOCS based on fluorescence quenching was used to measure directly metronidazole in serum and no pretreatment of serum sample was required. The pharmacokinetic parameters by this approach were in good agreement with those for a method based on liquid chromatography (LC).

* Corresponding author.

SSDI 0003-2670(94)00039-0

The FOCS was constructed with a sensing membrane that responds reversibly to metronidazole. The preparation and response characteristics of this optical sensor are described.

2. Experimental

2.1. PBA sensor system

The PBA sensor was based on a fluorescent membrane and its components were suitable amounts of cellulose triacetate, tributyl phosphate and pyrenebutyric acid (from Scientific Polymer Products and Molecular Probe). The materials were dissolved in 5.0 ml of dioxane and after using a vortex mixter to ensure that the solution was homogeneous, the solution was poured into a flat glass dish (2 × 8 cm) and the solvent allowed to evaporate, which required 24–72 h. The resulting membrane was cut into small sections, each weighing 2–5 mg and having an area of ca. 0.5–0.6 cm. The membrane thickness was ca. 0.08 mm. Fluorescent spectra of the membrane are shown in Fig. 1. Each section was held against the large end of a bifurcated fibre-optic bundle and the effect of distance between the membrane and the tip of the fibre bundle between 0.1 and 30 mm on sensitivity and linearity was investigated for metronidazole concentrations ranging from 5.0 to 100 μg ml^{-1}. Fig. 2 shows that a suitable distance is 1.0 mm.

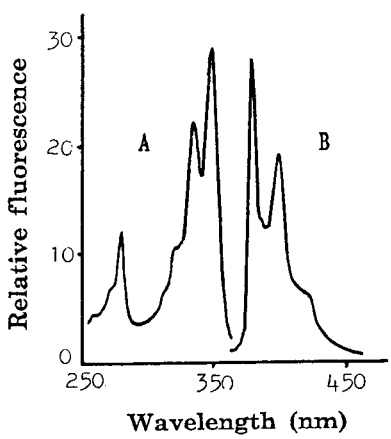

Fig. 1. Fluorescence spectra of membrane: (A) excitation spectrum; (B) emission spectrum.

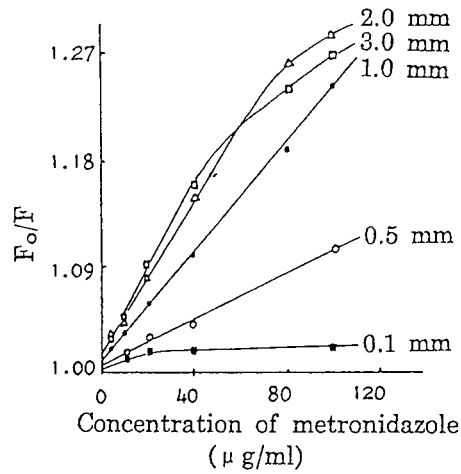

Fig. 2. Effect of distance between membrane and tip of fibre bundle on the sensor response to metronidazole.

A schematic diagram of the experimental set-up is shown in Fig. 3. The fluorescence of the membrane was excited at 347 nm using a 347-nm interference filter and a xenon lamp (Shimadzu) powered by a stabilized Shimadzu Model 12045 power supply. The excitation light was focused into one of the small heads of the bifurcated bundle. The emitted light was filtered by a 400-nm interference filter and detected using a model 9592B photomultiplier tube (UK) powered by a high-voltage supply/amplifier. The amplifier signal was displayed on a digital voltmeter.

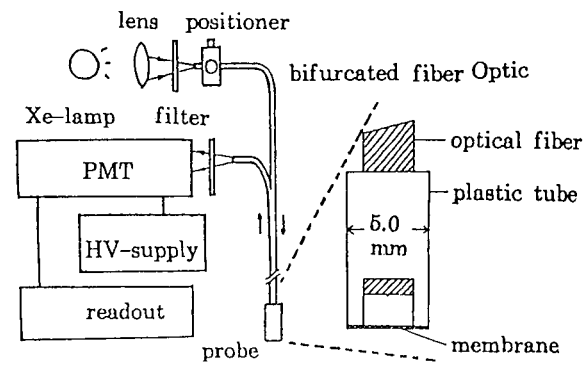

Fig. 3. Schematic diagram of the experimental set-up.

The PBA sensor did not need any preparation before use and was directly inserted into a serum sample to measure the concentration of metronidazole. Calibration graphs were obtained by measuring known amounts of metronidazole added to a serum sample from a normal donor and plotting the concentration against the corresponding F_0/F value obtained. In order to avoid ambient light interfering with the measurement, the ambient light intensity was constant (8-W fluorescent lamp) during the experimental period.

Metronidazole powder and tablets were obtained from Wuhan Pharmaceutical Factory and all the other chemicals were of analytical-reagent grade.

2.2. Liquid chromatographic procedure

Serum (0.5 ml) was pipetted into a test-tube (5 ml) followed by addition of ethanol (1 ml), in which a known amount of the required internal standard (nitrofurantoin) had been dissolved. The tube was capped and vortex mixed for 3 min, then centrifuged at 300 *g* at 25°C for 15 min. A suitable volume of clear solution was pipetted into a plastic tube (3 ml) and centrifuged at 900 *g* at 25°C for 5 min, and 10 μl of the solution were injected directly on to a 250 mm × 4.6 mm i.d. column packed with Nucleosil C_{18} (Shimadzu). The temperature of the column was set at 30°C. The mobile phase was ethyl cyanide (chromatographic grade)–redistilled water (18 : 82, v/v) at a flow-rate of 1 ml min^{-1}. UV detection was carried out at 340 nm. The identification and determination of metronidazole were based on the retention time and peak area relative to those of the internal standard.

3. Results and discussion

3.1. Characterization of PBA sensor

The most significant features of the PBA sensor are that it has a rapid response time and excellent reversibility with measurement. The response time did not exceed 2.0 s and the reversibility was 100.4 ± 0.5% ($n = 6$). The percentage reversibility of the PBA sensor was obtained by calculation using the equation

$$\text{reversibility} = [(F_0 - F)/(F_0' - F)] \times 100\%$$

where F_0, F and F_0' are the fluorescence intensity when the PBA sensor is inserted in the blank, analyte and blank solution in turn (Fig. 4).

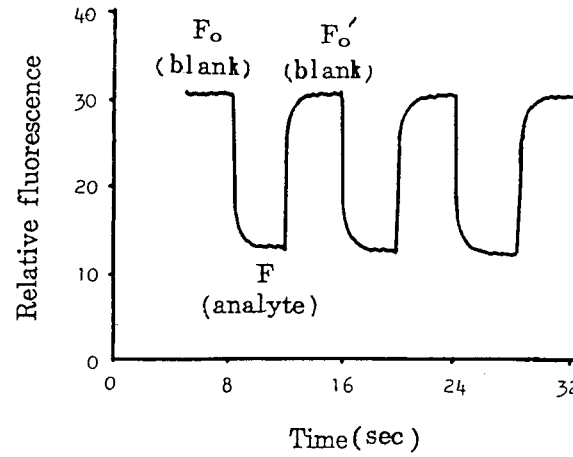

Fig. 4. Reversibility of PBA sensor (20 μg ml^{-1} metronidazole).

The stability of the PBA sensor was investigated over 12 months under the conditions used. About 200 analyses were carried out without a detectable change in its characteristics. After 18 months a slight decrease in membrane tenacity was observed, but this was not an obstacle for its further use. The long-term stability of the PBA sensor is therefore good.

As the technique is based on the measurement of fluorescence quenching, the interference by oxygen and by any other species that may co-exist with the analyte should be investigated. When many quenchers (1, 2, etc.) co-exist, the Stern–Volmer relationship becomes [6]

$$F_0/F = 1 + K_1[Q_1] + K_2[Q_2] + \ldots$$

If the concentration of the analyte is the sole variable among the concentrations of quenchers, the relationship between analyte concentration [Q] and measured fluorescence intensity F is similar for the Stern–Volmer law:

$$F_0/F = 1 + K[Q]$$

where F_0 is the fluorescence intensity in the absence of analyte, but K is inconsistent with the Stern–Volmer quenching constant K_{SV}; generally, K is less than K_{SV}. A blank assay showed that the PBA sensor response to sera from different normal donors at any time was identical, and therefore it can be considered that there is no interference by oxygen or any other quenchers that may co-exist with the analyte.

3.2. Linearity and detection limit

The calibration graph obtained for metronidazole in serum is linear over the concentration ranging 6.25–75 μg ml^{-1}. The least-squares regression equation for this graph is

$$F_0/F = 0.0118[Q]\ (\mu g\ ml^{-1}) + 0.992$$

$$(R^2 = 0.999,\ n = 6)$$

The detection limit, defined as the concentration of sample that yields a detector response equal to twice the detector noise, was determined to be 2.6 μg ml^{-1} for metronidazole in serum.

3.3. Precision and accuracy

The precision and accuracy of the proposed method for the determination of metronidazole in serum are summarized in Table 1. The relative standard deviations (R.S.D.) ranged from 2.3 to 6.4% for serum concentrations of metronidazole from 20 to 60 μg ml^{-1}. Large deviations were observed at low serum concentrations. The average recovery of the method was found to be 101.7 ± 3.9% over the concentration range 20–60 μg ml^{-1}. Therefore this probe presents adequate precision and accuracy for the determination of metronidazole in serum.

Table 1
Precision and accuracy of the proposed method ($n = 6$)

Metronidazole concentration (μg ml^{-1})	Measured concentration (mean ± S.D.) (μg ml^{-1})	R.S.D. (%)	Recovery (mean ± S.D.) (%)
20	19.5 ± 1.3	6.4	97.5 ± 6.3
40	42.1 ± 1.1	2.5	105.2 ± 2.7
60	61.5 ± 1.5	2.3	102.5 ± 2.4

Table 2
Comparison of results obtained for the pharmacokinetic parameters of metronidazole in rabbits using the proposed method and LC method

Parameter [a]	Labelled content obtained (μg ml^{-1}) [b]		t [c]	F [d]
	PBA sensor	LC		
K_a (h^{-1})	1.86 ± 1.31	1.68 ± 1.12	0.233	1.370
K (h^{-1})	0.66 ± 0.25	0.65 ± 0.10	0.083	6.25
V (l)	1.70 ± 0.90	2.80 ± 0.90	1.932	1.00
T_{max} (h)	0.98 ± 0.25	1.05 ± 0.33	0.378	1.74
$T_{1/2}$ (h)	1.19 ± 0.43	1.08 ± 0.18	0.522	5.71

[a] K_a = absorption rate constant; K = elimination rate constant; V = apparent volume of distribution; T_{max} = peak time; $T_{1/2}$ = half-time.
[b] Average for five rabbits with standard deviations.
[c] Theoretical value = 2.78 at 95% confidence limit.
[d] Theoretical value = 6.39 at 95% confidence limit.

3.4. Determination of metronidazole in serum

Metronidazole is an antimicrobial drug that has been increasingly used against anaerobic infections [7]. For the serum concentration of metronidazole as a function of time after oral administration of metronidazole (200 mg) to fasting rabbits, the best fit was found to be with an open one-compartment model. The validity of the proposed method for the pharmacokinetic determination of metronidazole in rabbits was examined by comparing it with the LC method. The results are presented in Table 2. Statistical analysis of the results reveals that at the 95% level of confidence, the calculated t values and F values indicate the proposed method to be as precise and accurate as the LC method.

The methods used to determine metronidazole in biological samples reported hitherto include spectrophotometry [8], bioassay [9] and chromatography [10–12]. However, extensive pretreatment of the samples is required when these methods are used. No pretreatment of the serum samples is required in the proposed method. This advantage represents a valuable contribution in various fields requiring metronidazole determination.

Acknowledgement

This work was supported by a Grant-in-Aid from the National Natural Science Foundation of China, No. 291References

[1] J.I. Peterson and G.G. Vurek, Science, 224 (1984) 123.
[2] P.R. Coulet, L.J. Blum and S.M. Gautier, J. Pharm. Biomed. Anal., 7 (1987) 1361.
[3] J.N. Roe, F.C. Szokaand, A.S. Verkman, Analyst, 115 (1990) 353.
[4] E. Vrbano, H. Offenbacher and O.S. Wolfbeis, Anal. Chem., 56 (1990) 353.
[5] M.J. Sepaniak, B.J. Tromberg and J.F. Eastham, Clin. Chem., 29 (1983) 1678.
[6] O.S. Wolfbeis, in S.G. Schulman (Ed.), Molecular Luminescence Spectroscopy: Method and Application. Part 2, Wiley, New York, 1988.
[7] R.N. Brogden, R.C. Heel, T.M. Speigh and G.S. Avery, Drugs, 16 (1978) 387.
[8] E.P.K. Lau, G. Yao, M. Lewis and B.Z. Senkowski, J. Pharm. Sci., 58 (1969) 55.
[9] E.D. Ralph and W.M.M. Kirby, J. Infect. Dis., 132 (1975) 587.
[10] J.C. Jensen and R. Gugler, J. Chromatogr., 277 (1983) 381.
[11] A. Gulaud, G.W. Houghton, O.R.W. Lewelen, J. Smith and P.S. Thorne, Br. J. Clin. Pharmacol., 6 (1978) 430.
[12] K.K. Mihda, I.J. McGilveray and J.K. Cooper, J. Chromatogr., 87 (1973) 491.

ELSEVIER

Analytica Chimica Acta 292 (1994) 317–324

ANALYTICA CHIMICA ACTA

Vaporization mechanisms for gold and for gold in the presence of vanadium in a graphite atomizer

A.J. Aller

Department of Biochemistry and Molecular Biology, University of León, E-24071 León, Spain

(Received 16th November 1993; revised manuscript received 4th January 1994)

Abstract

Time resolved absorbance profiles, the influence of gold concentration and the effect of vanadyl chloride have been established for graphite furnace atomic absorption signals of gold. Conventional furnace operating procedures with both wall and platform atomization modes showed similar results for the orders of reaction, but a few differences were noted in the activation energy values. On account of both the relatively narrow half widths and uniform peak profiles, gold–graphite interactions appear to be very strong for low gold concentrations, where the order of gold release is near to unity. However, gold–graphite interactions decrease for higher concentrations of gold, where the order of gold release deviates from unity. Absorbance profiles were found to be sensitive to the mass of the vanadium present showing larger integrated absorbances when the vanadium mass increases.

Key words: Atomic absorption spectrometry; Atomization kinetics; Gold atomization; Modifiers; Vanadyl chloride

1. Introduction

Although the main interest of gold lies in its economical importance, recent applications in geochemical [1] and clinical studies [2] have generated a lot of research in order to find satisfactory analytical methods for its determination in both geological [3–9] and biological [10–13] samples.

Graphite furnace atomic absorption spectrometry (GFAAS) has been widely used for the determination of gold, although some interferences [14,15] diminish its applicability. To cope with these interferences many methods have been employed, but particularly the solvent extraction [16–18] and chemical modification [15,18–21] procedures have found widespread use. Other alternatives for the separation/preconcentration of gold have also been recently developed [22]. Different chemical modifiers have been used in the GFAAS determination of gold in samples of different composition. Vanadium was recently found suitable for this purpose [21].

The optimal use of a chemical modifier requires knowledge of the atomization mechanism of any analyte alone and in the presence of modifier. Different mathematical models based on experimental studies have been evolved to describe the atomization in GFAAS [23–26]. However, for the evaluation of the mathematical expressions the rate order of the relevant chemical reactions is needed. Some authors have developed methods for determining the release order in different situations, "flash filament" desorp-

SSDI 0003-2670(94)00070-3

tion [27], vacuum conditions [28], using a Monte Carlo simulation technique [29] or under non-isothermal conditions [30,31]. The presence of a chemical modifier can alter the release order of an analyte in a graphite atomizer [32]. This work was undertaken to determine the release order of gold atoms alone and in the presence of vanadium, covering a wide gold concentration interval.

2. Experimental

2.1. Apparatus

The experiments were carried out using a Thermo Jarrel Ash SH 11 atomic absorption spectrophotometer equipped with a Model CTF-188 heated graphite atomizer and the Smith-Hieftje background correction system. The operating parameters used were as follows: wavelength, 242.8 nm, 267.6 nm and 274.8 nm; gold hollow cathode lamp, Visimax II; current, 2.5 mA; slit-width, 1 nm. Standard pyrolytic graphite-coated cylindrical and standard uncoated rectangular graphite tubes were used for wall and platform atomization, respectively. Standard pyrolytic graphite-coated platforms were used with rectangular tubes. Rectangular tubes can be placed in a such a way that platforms can be located vertically and horizontally. We have explored both possibilities in order to obtain better explanations about the vaporization mechanism of gold. The integrity of the pyrolytic coating was carefully monitored because the condition of the graphite strongly influences the characteristics of the gold peak profile and, therefore, the sensitivity of its determination. An Epson 118 recorder was used. Solutions were injected into the graphite atomizer by means of the Fastac automatic aerosol deposition system for wall and platform atomization and argon (99.995% purity) served as the purge gas. The temperature was measured with a calibrated automatic optical pyrometer via a hole in the graphite furnace. The temperature programme used is shown in Table 1. The volume of solution injected into the atomizer was 10 μl.

Table 1
Graphite atomizer temperature programme

Parameters	Steps				
	Dry	Ashing 1	Ashing 2	Atomization	Clean
Temperature, °C	150	450	600	2200	2400
Ramp time, s	2	20	20	0	–
Hold time, s	0	0	0	4	0
Ar flow, position	1	2	1	0	3
Read, s	–	–	–	5	–

2.2. Reagents

Gold stock solution (1000 μg/ml Au) was prepared by dissolving 1 g of 99.99% gold in aqua regia followed by dilution to 1000 ml in a calibrated flask. The test solutions were prepared by appropriate dilution of the stock solution immediately prior to their use. Inorganic acids and other chemicals were of analytical-reagent grade. Distilled, deionized water was used for the preparation of samples and standards.

2.3. Procedure

The atomic absorption spectrometer provides simultaneous measurements of peak height (PH) and integrated absorbance (PA). The integrated absorbance mode was mainly used because it was less prone to interferences. In the atomic absorption determination of gold using graphite furnace atomization, optimum conditions with respect to the analyte wavelength and spectral band-pass were established in order to get the best sensitivity. Ashing temperature, atomization temperature and inert gas flow-rate were also optimized. Results presented in this paper are the average of at least three measurements. Activation energies were obtained from a least-squares fit of the data. In order to reduce all results to the usual working conditions and to isolate background contribution to the analyte signal the Smith-Hieftje background correction system was used in all measurements. Although AAS is usually employed for the determination of trace metals, it can also occasionally be used for the determination of metals at higher concentration levels by selecting adequate instrumental settings. This is

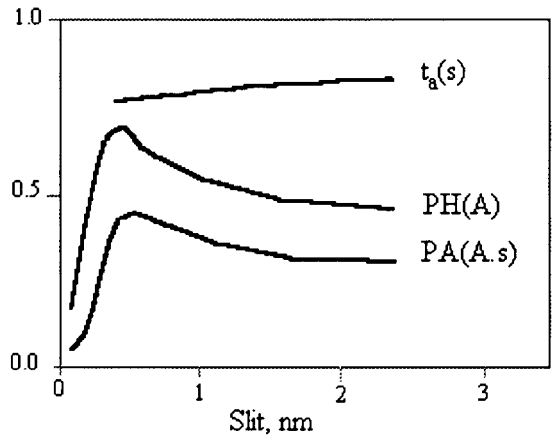

Fig. 1. Integrated absorbance (PA), peak height (PH) and appearance time (t_a) of the gold (1 ng) platform atomization as a function of the slitwidth. The scale for PA, PH and t_a is numerically the same, each one with the units shown in parenthesis inside the figure.

the reason why gold was used in a wide mass range (up to 20 μg). It is common practice for these measurements to have the gas flow on during the atomization, but zero gas flow was used in this work (Table 1) because this value is recommended by the manufactures and for a better isolation of the source function. All temperature and signal intensity data were recorded simultaneously during each atomization cycle.

3. Results and discussion

3.1. Influence of band-pass

Fig. 1 shows the effect of band-pass on the gold signal in the case of platform atomization with the Smith-Hieftje background correction system. This figure shows that the appearance time (t_a) slightly increases with the band-pass, but that above 1 nm the curve levels off. On the other hand, both integrated absorbance (PA) and peak height (PH) show a maximum value around 0.5–0.8 nm of the band-pass. It is clear from this figure that the gold atomic absorption signal is affected by band-pass. These results are opposed to the fact that, at very small band-pass values and corresponding narrow slit-widths, the light-gathering power of the monochromator decreases because of diffraction and that, consequently, the detection limit increases [33]. However, we can see from Fig. 1 that above a band-pass value of 0.5 the absorbance once decreases again. This is probably due to the broadening of the emission line profile during the high current pulse of the lamp. As a result of this broadening, the Lorentzian components show a stronger contribution to the background signal above a band-pass of 0.5 nm. This means that the detection limit becomes higher and that it is necessary to have a larger amount of analyte in the atomizer before it can be detected. For certain amounts of gold deposited in the atomizer, the amount of gold required for detection is attained later with increasing slit-width. A wide slit is not essential for maximum sensitivity, because the background noise (shot noise) and the throughput of broad-band background signals depend on the spectral band-pass and on the square of the spectral band-pass, respectively [34]. The best band-pass value for the Au determination based on GFAAS is in the range of 0.5–1.0 nm and a band-pass of 1 nm was used throughout this study.

3.2. Effect of gold concentration on peak profile characteristics

The atomization of gold was performed in both wall and platform atomization modes. Integrated absorbances and appearance temperatures for platform atomization are higher than the corresponding values for wall atomization. The range of gold amounts deposited in the graphite tube was between 0.01 ng and 20 μg. Thus, for the determination of gold over such a wide range, different sensitivities are needed and consequently both wall and platform atomization techniques as well as different wavelengths were used.

The influence of the gold concentration (from 0.5 to 5 ng Au deposited) on the peak-profile of gold atomic absorption signals in GFAAS from wall atomization are depicted in Fig. 2A and B. According to McNally and Holcombe [29], the order of atom desorption can be predicted from the concentration dependence of absorbance–time profile characteristics. Thus, an increase of

the amount of analyte deposited into the graphite tube results in peak shifts to higher temperatures for a zero- or fractional-order desorption, while in a first-order signal process the peak maximum occurs at the same temperature, independent of the amount of gold deposited. As a result, we can deduce from this figure that the gold atom release from the graphite surface follows a fractional order. From the Fig. 2A it is possible to derive an order of desorption between 1 and 2/3 for the gold atomization in the quoted range. These results agree with those obtained using the 242.8 nm wavelength. However, the gold atom desorption changes when the amount of gold deposited is increased. Thus, if we introduce in the atomizer a gold mass between 50 ng and 20 μg, the release order changes again, apparently to a quasi half-order desorption (Fig. 2B).

Results for the masses of gold between 0.01 and 1 ng obtained by platform (horizontal) atomization are shown in Fig. 2C. An order of desorption near to unity can be deduced from this figure. However, a lower order of gold desorption appeared for higher concentrations of gold (2.5–30 ng Au deposited) for platform (vertical) atomization (Fig. 2D).

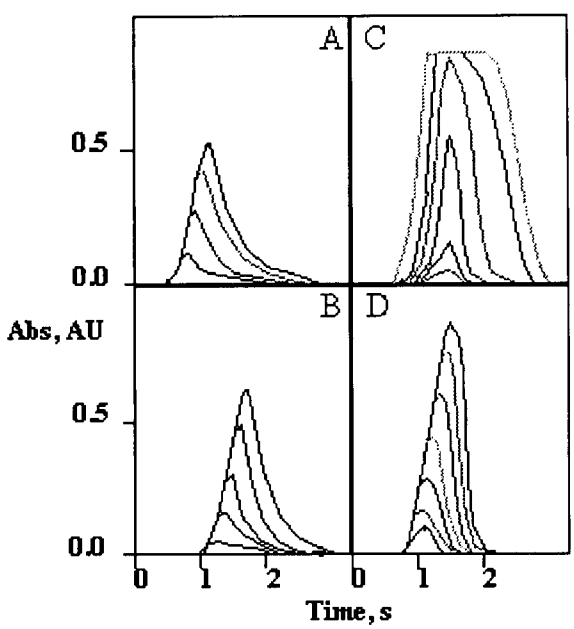

Fig. 2. Superimposed absorbance–time profiles for different concentrations of gold obtained by wall atomization [(A) 0.5–5.0 ng Au, λ = 267.6 nm; (B) 5–20 μg Au, λ = 274.8 nm] and platform atomization [(C) 0.01–1 ng Au (platform horizontally used), (D) 2.5–30 ng Au (platform vertically used); λ = 242.8 nm].

Table 2
Appearance time (t_a), integrated absorbance (PA) and peak height (PH) of the gold (1 ng) platform atomization alone and in the presence of some metals (10 ng) for two slit values (A = absorbance units)

System	t_a (s)	PA (A s)	PH (A)
Slit = 1 nm			
Au	0.72 ± 0.01	0.480 ± 0.015	0.765 ± 0.012
Au + Al	0.71 ± 0.01	0.511 ± 0.015	0.749 ± 0.016
Au + Mg	0.74 ± 0.02	0.488 ± 0.014	0.746 ± 0.018
Au + Ca	0.72 ± 0.01	0.545 ± 0.016	0.747 ± 0.017
Au + Cu + Ag	0.90 ± 0.03	0.109 ± 0.015	0.283 ± 0.018
Slit = 2 nm			
Au	0.88 ± 0.03	0.314 ± 0.015	0.476 ± 0.013
Au + Pd	0.98 ± 0.02	0.354 ± 0.016	0.475 ± 0.017
Au + Cu	1.00 ± 0.01	0.281 ± 0.016	0.527 ± 0.016
Au + Co	0.85 ± 0.03	0.197 ± 0.017	0.322 ± 0.017

The presence of some metals during the atomization of gold modifies the characteristics of the Au atomic absorption signals (Table 2), although our results do not agree with those found in the literature [15,35]. Previous results, using a deuterium correction system, did not show interference from copper, but show a positive effect from aluminium, magnesium and cobalt and a negative influence from calcium [35]. The reason for this disagreement could be based on the different instrumental conditions used in the experiments. Savel'eva and Agapova [35] used the deuterium background correction system, but Egila et al. [15] did not use background correction at all. Different temperature programmes [15,35] are also reported in each paper. When the matrix composition of a sample is very complex the gold atomic absorption signal is strongly distorted. Therefore, a complex peak profile (two peaks) [21] is obtained for the atomization of gold from a complex matrix containing Cr, Fe, Al, Mg, Ca and Si. The second peak results from the participation of a few of the metals present in the sample, and so modifying the atomization path of gold (Fig. 3A). These results suggest that the atomization of gold in the presence of some met-

als takes place by a complex mechanism. The influence of the amount of gold deposited in the graphite tube, from both the complex sample and together with vanadium as chemical modifier, is shown in Fig. 3A and B, respectively. From these figures it can be deduced that a first-order process occurs. In conclusion, the gold atom formation process is altered by the presence of some concomitant metals. When background correction is not used, the signals in Fig. 3 show the same shape, which eliminates the possibility of any spectral interference.

In order to confirm the above assumptions for the desorption order of gold, they were experimentally determined for all the situations described above by using the method described by Cathum et al. [30] (Table 3). The activation energy was also calculated by using the method of Sturgeon et al. [36] (Table 3). The orders of gold desorption from Table 3 are in good agreement with those deduced from the shapes of the gold atomic absorption signals in GFAAS with changes in concentration and in a general way with those obtained by other authors [29,32,37] for the gold solutions and for a similar concentration interval. However, the orders of gold desorption experimentally found in this paper are a little higher than those previously reported [29,37], while the activation energies are a little lower here. It was recently shown that the net rate of atom supply

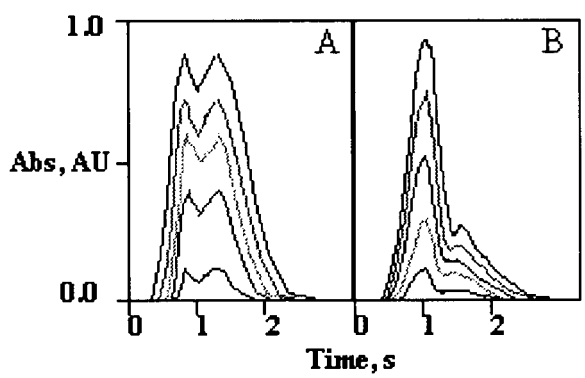

Fig. 3. Superimposed absorbance–time profiles for the wall atomization of different concentrations of gold (0.5–5.0 ng Au) from a complex matrix (A) and from a complex matrix together with vanadium (0.1% V, v/v) as chemical modifier (B), at $\lambda = 242.8$ nm.

Table 3
The order of reaction, n, calculated according to the method of Cathum et al. [30] and the activation energy, E_a, obtained by Sturgeon et al. [36] for different concentrations of gold

Amount deposited	Atomization mode	n	E_a (kJ/mol)
Au (0.01–1 ng)	Platform (horizontal)	0.79±0.05	269.7±14
Au (2.5–30 ng)	Platform (vertical)	0.55±0.05	308.2±18
Au (0.5–5 ng)	Wall	0.80±0.07	278.7±14
Au (50–500 ng)	Wall	0.59±0.06	263.4±12
Au (5–20 μg)	Wall	0.45±0.06	255.4±12
Au (1 ng) +V (0.1%)	Wall [a]	0.94±0.06	741.6±20

[a] Results for horizontal platform atomization were similar.

and removal are identical for both gas-stop and gas-flow conditions during the atomization stage using either uncoated and pyrolytic graphite coated graphite tubes [38]. Consequently, the activation energy obtained in both cases is the same. However, the peak maximum shifts to a later time as the gas flow decreases [38]. This suggests that the desorption order obtained through the peak maximum, could show some differences when comparing them with those previously reported. The method of Sturgeon et al. [36] was used for the calculation of activation energy because this procedure does not invoke the first order assumption. However, in other articles [29,37], the activation energy was reported to be calculated employing the Smets method, which is stronger at lower temperatures but has a limited value to be used over a wide temperature range. This could be another point of discrepancy between our results and those obtained in previous papers.

3.3. Influence of vanadium concentration

The suitability of vanadium as a chemical modifier for the determination of gold was recently demonstrated [20,21]. It has been shown above that the presence of chemical modifiers and/or interferents can modify the peak profile characteristics of the gold atomic absorption signal (Table 2) varying also the release order.

The effect of the vanadium concentration on the atomization of gold (Fig. 4) shows that the gold atom desorption is always a first-order process for the whole concentration range studied. The fact that the atomization temperature has not been sufficiently increased to accommodate the higher activation energy could also be responsible for the slow desorption (Table 3). However, when the vanadium content increases in the quoted range the integrated absorbance also increases. Nevertheless, at higher values of the integrated absorbances the roll-over phenomenon appears (line d in Fig. 4) [21,39].

3.4. Influence of ashing temperature on the gold atomization

The highest ashing temperature used was 900°C because above this temperature a decrease of the gold signal was observed. The effect of ashing temperature (600–900°C) on the gold peak profile is shown in Fig. 5. This figure shows that the peak temperatures (T_p) of the atomic absorption signals for gold alone and together with vanadium are unaltered for increased ashing temperatures. However, the appearance temperatures (T_a) are slightly increased for the higher ashing temperatures, both for gold alone and for gold in the presence of vanadium. Only at the ashing temperature of 900°C little alteration of the mechanism of gold atomization seems to occur. Losses of gold can also be the reason for this alteration.

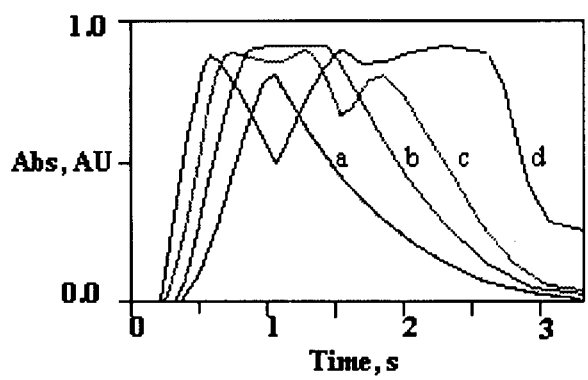

Fig. 4. Effect of vanadium concentration (a, 0% v/v; b, 0.2% v/v, c, 1% v/v; d, 2% v/v) on the peak profiles of the gold (1 ng) wall atomization at the 242.8 nm wavelength.

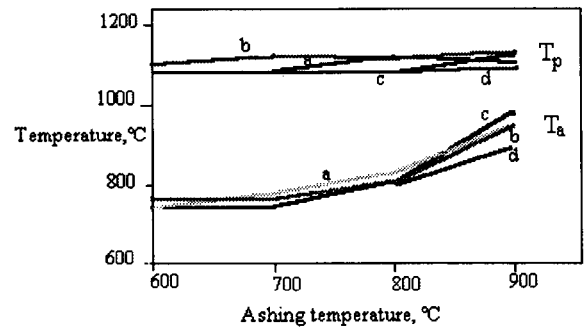

Fig. 5. Effect of ashing temperature (600–900°C) on the appearance (T_a) and peak (T_p) temperatures of the gold (1 ng) wall atomization alone and in the presence of vanadium. [a, Au alone; b, Au in an ore matrix; c, Au alone plus 0.5% (v/v) V; and d, Au in an ore matrix plus 0.5% (v/v) V].

3.5. Vaporization and atomization mechanisms

The appearance temperature (Fig. 5) for the gold atomization is lower than the melting point (1063°C), suggesting that gold is present in its elemental state on the graphite surface prior to its vaporization. Consequently, the final process of the gold atomization will involve vaporization of free metal at the appearance temperature and above. These results, supported by the activation energies (Table 3), agree with those reported in other papers [37,40].

The kinetics and mechanism of gold vaporization can be alternatively explained by two different approaches, the adsorption/desorption and condensation/evaporation processes. In the first process, the analyte desorption takes place from a monolayer of the sample distributed over the tube surface or from individual atoms or molecules which are physically sorbed or chemisorbed to the surface. In the second process, the analyte is released from individual microcrystallites or microdroplets. However, the results of this paper suggest that the behaviour of gold in GFAAS shows characteristics of both approaches. This can be explained by the simultaneous influence of the number of droplets and a coalescence process, which in turn are affected by both the

Fastac automatic sample introduction system and the physical properties of sample solution. The average crystal size produced by the Fastac system depends on the average aerosol droplet diameter [41], being also larger than those produced by the manual injection mode [42].

Gold vaporization mechanisms for wall and platform atomization seems to be similar for the same concentration interval, because both the desorption order and activation energy are similar for each atomization mode (Table 3). The order of desorption for low concentrations of gold (0.01–5 ng deposited) is near unity (Table 3) for both platform and wall atomization. This can be explained by the formation of very small droplets, simulating a submonolayer coverage of gold upon the graphite surface, where desorption of gold takes place from a monolayer (for unit desorption orders) [23], or the droplet surface (for a 2/3 desorption order) [43]. The average number of droplets would be high and probably nearly constant for the whole concentration range studied. On the other hand, for higher amounts of gold (up to μg level), where the desorption order is 1/2 (Table 3) for both platform and wall atomization, the desorption of gold can be explained by evaporation from the edges of hemispherical droplets or by a Langmuirian vaporization from a droplet [29,44]. The number of droplets (the total evaporation area) increases with gold concentration, but with a larger average size [45], owing to the coalescence process. The decrease of desorption order with gold concentration could also be affected by the fact that the desorption of large amounts of gas, where gas expansion is far greater, influences the transport mechanisms within the tube. If gold is deposited together with some concomitants, the formation of macro-droplets on the graphite surface appears to occur. In this case, the submonolayer of gold is probably covered to some extent by concomitant species (forming probably an intermetallic compound) and the desorption of single gold atoms simulates the desorption from a graphite or metal surface. Larger peak half-widths appear for a quasi-first-order of gold desorption, suggesting an adsorption/desorption equilibrium with strong gold–graphite interactions. However, narrower peak half-widths are obtained for fractional orders, and weak and relatively elastic gold–graphite interactions occur; consequently, the gold residence time within the furnace will be subsequently shortened and gold atoms would show a diffusion controlled distribution [29,46].

The activation energy of the desorption of gold might be dependent on the desorption order and, consequently, on the amount of gold deposited in the graphite tube. This was recently confirmed for the secondary desorption of gold [37], but our results do not totally confirm this hypothesis (Table 3), probably owing to differences in the sample deposition mode and in the rate of solvent evaporation [37]. However, a few differences in this trend are noted for wall and platform atomization modes. For wall atomization lower values of the activation energy are obtained as the gold concentration increases. Thus, the concentration-dependent activation energy values suggest also that the number of droplets increases with gold concentration, but with a lower rate than expected owing to the coalescence of molten droplets. Another possible explanation takes into consideration the two types of graphite tubes used. Thus, pyrolytic graphite-coated graphite, used to form the cylindrical graphite tubes (wall atomization) and the platforms, has a less reactive nature with a lower number of active sites than shown by the uncoated rectangular graphite tubes (vertical platform atomization). When the platform is used in a vertical manner, the sample is mainly deposited on the surface of the non-pyrolytic graphite tube due to the orientation of the platform, but not on the platform itself. This explains the differences of the two modes as the platform is used. However, the activation energy for the atomization of gold in the presence of vanadium shows a higher value, suggesting the presence of a dissociation process of gold–vanadium intermetallic compounds, that rules the subsequent vaporization step of gold atoms.

4. Conclusion

This paper shows that the vaporization mechanism of gold depends on both gold concentration

and concomitant species. Thus, the vaporization of low amounts of gold alone from a wall shows a fractional desorption order near to 0.80. This fractional order lowers as the gold concentration increases. On the other hand, desorption of gold for platform atomization also exhibits a fractional (0.79) order, decreasing also with the gold concentration. The desorption of gold in the presence of vanadium as chemical modifier is a first-order process for wall and platform atomization modes. Gold–graphite interactions are lower as gold concentration increases.

References

[1] C.J.B. Smit, J.S. Afr. Inst. Min. Metall., 85 (1985) 417.
[2] A.C. Johnsen, J. Aaseth, F.J. Langmyhr and G. Wibetoe, Anal. Chim. Acta, 135 (1982) 243.
[3] E. Taskaev, I. Penev, H. Schelhorn and M. Geisler, Geostandards Newsletter, 11 (1987) 103.
[4] F. Me, R. Sera, R. Enne, I. Trudu and E. Contini, At. Spectrosc., 11 (1990) 128.
[5] R.K. Tewari, V.K. Tarsekar and M.B. Lokhande, At. Spectrosc., 11 (1990) 125.
[6] S.K. Xu, L.J. Sun and Z.L. Fang, Anal. Chim. Acta, 245 (1991) 7.
[7] M. Asif and S.J. Parry, Analyst, 116 (1991) 1071.
[8] X. Peiqing, J. Anal. At. Spectrom., 7 (1992) 775.
[9] L.C. Robles, C. García-Olalla and A.J. Aller, Fresenius' J. Anal. Chem., 345 (1993) 441.
[10] S. Xiao-quan, J. Egila, D. Littlejohn and J.M. Ottaway, J. Anal. At. Spectrom., 2 (1987) 299.
[11] D.F. Kehoe, D.M. Sullivan and R.L. Smith, J. Assoc. Off. Anal. Chem., 71 (1988) 1153.
[12] S.G. Matz, R.C. Elder and K. Tepperman, J. Anal. At. Spectrom., 4 (1989) 767.
[13] L. Thunus and J.F. Dauphin, Anal. Chim. Acta, 235 (1990) 393.
[14] Z.H. Hou, J. Geochem. Explor., 27 (1987) 323.
[15] J. Egila, D. Littlejohn, J.M. Ottaway and S. Xiaoquan, J. Anal. At. Spectrom., 2 (1987) 293.
[16] K.S. Patel and K.H. Lieser, Fresenius' Z. Anal. Chem., 323 (1986) 494.
[17] C.H. Branch and D. Hutchison, Analyst, 111 (1986) 231.
[18] J.M. Vermeulen, J. Anal. At. Spectrom., 4 (1989) 77.
[19] D.O. Matthews and M.C. Mcgahan, Spectrochim. Acta, 42B (1987) 909.
[20] D.L. Tsalev, T.A. Dimitrov and P.B. Mandjukov, J. Anal. At. Spectrom., 5 (1990) 189.
[21] C. García-Olalla and A.J. Aller, Anal. Chim. Acta, 252 (1991) 97.
[22] L.C. Robles, C. García-Olalla and A.J. Aller, J. Anal. At. Spectrom., 8 (1993) 1015.
[23] B. Smets, Spectrochim. Acta, 35B (1980) 33.
[24] C.H. Chung, Anal. Chem., 56 (1984) 2714.
[25] N.G. Zhou, W. Frech and L. de Galan, Spectrochim. Acta, 39B (1984) 225.
[26] C. Hsiech and H.L. Pardue, Anal. Chem., 65 (1993) 1809.
[27] P.A. Redhead, Vacuum, 12 (1962) 203.
[28] J.R. Arthur and A.Y. Cho, Surf. Sci., 36 (1973) 641.
[29] J. McNally and J.A. Holcombe, Anal. Chem., 59 (1987) 1105.
[30] S.J. Cathum, C.L. Chakrabarti and J.C. Hutton, Spectrochim. Acta, 46B (1991) 35.
[31] D. Rojas and W. Olivares, Spectrochim. Acta, 47B (1992) 387.
[32] H. Qiao and K.W. Jackson, Spectrochim. Acta, 46B (1991) 1841.
[33] M.-L.W. Wu and R.G. Michel, Analyst, 110 (1985) 937.
[34] T.L. Chester and J.D. Winefordner, Anal. Chem., 49 (1977) 119.
[35] A.N. Savel'eva and T.E. Agapova, J. Anal. Chem. USSR, 34 (1979) 1344.
[36] R.E. Sturgeon, C.L. Chakrabarti and C.H. Langford, Anal. Chem., 48 (1976) 1792.
[37] S. Lynch, R.E. Sturgeon, V.T. Luong and D. Littlejohn, J. Anal. At. Spectrom., 5 (1990) 311.
[38] C.W. Huie and C.J. Curran, Jr., Appl. Spectrosc., 44 (1990) 1329.
[39] A.J. Aller, Anal. Chim. Acta, 284(2) (1993) 361.
[40] W.B. Rowston and J.M. Ottaway, Analyst, 104 (1979) 645.
[41] J.G. Shabushing and G.M. Hieftje, Anal. Chim. Acta, 148 (1983) 181.
[42] A.G. Howell and S.R. Koirtyohann, Appl. Spectrosc., 46 (1992) 953.
[43] A.E. Seaver, Aerosol Sci. Technol., 3 (1984) 177.
[44] B.V. L'vov and P.A. Bayunov, Zh. Anal. Khim., 40 (1985) 614.
[45] B.V. L'vov, A.V. Novichikhin nd L.K. Polzik, Spectrochim. Acta, 47B (1992) 289.
[46] J. McNally and J.A. Holcombe, Anal. Chem., 63 (1991) 1918.

ELSEVIER

Analytica Chimica Acta 292 (1994) 325–328

ANALYTICA CHIMICA ACTA

Determination of boron in iron- and nickel-based alloys by graphite furnace atomic absorption spectrometry with a zirconium–nickel chemical modifier and a zirconium-pretreated graphite tube

Yongming Liu *, Benling Gong, Yuli Xu, Zhuanhe Li, Tiezheng Lin

Dalian Institute of Chemical Physics, Academia Sinica, 161 Zhongshan Road, Dalian, China

(Received 6th May 1993; revised manuscript received 14th July 1993)

Abstract

A chemical modifier composed of nickel and zirconium salts and treatment of the graphite tube with zirconium solution were studied for the determination of boron in cast iron, Fe-, Ni- and Fe–Ni-based alloys. A combination of 3000 mg l^{-1} nickel and 1000 mg l^{-1} zirconium as chemical modifier and soaking the graphite tube in 10 g l^{-1} zirconium solution gave the highest analytical sensitivity. The interference effects of a major component (iron) and eight minor components (Cr, W, Nb, Ta, Mo, Ti, Al and Mn) were studied.The relative standard deviation for the determination of 0.013% of boron in a nickel-based alloy was 5.6% ($n = 8$). The characteristic mass was 500 pg per 0.0044 absorbance.

Key words: Atomic absorption spectrometry; Alloys; Boron; Chemical modification; Zirconium–nickel chemical modifier

1. Introduction

Boron is a minor component with a large effect on the performance of steels and alloys, hence the exact determination of boron is important in the metallurgical industry.

Inductively coupled plasma atomic emission spectrometry is widely used for the determination of micro amounts of boron [1–9], but it suffers severely from spectral interferences from samples having a complex matrix such as steels and alloys. To remove these interferences, tedious pretreatment for separation of the matrix from the sample is usually necessary, and this can easily cause contamination or losses.

Graphite furnace atomic absorption spectrometry (GFAAS) could be used as an alternative sensitive method to determine this element. However, boron very easily combines with the carbon of the graphite tube, resulting in low analytical results and severe memory effects.

The application of a suitable chemical modifier and treatment of the graphite tube could resolve these problems. Chemical modifiers such

* Corresponding author.

Elsevier Science B.V.
SSDI 0003-2670(94)00036-L

as calcium [10,11], strontium [12] and magnesium [11,12] and methods for treatment of graphite tubes have already been proposed.

In this paper a mixture of nickel and zirconium as a chemical modifier and coating of the graphite tube with zirconium solution are proposed, because zirconium is often used for coating graphite tubes to protect them against the formation of carbide during analyses of carbide-forming elements and nickel is used as a chemical modifier for some elements such as arsenic, gold, bismuth and selenium. This combination of the proposed chemical modifier and zirconium coating of the graphite tube showed excellent performance, increasing the analytical sensitivity and suppressing memory effects in the determination of boron. With this procedure satisfactory results were obtained for the determination of boron in cast iron and Fe-, Ni- and Fe–Ni-based alloys by GFAAS without preseparation of the matrix.

2. Experimental

2.1. Apparatus

A Perkin-Elmer Model 5000 atomic absorption spectrometer equipped with a Model HGA 500 graphite furnace, a Data Station 10 and a PR 100 printer was used. An Eppendorf micropipette was used for injecting sample solutions into the graphite furnace.

The instrumental parameters and operating conditions were optimized experimentally and are shown in Table 1.

The pyrolytic graphite tube was soaked in a 10 g l^{-1} solution of zirconium for 2 days, then dried at 120°C for 2 h and stored in a desiccator. Such a tube can be used for 200–300 firings.

2.2. Reagents

All chemicals were of analytical-reagent grade and distilled, deionized water was used throughout.

A stock standard solution of boron (1000 mg l^{-1}) was prepared by dissolving boric acid in water and stored in a polyethylene bottle. A working standard solution (10 mg l^{-1}) was prepared by diluting the stock standard solution with 0.2% nitric acid.

A 12.5 g l^{-1} solution of zirconium was prepared by dissolving zirconium oxychloride ($ZrOCl_2 \cdot 8H_2O$) in water.

A 25 g l^{-1} solution of nickel was prepared by dissolving nickel acetate [$Ni(CH_3COO)_2 \cdot 4H_2O$] in water.

Solutions of 0 (blank), 250, 500, 750 and 1000 μg l^{-1} of boron were prepared by diluting the working standard solution and each solution, containing 3000 mg l^{-1} of nickel and 1000 mg l^{-1} of zirconium, was used for constructing a calibration graph.

Table 1
Instrumental parameters and operating conditions

Instrumental parameters					
Wavelength (nm)	249.7				
Slit width (nm)	0.7				
Lamp current (mA)	15				
Integration time (s)	6				
Sample injection volume (μl)	20				
Heating programme					
	Step				
	1	2	3	4	5
Temperature (°C)	120	1200	2700	2650	20
Ramp time (s)	10	10	1	1	1
Hold time (s)	20	20	3	3	5
Read (s)		0			
Int. gas flow-rate (ml min^{-1})	300	300	50	300	300

2.3. Procedures for alloy analysis

A 50–100-mg amount of finely granulated sample was weighed in a quartz beaker, 2.5–3 ml of aqua regia were added and the solution was allowed to stand for 1 h at room temperature. The beaker was then heated in a water-bath at 60–70°C to decompose the sample completely until only a few carbon particles remained in the sample solution.

After cooling, the sample solution was transferred into a 25-ml volumetric flask with 0.3% nitric acid. For cast iron and Fe-based alloy samples that contain no or only small amounts of

nickel, 3 ml of nickel solution and 2 ml of zirconium solution were added in the flask, and for Ni- and Fe–Ni-based alloys, which contain the bulk of nickel, 2 ml of zirconium solution were added. The sample solution was then neutralized to pH 6–7 with concentrated ammonia solution (1 + 1). Finally, if necessary, water was added to the mark. Using an Eppendorf micropipette, 20-μl portions of the sample solution were injected into the graphite furnace and the peak height was measured.

3. Results and discussion

3.1. Acidity of prepared sample solution

The sample solution obtained via decomposition must be carefully neutralized with ammonia solution to pH 6–7 to match that of the working standard solution used to prepare the calibration graph. The acidity of the sample solution injected affects the analytical sensitivity appreciably, that is, the sensitivity decreases with increasing acidity.

3.2. Effect of coating of graphite tube

The effect of coating of the pyrolytic graphite tube was studied for the determination of 500 μg l^{-1} of boron containing 3000 mg l^{-1} of nickel and 1000 mg l^{-1} of zirconium with the use of a zirconium-coated and an uncoated pyrolytic graphite tube. The uncoated tube gave an absorbance of 0.048, compared with 0.090 for the coated tube.

3.3. Effect of proposed chemical modifier

The Zr–C bond strength (134 ± 6 kcal mol^{-1}) is larger than that of B–C (107 ± 7 kcal mol^{-1}) [13]. Therefore, when boron and zirconium are atomized simultaneously, zirconium may combine predominantly with carbon in the graphite tube, thus retarding the combination of boron with carbon and hence increasing the analytical sensitivity, and at the same time suppressing any memory effect. Nickel has been demonstrated to be useful as a chemical modifier for some elements, but its use in the determination of boron has not been reported. The use of nickel was found to enable the ashing temperature for the analyses of metals and alloys to be raised to 1200°C, which is useful for decreasing the matrix effect.

Table 2
Effects of nickel, zirconium and nickel–zirconium as chemical modifiers for 500 μg l^{-1} boron

Nickel (mg l^{-1})	0	0	3000	3000
Zirconium (mg l^{-1})	0	1000	0	1000
Absorbance	0.015	0.024	0.036	0.090
Nickel (mg l^{-1})	1000	3000	5000	10000
Zirconium (mg l^{-1})	1000	1000	1000	1000
Absorbance	0.075	0.090	0.042	0.043
Zirconium (mg l^{-1})	0	1000	2000	
Nickel (mg l^{-1})	3000	3000	3000	
Absorbance	0.033	0.090	0.000	

The effect of the chemical modifier composed from nickel and zirconium was studied for the determination of 500 μg l^{-1} boron with use of a zirconium-coated pyrolytic graphite tube. The results obtained are given in Table 2.

Table 2 shows that, although nickel and zirconium each enhance the analytical sensitivity, the combination of these two elements has a synergistic effect. The combination of 3000 mg l^{-1} nickel and 1000 mg l^{-1} zirconium can be seen to give the highest analytical sensitivity. A number of Ni- and Ni–Fe-based alloys contain 50–70% nickel. Therefore, the sample weight should be selected so that the final sample solution to be injected into the graphite furnace contains about 3000 mg l^{-1} nickel. In such cases only the addition of

Table 3
Maximum permissible concentrations of co-existing elements for the determination of 500 μg l^{-1} boron

Element	Maximum permissible amount (mg l^{-1})	Element	Maximum permissible amount (mg l^{-1})
Fe	4500	Mn	250
Cr	450	Al	175
W	450	Mo	125
Nb	450	Ti	30
Ta	300		

Table 4
Determination of boron in metal samples

Sample	Identification No.	Certified value (%)	Value obtained (%)	Difference (%)	Permissible difference (%) [a]
Cast iron	59	0.0160	0.0169	+0.0009	0.003
Fe-based alloy	1	0.0014	0.0014	0	0.0005
	14	0.0082	0.0075	−0.0007	0.001
Ni-based alloy	38	0.0090	0.0088	−0.0002	0.002
	36	0.0130	0.0132	+0.0002	0.003
Fe–Ni-based alloy	2	0.0045	0.0042	−0.0003	0.0005
	18	0.0040	0.0037	−0.0003	0.0005

[a] Permissible difference is based on Chinese National Standard GB 223.6-81 for the determination of the amounts of boron in steels and alloys.

zirconium solution to the sample solution is required. Any memory effect decreased rapidly with increasing amount of zirconium.

3.4. Interference of co-existing elements

Cast iron and Fe-, Ni- and Fe–Ni-based alloys contain minor components (Cr, W, Nb, Ta, Mo, Ti, Al, Mn, etc.). The interference effects of these elements on the determination of boron were studied with use of the chemical modifier composed of 3000 mg l^{-1} nickel and 1000 mg l^{-1} zirconium and the zirconium-coated pyrolytic graphite tube. Table 3 shows the maximum concentrations of these elements that can be tolerated in the determination of 500 μg l^{-1} boron. These limits exceed the concentrations that would be obtained by dissolving the alloys discussed above.

3.5. Determination of boron in cast iron and alloys

Boron in seven samples, viz., one cast iron, two Fe-based alloys, two Ni-based alloys and two Fe–Ni-based alloys, was determined with use of the chemical modifier composed of 3000 mg l^{-1} nickel and 100 mg l^{-1} zirconium and the zirconium-coated pyrolytic graphite tube. The results are given in Table 4.

The relative standard deviation for alloy No. 36 is 5.6% (n = 8, boron = 0.0130%). The characteristic mass is 500 pg per 0.0044 absorbance.

References

[1] G. Mezger, E. Grallath, U. Stix and G. Tolg, Fresenius' Z. Anal. Chem., 317 (1984) 765.
[2] V.K. Pin, Anal. Chim. Acta, 159 (1984) 387.
[3] J.N. Walsh, Analyst, 110 (1985) 959.
[4] K. Fujimoto, T. Okano, Y. Matumura and S. Harima, Bunseki Kagaku, 35 (1986) 651.
[5] Y. Takahashi, Bunseki Kagaku, 36 (1987) 693.
[6] G. Bauer, I. Rehana, W. Wegscheider and H.M. Ortner, Spectrochim. Acta, Part B, 43 (1988) 971.
[7] G. Zeibig, Mikrochim. Acta, III (1989) 389.
[8] I. Hlavacek, Mikrochim. Acta, III (1989) 309.
[9] H. Bin, Fresenius' J. Anal. Chem., 340 (1991) 435.
[10] Perkin-Elmer Model HGA-500 Operation Manual, Perkin-Elmer, Norwalk, CT.
[11] Y.-Q. Jiang, J.-Y. Yao and B.-L. Huang, Fenxi Huaxue, 17 (1989) 456.
[12] Y.-Q. Jiang, J.-Y. Yau and B.-L. Huang, Fenxi Shiyanshi, 17 (1988) 21.
[13] R.C. Weast (Ed.), CRC Handbook of Chemistry and Physics, CRC Press, Boca Raton, FL, 70th edn., 1990, pp. F197–198.

ELSEVIER

Analytica Chimica Acta 292 (1994) 329–331

ANALYTICA CHIMICA ACTA

AUTHOR INDEX

PUBLICATION SCHEDULE FOR 1994

	S'93	O'93	N'93	D'93	J	F	M	A	M	J	J	A
Analytica	281/1	282/1	283/1	283/3	284/3	286/1	287/1-2	288/3	289/3	291/1-2	292/3	294/1
Chimica	281/2	282/2	283/2	284/1	285/1-2	286/2	287/3	289/1	290/1-2	291/3	293/1-2	294/2
Acta	281/3	282/3		284/2	285/3	286/3	288/1-2	289/2	290/3	292/1-2	293/3	294/3
Vibrational Spectroscopy		6/1			6/2		6/3		7/1		7/2	

INFORMATION FOR AUTHORS

Detailed "Instructions to Authors" for *Analytica Chimica Acta* was published in Volume 289, No. 3, pp. 381–384. Free reprints of the "Instructions to Authors" of *Analytica Chimica Acta* and *Vibrational Spectroscopy* are available from the Editors or from: Elsevier Science B.V., P.O. Box 330, 1000 AH Amsterdam, The Netherlands. Telefax: (+31-20) 5862459.

Manuscripts. The language of the journal is English. English linguistic improvement is provided as part of the normal editorial processing. Authors should submit three copies of the manuscript in clear double-spaced typing on one side of the paper only. *Vibrational Spectroscopy* also accepts papers in English only.

Rapid publication letters. *Letters* are short papers that describe innovative research. Criteria for letters are novelty, quality, significance, urgency and brevity. Submission data: max. of 2 printed pages (incl. Figs., Tables, Abstr., Refs.); short abstract (e.g., 3 lines); *no* proofs will be sent to the authors; submission on floppy disc; *no* revision will be possible.

Abstract. All papers and reviews begin with an Abstract (50–250 words) which should comprise a factual account of the contents of the paper, with emphasis on new information.

Figures. Figures should be prepared in black waterproof drawing ink on drawing or tracing paper of the same size as that on which the manuscript is typed. One original (or sharp glossy print) and two photostat (or other) copies are required. Attention should be given to line thickness, lettering (which should be kept to a minimum) and spacing on axes of graphs, to ensure suitability for reduction in size on printing. Axes of a graph should be clearly labelled, along the axes, outside the graph itself. All figures should be numbered with Arabic numerals, and require descriptive legends which should be typed on a separate sheet of paper. Simple straight-line graphs are not acceptable, because they can readily be described in the text by means of an equation or a sentence. Claims of linearity should be supported by regression data that include slope, intercept, standard deviations of the slope and intercept, standard error and the number of data points; correlation coefficients are optional.

Photographs should be glossy prints and be as rich in contrast as possible; colour photographs cannot be accepted. Line diagrams are generally preferred to photographs of equipment. Computer outputs for reproduction as figures must be good quality on blank paper, and should preferably be submitted as glossy prints.

Nomenclature, abbreviations and symbols. In general, the recommendations of IUPAC should be followed, and attention should be given to the recommendations of the Analytical Chemistry Division in the journal *Pure and Applied Chemistry* (see also *IUPAC Compendium of Analytical Nomenclature, Definitive Rules*, 1987).

References. The references should be collected at the end of the paper, numbered in the order of their appearance in the text (*not* alphabetically) and typed on a separate sheet.

Reprints. Fifty reprints will be supplied free of charge. Additional reprints (minimum 100) can be ordered. An order form containing price quotations will be sent to the authors together with the proofs of their article.

Papers dealing with vibrational spectroscopy should be sent to: Dr J.G. Grasselli, 150 Greentree Road, Chagrin Falls, OH 44022, U.S.A. Telefax: (+1-216) 2473360 (Americas, Canada, Australia and New Zealand) or Dr J.H. van der Maas, Department of Analytical Molecular Spectrometry, Faculty of Chemistry, University of Utrecht, P.O. Box 80083, 3508 TB Utrecht, The Netherlands. Telefax: (+31-30) 518219 (all other countries).

0003-2670/94/$07.00

Flow-Through (Bio)Chemical Sensors

By **M. Valcárcel** and **M.D. Luque de Castro**, Department of Analytical Chemistry, University of Córdoba, 14004 Córdoba, Spain

Techniques and Instrumentation in Analytical Chemistry Volume 16

Flow-through sensors are more suitable than classical probe-type sensors for addressing real (non-academic) problems. The external shape and operation of flow-through (bio)chemical sensors are of great practical significance as they facilitate sample transport and conditioning, as well as calibration and sensor preparation, maintenance and regeneration, all of which result in enhanced analytical features and a wider scope of application.
This is a systematic presentation of flow-through chemical and biochemical sensors based on the permanent or transient immobilization of any of the ingredients of a (bio)chemical reaction (i.e. the analyte, reagent, catalyst or product) where detection is integrated with the analytical reaction, a separation process (dialysis, gas diffusion, sorption, etc.) or both.

The book deals critically with most types of flow-through sensors, discussing their possibilities and shortcomings to provide a realistic view of the state-of-the-art in the field. The large numbers of figures, the wealth of literature references and the extensive subject index complement the text.

© 1994 332 pages Hardbound
Price: Dfl. 355.00 (US$ 202.75)
ISBN 0-444-89866-2

ELSEVIER SCIENCE

ORDER INFORMATION
ELSEVIER SCIENCE B.V.
P.O. Box 330
1000 AH Amsterdam
The Netherlands
Fax: (+31-20) 5862 845
For USA and Canada
P.O. Box 945
Madison Square Station
New York, NY 10159-0945
Fax: (212) 633 3680
US$ prices are valid only for the USA & Canada and are subject to exchange rate fluctuations; in all other countries the Dutch guilder price (Dfl.) is definitive. Customers in the European Union should add the appropriate VAT rate applicable in their country to the price(s). Books are sent postfree if prepaid.

0003-2670(19940711)292:3;1-8